

**Universidade Federal do Rio Grande – FURG**

**Instituto de Oceanografia**

Programa de Pós-Graduação em Oceanologia

**DISTRIBUIÇÃO DAS ÁGUAS-FONTE DA  
ÁGUA PROFUNDA DO ATLÂNTICO NORTE  
E DA ÁGUA DE FUNDO ANTÁRTICA NO  
OCEANO GLOBAL**

**DAVID ANTONIO DE LIMA SILVA**

Dissertação apresentada ao  
Programa de Pós-graduação em  
Oceanologia, como parte dos  
requisitos para a obtenção do Título  
de Mestre.

Orientador: *Prof. Dr. RODRIGO KERR DUARTE PEREIRA*  
Universidade Federal do Rio Grande (FURG), Brasil.

Rio Grande, RS, Brasil

Maio 2024

# **DISTRIBUIÇÃO DAS ÁGUAS-FONTE DA ÁGUA PROFUNDA DO ATLÂNTICO NORTE E DA ÁGUA DE FUNDO ANTÁRTICA NO OCEANO GLOBAL**

Dissertação apresentada ao Programa de Pós-Graduação em Oceanologia,  
como parte dos requisitos para a obtenção do Título de Mestre

por

**DAVID ANTONIO DE LIMA SILVA**

Rio Grande, RS, Brasil

Maio 2024

© A cópia parcial e a citação de trechos desta tese são permitidas sobre a condição de que qualquer pessoa que a consulte reconheça os direitos autorais do autor. Nenhuma informação derivada direta ou indiretamente desta obra deve ser publicada sem o consentimento prévio e por escrito do autor.

Lima Silva, David A.

Distribuição das águas-fonte da Água Profunda do Atlântico Norte e da Água de Fundo Antártica no Oceano Global./ David Antonio de Lima Silva. – Rio Grande: FURG, 2024.

Número de páginas p.

Dissertação (Mestrado) – Universidade Federal do Rio Grande. Mestrado em Oceanologia. Área de Concentração: Física dos Oceanos e Clima.

1. Águas-fonte.
  2. Massas de água.
  3. Análise OMP.
  4. Oceano global.
- I. Distribuição das águas-fonte da Água Profunda do Atlântico Norte e da Água de Fundo Antártica no Oceano Global.



## ATA ESPECIAL DE DEFESA DE DISSERTAÇÃO DE MESTRADO – 05/2024

Às nove horas do dia vinte e quatro de maio do ano dois mil e vinte e quatro, por videoconferência através da sala: <https://conferenciaweb.rnp.br/sala/rodrigo-rodrigo-kerr-duarte-pereira>, reuniu-se a Comissão Examinadora da Dissertação de **MESTRADO** intitulada “**Distribuição das águas-fonte da Água Profunda do Atlântico Norte e da Água de Fundo Antártica no Oceano Global**”, do Acad. **David Antonio de Lima Silva**. A Comissão Examinadora foi composta pelos seguintes membros: Prof. Dr. Rodrigo Kerr Duarte Pereira – Orientador – (FURG), Prof. Dr. Marcos Henrique Maruch Tonelli (IEAPM) e Prof. Dr. Mauricio M. Mata (FURG). Dando início à reunião, a Coordenadora do PPGO, Profa. Dra. Grasiela L. L. Pinho, agradeceu a presença de todos e fez a apresentação da Comissão Examinadora. Logo após esclareceu que o candidato teria um tempo de 45 a 60 minutos para explanação do tema, e cada membro da Comissão Examinadora, um tempo máximo de 30 minutos para perguntas. A seguir, passou à palavra ao candidato, que apresentou o tema e respondeu às perguntas formuladas pela banca. Após ampla explanação, a Comissão Examinadora reuniu-se em reservado para discussão do conceito a ser atribuído ao candidato. Foi estabelecido que as sugestões de todos os membros da Comissão Examinadora, que seguem em pareceres em anexo, foram aceitas pelo Orientador/Candidato para incorporação na versão final da Dissertação. Finalmente, a Comissão Examinadora considerou o candidato **aprovado**, por unanimidade. Nada mais havendo a tratar, foi lavrada a presente ATA, pela Coordenadora do PPGO, que após lida e aprovada, será assinada pela Comissão Examinadora, pelo Candidato e pela Coordenação do Programa de Pós-Graduação em Oceanologia.

Documento assinado digitalmente



RODRIGO KERR DUARTE PEREIRA

Data: 26/05/2024 12:37:34-0300

Verifique em <https://validar.iti.gov.br>

Prof. Dr. Rodrigo Kerr Duarte Pereira  
Orientador

Documento assinado digitalmente



MARCOS HENRIQUE MARUCH TONELLI

Data: 28/05/2024 17:49:22-0300

Verifique em <https://validar.iti.gov.br>

Prof. Dr. Mauricio M. Mata

Documento assinado digitalmente



MAURICIO MAGALHAES MATA

Data: 26/05/2024 15:57:44-0300

Verifique em <https://validar.iti.gov.br>

Prof. Dr. Marcos Henrique M. Tonelli

Documento assinado digitalmente



GRASIELA LOPEZ LEAES PINHO

Data: 24/05/2024 13:31:02-0300

Verifique em <https://validar.iti.gov.br>

Acad. David Antonio de L. Silva

Profª. Drª Grasiela L. L. Pinho  
Coordenadora do PPGO

Documento assinado digitalmente



DAVID ANTONIO DE LIMA SILVA

Data: 26/05/2024 20:35:37-0300

Verifique em <https://validar.iti.gov.br>

# Agradecimentos

Agradeço ao meu orientador, professor Rodrigo Kerr, pela oportunidade dada, por ter me aceitado como orientando, por toda a ajuda fornecida, pela disponibilidade e por toda a orientação durante este período.

À Allana, por todo o amor, pelo companheirismo, por toda a paciência, pelos momentos mais felizes da minha vida e por todo o apoio ao longo desses anos.

Ao Fósforo, pela parceria de anos e por me acompanhar em mais uma importante fase da vida.

À minha família, por todo o apoio e amor ao longo desses anos.

Ao pessoal do Laboratório de Estudos dos Oceanos e Clima e ao CARBON Team, pelas conversas, sugestões e discussões durante o período em que estive na FURG.

Aos membros da banca Mauricio Mata e Marcos Tonelli, por aceitarem o convite e pelas sugestões ao trabalho.

À Coordenação de Aperfeiçoamento de Pessoal de Nível Superior (CAPES), pelo financiamento da bolsa de mestrado. À FURG, ao PPGO e aos professores do PPGO, que contribuíram para minha formação ao longo desta caminhada.

Por fim, agradeço a todas as pessoas que contribuíram de alguma forma para que eu pudesse chegar até aqui.

*“O mar não é um obstáculo, é um caminho”*

Amyr Klink

# Índice

<b>Agradecimentos.....</b>	v
<b>Lista de Figuras.....</b>	viii
<b>Lista de Tabelas.....</b>	xii
<b>Lista de Acrônimos e Abreviações.....</b>	xiii
<b>Resumo.....</b>	xv
<b>Abstract.....</b>	xvi
<b>Capítulo I: Introdução.....</b>	01
<b>1.1. Formação e distribuição das águas-fonte da NADW e AABW.....</b>	06
<b>Capítulo II: Objetivos.....</b>	12
<b>Capítulo III: Dados e Métodos.....</b>	13
<b>3.1. Dados oceanográficos.....</b>	13
<b>3.2. Análise Otimizada com Parâmetros Múltiplos.....</b>	14
<b>3.3. Definição das águas-fonte.....</b>	17
<b>3.3.1. Cálculo dos índices das águas-fonte.....</b>	19
<b>3.3.2. Teste de sensibilidade.....</b>	20
<b>Capítulo IV: Artigo Científico.....</b>	22
<b>4.1. Introduction.....</b>	23
<b>4.2. Formation and distribution context: source water masses of             NADW and AABW.....</b>	26
<b>4.3. Data and Methods.....</b>	29

<i>4.3.1. Databases compiled and used in this study.....</i>	29
<i>4.3.2. Optimum Multiparameter analysis.....</i>	31
<i>4.3.3. Source waters type definition.....</i>	34
<i>4.3.4. Calculation of source waters type indices.....</i>	35
<i>4.3.5. Sensitivity test.....</i>	36
<b>4.4. Results.....</b>	37
<i>4.4.1. Water mass distributions in the Atlantic basin.....</i>	37
<i>4.4.2. Water mass distributions in the Indian basin.....</i>	45
<i>4.4.3. Water mass distributions in the Pacific basin.....</i>	49
<b>4.5. Discussion.....</b>	52
<i>4.5.1. Water mass distributions in the Atlantic basin.....</i>	52
<i>4.5.2. Water mass distributions in the Indian basin.....</i>	56
<i>4.5.3. Water mass distributions in the Pacific basin.....</i>	58
<b>4.6. Conclusions.....</b>	60
<b>Capítulo V: Síntese da Discussão e Conclusões.....</b>	64
<b>Capítulo VI: Referências Bibliográficas.....</b>	67

# Listas de Figuras da Dissertação

**Figura 1.** Esquema simplificado da Circulação de Revolvimento Meridional Global (MOC). As águas superficiais aquecidas são representadas pela seta roxa. As setas vermelhas representam as águas intermediárias. As águas profundas do Atlântico Norte são representadas pela seta verde que se espalham para sul no Atlântico e são transportadas pela Corrente Circumpolar Antártica (ACC) para outras bacias oceânicas. A seta azul representa as águas de fundo formadas no oceano Austral, que fluem para norte e para o entorno do continente Antártico carregas pela Corrente Circumpolar Antártica (ACC), no Atlântico Norte são absorvidas pelas águas-fonte da Água Profunda do Atlântico Norte (NADW). Fluxos do Mediterrâneo são representados pela seta cinza. Figura de [Talley \[2013\]](#).....**2**

**Figura 2.** Distribuição superficial da temperatura conservativa obtida do banco de dados Global Ocean Data Analysis Project (GLODAP) e World Ocean Database 2018 (WOD18). (a) Localização das três áreas de formação das águas-fonte da Água Profunda do Atlântico Norte (NADW) (Mar do Labrador, Mares Nórdicos e Mar Mediterrâneo) no oceano Atlântico Norte. (b) Localização das três áreas de formação das águas-fonte da Água de Fundo Antártica (AABW) (Mar de Weddell, Mar de Ross e Terra de Adelie) no oceano Austral.....**3**

**Figura 3.** Distribuição da Água Profunda do Atlântico Norte (NADW) e da Água de Fundo Antártica (AABW) nas camadas profundas do oceano global, com a barra em cores representando as frações dessas massas de água em um intervalo de 0 a 1. As maiores frações de Água Profunda do Atlântico Norte (NADW) são encontradas na bacia do Atlântico Norte e as maiores frações da Água de Fundo Antártica (AABW) são encontradas no sul das bacias do Atlântico, Índico e Pacífico. Figura de [Johnson \[2008\]](#).....**4**

**Figura 4.** Esquema de formação da Água Profunda do Atlântico Norte (NADW). As setas em vermelho escuro indicam a perda de calor da superfície do oceano para a atmosfera; setas em vermelho claro indicam a convecção profunda das águas superficiais após perder flutuabilidade e aumentar suas densidades. As águas mais densas fluem por camadas mais profundas, compondo a Água Profunda do Atlântico Norte (NADW) inferior, enquanto as águas ventiladas para profundidades menos profundas compõem a Água Profunda do Atlântico Norte (NADW) superior. Figura de [Weijer et al. \[2022\]](#).....**7**

**Figura 5.** Esquema de formação da Água de Fundo Antártica (AABW) por meio do processo de convecção profunda na plataforma. As setas laranjas indicam a perda de calor da superfície do oceano para a atmosfera na polínia costeira; a seta laranja para baixo indica a rejeição de sal e a convecção profunda das águas superficiais após perder flutuabilidade e aumentar suas densidades. A SW e a ISW misturam-se com a Circumpolar Deep Water (CDW) e formam a Água de Fundo Antártica (AABW). Figura de [Silvano et al. \[2023\]](#).....**10**

**Figura 6.** Diagrama TS de dados dos oceanos Atlântico e Antártico obtidos do banco de dados WOD18 e GLODAP, com os pontos pretos definindo as massas

de água profundas usadas na análise: Água do Mar de Labrador (LSW), Água da Islândia-Escócia (ISOW), Água do Estreito da Dinamarca (DSOW), Água Profunda do Mar de Weddell (WSDW), Água de Fundo do Mar de Weddell (WSBW), Água de Fundo da Terra de Adelie (ADLBW) e Água de Fundo do Mar de Ross (RSBW). As cores representam a densidade neutra ( $\sigma_n$ , kg m<sup>-3</sup>).....20

## Listas de Figuras do Artigo

**Figure 1.** Surface distribution of conservative temperature from the compiled data of GLODAP and WOD18 databases. (a) Location of the three formation areas of the North Atlantic Deep Water (NADW) source waters (Labrador Sea, Nordic Seas, and Mediterranean Sea) in the North Atlantic Ocean. (b) Location of the three formation areas of the Antarctic Bottom Water (AABW) source waters (Weddell Sea, Ross Sea, and Adelie Land) in the Southern Ocean.....24

**Figure 2.** (a) Distribution of the hydrographic stations and locations of the three WOCE hydrographic sections (black lines) running through the Atlantic (A16 and A14), the Indian (I09N and I08S) and the Pacific (P16) basins. The black outlined ellipses represent the source areas where parameters were obtained to determine the source waters of North Atlantic Deep Water in the North Atlantic Ocean and Antarctic Bottom Water in the Southern Ocean, in addition to three more intermediate waters (Antarctic Intermediate Water - AAIW, Red Sea Overflow Water - RSOW, and North Pacific Intermediate Water - NPIW) in the Indian and Pacific basins. The histogram shows the number of stations per year for the global ocean basin. (b) Ocean Basins bathymetric features. The acronyms for bathymetric features in the Atlantic Ocean basin are Irminger Basin (IrB), Reykjanes Ridge (RR), Charlie-Gibbs Fracture Zone (CGFZ), Mid-Atlantic Ridge (MAR), Angola Basin (AB), South Scotia Ridge (SSR), South Sandwich Trench (SSTr), North Weddell Ridge (NWR), and Southwest Indian Ridge (SWIR). The acronyms for bathymetric features in the Indian Ocean basin are Southwest Indian Ridge (SWIR), Mozambique Basin (MoB), Madagascar Ridge (MR), Madagascar Basin (MB), Kerguelen Plateau (KP), and Southeast Indian Ridge (SEIR). The acronyms for bathymetric features in the Pacific Ocean basin are Campbell Plateau (CP), Pacific Antarctic Ridge (PAR), East Pacific Rise (EPR), and Chile Ridge (CR).....30

**Figure 3.**  $\Theta$ - $S_A$  diagram ( $^{\circ}\text{C}$ -g kg<sup>-1</sup>) of Atlantic and Southern Oceans data obtained from the GLODAP and WOD18 database, with the black dots defining each source waters type used in the analysis: Labrador Sea Water (LSW), Iceland-Scotland Overflow Water (ISOW), Denmark Strait Overflow Water (DSOW), Weddell Sea Deep Water (WSDW), Weddell Sea Bottom Water (WSBW), Adelie Land Bottom Water (ADLBW), and Ross Sea Bottom Water (RSBW). The colorbar represent the neutral density ( $\sigma_n$ ; kg m<sup>-3</sup>).....36

**Figure 4.** Distribution and contribution (%) of North Atlantic Deep Water (NADW) source waters in the Atlantic basin. Labrador Sea Water (LSW) at (a) 2200 m, (b) 2400 m and (c) 2800 m. Iceland-Scotland Overflow Water (ISOW) at (d) 2700 m and (e) 3200 m. Denmark Strait Overflow Water (DSOW) at (f) 3800 m.....39

**Figure 5.** Distribution and contribution (%) of North Atlantic Deep Water (NADW) source waters in the Atlantic basin along the WOCE A16 section (Fig. 2a). The names of the source waters type (SWT) are on the bathymetry: (a) Labrador Sea Water (LSW), (b) Iceland-Scotland Overflow Water (ISOW), (c) Denmark Strait Overflow Water (DSOW), and (d) Mediterranean Water (MW). The acronyms of the bathymetric features are the North Weddell Ridge (NWR) and Mid-Atlantic Ridge (MAR).....40

**Figure 6.** Distribution and contribution (%) of Iceland-Scotland Overflow Water (ISOW) in the Atlantic basin along the WOCE A14 section (Fig. 2a).....41

**Figure 7.** Distribution and contribution (%) of North Atlantic Deep Water (NADW) source water in the Atlantic basin. Mediterranean Water (MW) at (a) 1500 m and (b) 1900 m.....43

**Figure 8.** Distribution and contribution (%) of Antarctic Bottom Water (AABW) source waters in the Atlantic basin. Weddell Sea Deep Water (WSDW) at (a) 4000 m and (b) 4200 m. Weddell Sea Bottom Water (WSBW) at (c) 4000 m and (d) 4600 m.....44

**Figure 9.** Distribution and contribution (%) of Antarctic Bottom Water (AABW) source waters in the Atlantic basin along the WOCE A16 section (Fig. 2a). The names of the source waters type (SWT) are on the bathymetry: (a) Weddell Sea Deep Water (WSDW), and (b) Weddell Sea Bottom Water (WSBW). The acronyms of the bathymetric features are the North Weddell Ridge (NWR) and Mid-Atlantic Ridge (MAR).....45

**Figure 10.** Distribution and contribution (%) of North Atlantic Deep Water (NADW) source waters in the Indian basin. Labrador Sea Water (LSW) at (a) 2200 m. Iceland-Scotland Overflow Water (ISOW) at (b) 3200 m and (c) 4000 m.....46

**Figure 11.** Distribution and contribution (%) of Antarctic Bottom Water (AABW) source waters in the Indian basin. Weddell Sea Deep Water (WSDW) (a) at 3200 m and (b) 4000 m. Weddell Sea Bottom Water (WSBW) (c) at 4000 m and (d) 4300 m. Adelie Land Bottom Water (ADLBW) (e) at 2400 and (f) 3000 m.....47

**Figure 12.** Distribution and contribution (%) of North Atlantic Deep Water (NADW) and Antarctic Bottom Water (AABW) source waters in the Indian basin along the WOCE I09N and I08S sections (Fig. 2a). The names of the source waters type (SWT) are on the bathymetry: (a) Labrador Sea Water (LSW), (b) Iceland-Scotland Overflow Water (ISOW), (c) Weddell Sea Deep Water (WSDW), (d) Weddell Sea Bottom Water (WSBW), and (e) Adelie Land Bottom Water (ADLBW). The acronym of the bathymetric feature is the Southeast Indian Ridge (SEIR).....48

**Figure 13.** Distribution and contribution (%) of North Atlantic Deep Water (NADW) and Antarctic Bottom Water (AABW) source waters in the Indian basin. Labrador Sea Water (LSW) (a) at 2200 m and, Iceland-Scotland Overflow Water (ISOW) (b) at 3200 m. Weddell Sea Deep Water (WSDW) at (c) 4000 m, Adelie

Land Bottom Water (ADLBW) (d) at 3500 m and, Ross Sea Bottom Water (RSBW) (e) at 4000.....	<b>50</b>
--	-----------

<b>Figure 14.</b> Distribution and contribution (%) of North Atlantic Deep Water (NADW) and Antarctic Bottom Water (AABW) source waters in the Pacific basin along the WOCE P16 section ( <a href="#">Fig. 2a</a> ). The names of the source waters type (SWT) are on the bathymetry: (a) Labrador Sea Water (LSW), (b) Iceland Scotland Overflow Water (ISOW), (c) Weddell Sea Deep Water (WSDW), (d) Adelie Land Bottom Water (ADLBW), and (e) Ross Sea Bottom Water (RSBW).....	<b>51</b>
--	-----------

# **Lista de Tabelas da Dissertação**

**Tabela 1.** Índices das águas-fonte (SWT) com os respectivos desvios padrão considerados no estudo. Os pesos e a Razão de Redfield para cada parâmetro utilizado na análise Otimizada com Parâmetros Múltiplos (OMP) também são fornecidos. As siglas das massas de água correspondem à a Água do Mar de Labrador (LSW), Água do Estreito da Dinamarca (DSOW), Água da Islândia-Escócia (ISOW), Água do Mediterrâneo (MW), Água Profunda do Mar de Weddell (WSDW), Água de Fundo do Mar de Weddell (WSBW), Água de Fundo da Terra de Adelie (ADLBW), Água de Fundo do Mar de Ross (RSBW), Água Intermediária da Antártica (AAIW), Água do Mar Vermelho (RSOW) e Água Intermediária do Pacífico Norte (NPIW).....**17**

**Tabela 2.** Bacias oceânicas com as respectivas massas de água e parâmetros utilizados em cada uma das aplicações da análise Otimizada com Parâmetro Múltiplos (OMP). As siglas das massas de água correspondem à a Água do Mar de Labrador (LSW), Água do Estreito da Dinamarca (DSOW), Água da Islândia-Escócia (ISOW), Água do Mediterrâneo (MW), Água Profunda do Mar de Weddell (WSDW), Água de Fundo do Mar de Weddell (WSBW), Água de Fundo da Terra de Adelie (ADLBW), Água de Fundo do Mar de Ross (RSBW), Água Intermediária da Antártica (AAIW), Água do Mar Vermelho (RSOW) e Água Intermediária do Pacífico Norte (NPIW).....**18**

# **Lista de Tabelas do Artigo**

**Table 1.** Source waters type (SWT) indices with the respective standard deviations considered in the study. The weights and Redfield ratio for each oceanic parameter used in the Optimum Multiparameter analysis (OMP) are also given. The acronyms for the water masses correspond to Labrador Sea Water (LSW), Denmark Strait Overflow Water (DSOW), Iceland-Scotland Overflow Water (ISOW), Mediterranean Water (MW), Weddell Sea Deep Water (WSDW), Weddell Sea Bottom Water (WSBW), Adelie Land Bottom Water (ADLBW), Ross Sea Bottom Water (RSBW), Antarctic Intermediate Water (AAIW), Red Sea Overflow Water (RSOW), and North Pacific Intermediate Water (NPIW).....**34**

**Table 2.** Total contributions and average contributions with the respective standard deviations - CT% (mean  $\pm$  std%) of source waters in ocean basins. The acronyms represent the source waters: Labrador Sea Water (LSW), Denmark Strait Overflow Water (DSOW), Iceland-Scotland Overflow Water (ISOW), Mediterranean Water (MW), Weddell Sea Deep Water (WSDW), Weddell Sea Bottom Water (WSBW), Adelie Land Bottom Water (ADLBW)and, Ross Sea Bottom Water (RSBW).....**38**

# Listas de Acrônimos e Abreviações

## A

**AABW** – Água de Fundo Antártica  
(*Antarctic Bottom Water*)

**AAIW** – Água Intermediária da Antártica (*Antarctic Intermediate Water*)

**ADLBW** – Água de Fundo da Terra de Adelie (*Adélie Land Bottom Water*)

**ACC** – Corrente Circumpolar Antártica (*Antarctic Circumpolar Current*)

## C

**CDW** – Água Profunda Circumpolar (*Circumpolar Deep Water*)

**CGFZ** – Zona de Fratura Charlie-Gibbs (*Charlie-Gibbs Fracture Zone*)

**CP** – Platô Campbell (*Campbell Plateau*)

**CR** – Cordilheira do Chile (*Chile Ridge*)

## D

**DSOW** – Água do Estreito da Dinamarca (*Denmark Strait Overflow Water*)

**DWBC** – Corrente Profunda de Contorno Oeste (*Deep Western Boundary Current*)

## E

**EPR** – Elevação do Pacífico Leste (*East Pacific Rise*)

## G

**GLODAP** – Projeto Global de Análise de Dados Oceânicos (*Global Ocean Data Analysis Project*)

**GOAL** – Grupo de Oceanografia de Altas Latitudes

## I

**IrB** – Bacia Irminger (*Irminger Basin*)

**ISOW** – Água da Islândia-Escócia (*Iceland-Scotland Overflow Water*)

## K

**KP** – Platô de Kerguelen (*Kerguelen Plateau*)

## L

**LSW** – Água do Mar de Labrador (*Labrador Sea Water*)

## M

**MAR** – Dorsal Meso-Atlântica (*Mid-Atlantic Ridge*)

**MB** – Bacia de Madagascar (*Madagascar Basin*)

**MoB** – Bacia de Moçambique  
(*Mozambique Basin*)

**MOC** – Célula de Revolvimento Meridional (*Meridional Overturning Circulation*)

**MR** – Elevação de Madagascar  
(*Madagascar Ridge*)

**MW** – Água do Mediterrâneo  
(*Mediterranean Water*)

## N

**NAC** – Corrente do Atlântico Norte  
(*North Atlantic Current*)

**NADW** - Água Profunda do Atlântico Norte (*North Atlantic Deep Water*)

**NPIW** – Água Intermediária do Pacífico Norte (*North Pacific Intermediate Water*)

**NWR** – Cordilheira do Norte de Weddell (*North Weddell Ridge*)

## O

**OMP** – Análise Otimizada com Parâmetros Múltiplos (*Optimum Multiparameter Analysis*)

## P

**PAR** – Cordilheira Antártica do Pacífico (*Pacific Antarctic Ridge*)

## R

**RR** – Cordilheira de Reykjanes (*Reykjanes Ridge*)

**RSBW** – Água de Fundo do Mar de Ross (*Ross Sea Bottom Water*)

**RSOW** – Água do Mar Vermelho  
(*Red Sea Overflow Water*)

## S

**SEIR** – Cordilheira Sudeste do Índico (*Southeast Indian Ridge*)

**SW** – Águas de Plataforma (*Shelf Water*)

**SWIR** – Cordilheira Sudoeste do Índico (*Southwest Indian Ridge*)

**SWT** – Água-fonte (*Source Water Type*)

**SSR** – Cordilheira da Escócia do Sul (*South Scotia Ridge*)

**SSTr** – Fossa Sandwich do Sul (*South Sandwich Trench*)

## V

**VC** – Canal de Vema (*Vema Channel*)

## W

**WOD** – Banco de Dados do Oceano Mundial (*World Ocean Database*)

**WR** – Cordilheira Walvis (*Walvis Ridge*)

**WSBW** – Água de Fundo do Mar de Weddell (*Weddell Sea Bottom Water*)

**WSDW** – Água Profunda do Mar de Weddell (*Weddell Sea Deep Water*)

# Resumo

Investigamos a distribuição e contribuição das águas-fonte da Água Profunda do Atlântico Norte e da Água de Fundo Antártica com base na porcentagem de mistura destas águas-fonte nas bacias dos oceanos Atlântico, Índico e Pacífico. Neste trabalho, os dados utilizados foram obtidos do World Ocean Database 2018 e do Global Ocean Data Analysis Project, abrangendo um período de 46 anos (1973–2019). Um total de 11 águas-fonte foram selecionadas e utilizadas na análise Otimizada com Parâmetro Múltiplos para obter as distribuições e contribuições percentuais das massas de água no oceano global. As águas-fonte da Água Profunda do Atlântico Norte mostraram um fluxo para o sul principalmente através da bacia oeste do Atlântico Norte, com diminuição em suas contribuições longe de suas áreas de formação, exceto a Água do Mar de Labrador, que apresentou um aumento em sua contribuição entre 30°S e 50°S na bacia do Atlântico. A Água do Mar de Labrador e a Água da Islândia-Escócia são as únicas águas-fonte da Água Profunda do Atlântico Norte exportadas para outras bacias oceânicas, com a Água do Mar de Labrador ocupando toda a extensão das bacias do Índico e do Pacífico, enquanto a Água da Islândia-Escócia está restrita ao sul das bacias destes oceanos onde apresentou baixas contribuições. As águas-fonte da Água de Fundo Antártica apresentaram distribuições próximas de suas áreas de formação, exceto a Água Profunda do Mar de Weddell, que se espalhou por todas as bacias do oceano global, estendendo-se até 50°N na bacia do Atlântico e preenchendo as bacias profundas do Índico e do Pacífico, enquanto as outras águas-fonte da Água de Fundo Antártica estão restritas às bacias do sul do oceano global e à bacia da Antártica. A Água do Mar de Labrador e Água Profunda do Mar de Weddell foram as águas dominantes nas bacias oceânicas, apresentaram maiores contribuições e mostraram caminhos semelhantes de exportação a partir da bacia do Atlântico Sul, espalhando-se de oeste para leste, entrando nas bacias do Índico e do Pacífico, onde fluem para norte, com a Água Profunda do Mar de Weddell espalhando-se principalmente ao longo das bacias ocidentais nas camadas inferiores.

**Palavras-Chave:** Águas-fonte; Massas de água profundas; Análise OMP; Oceano global.

# Abstract

Here, we investigate the distribution and contribution of source water masses of North Atlantic Deep Water (NADW) and Antarctic Bottom Water (AABW) in the Atlantic, Indian, and Pacific basins based on results of the Optimum Multiparameter Analysis. The data used were compiled from World Ocean Database 2018 and Global Ocean Data Analysis Project over a period of 46 years (1973–2019). Eighth source water masses (4 for NADW and 4 for AABW) were selected to map the pathway and quantify the contributions for NADW and AABW in the global ocean. Three additional water masses were used to reduce the mass conservation residuals at the upper edge of NADW. The distribution of NADW source waters showed a southward flow, mainly through the western North Atlantic basin, with a decrease in their contributions away from their areas of formation, except Labrador Sea Water (LSW), which showed an increase in its contribution between 30°S and 50°S in the Atlantic basin. LSW and Iceland-Scotland Overflow Water (ISOW) are the major source water masses of NADW exported to other ocean basins from the South Atlantic, with LSW occupying the entire extent of the Indian and Pacific basins, while ISOW is restricted to the south of the basins of these oceans where it presented relatively low contributions. The source waters of the AABW presented distributions close to their areas of formation, except for the Weddell Sea Deep Water (WSDW), which spread throughout all basins of the global ocean, extending up to 50°N in the Atlantic basin and filling the deep Indian and Pacific basins, while the other source waters of the AABW are restricted to the southern basins of the global ocean and the Antarctic basin. LSW and WSDW were the dominant source waters in the oceanic basins, showing similar export pathways from the South Atlantic basin, spreading to the Indian Ocean basin and subsequently to the Pacific basin from east to west. In these basins, they also spread northward, with WSDW spreading mainly along the western basins in the bottom layers. Finally, this study updated the global distribution (and contributions) of NADW and AABW mapping their source water masses by using the most recent available database and give new insights for discussion about diapycnal upwelling mixing.

**Keywords:** Source waters; Deep water masses; OMP analysis; Global Ocean.

# Capítulo I: Introdução

O oceano global desempenha um papel fundamental na modulação do equilíbrio do clima devido ao transporte de calor das regiões de baixas latitudes para as regiões polares através da Célula de Revolvimento Meridional (MOC, do inglês *Meridional Overturning Circulation*, Fig. 1) [Gordon 1986, Orsi *et al.* 1999, Wunsch 2005, Stocker 2013, Bryden *et al.* 2020]. O ramo inferior da MOC é impulsionado por águas profundas e de fundo que se movem através das bacias profundas do oceano global, transportando CO<sub>2</sub> [Yu *et al.* 2014, Rae *et al.* 2018], nutrientes, sal e minerais, os quais são traçadores de mudanças oceanográficas em diferentes escalas de tempo [Goodman 1988, Williams *et al.* 2019, Mokedemm & McManus 2017, Martínez-Fontaine *et al.* 2019]. Este ramo é amplamente representado pela Água Profunda do Atlântico Norte (NADW, do inglês *North Atlantic Deep Water*) e pela Água de Fundo Antártica (AABW, do inglês *Antarctic Bottom Water*) [Gordon 1986, Broecker & Denton 1989, Elliot *et al.* 2002, Lynch-Stieglitz *et al.* 2007], que são formadas em regiões de altas

latitudes nos hemisférios norte e sul, respectivamente [Foster & Carmack 1976, Mantyla & Reid 1983, Orsi *et al.* 1999, Ferreira & Kerr 2017].

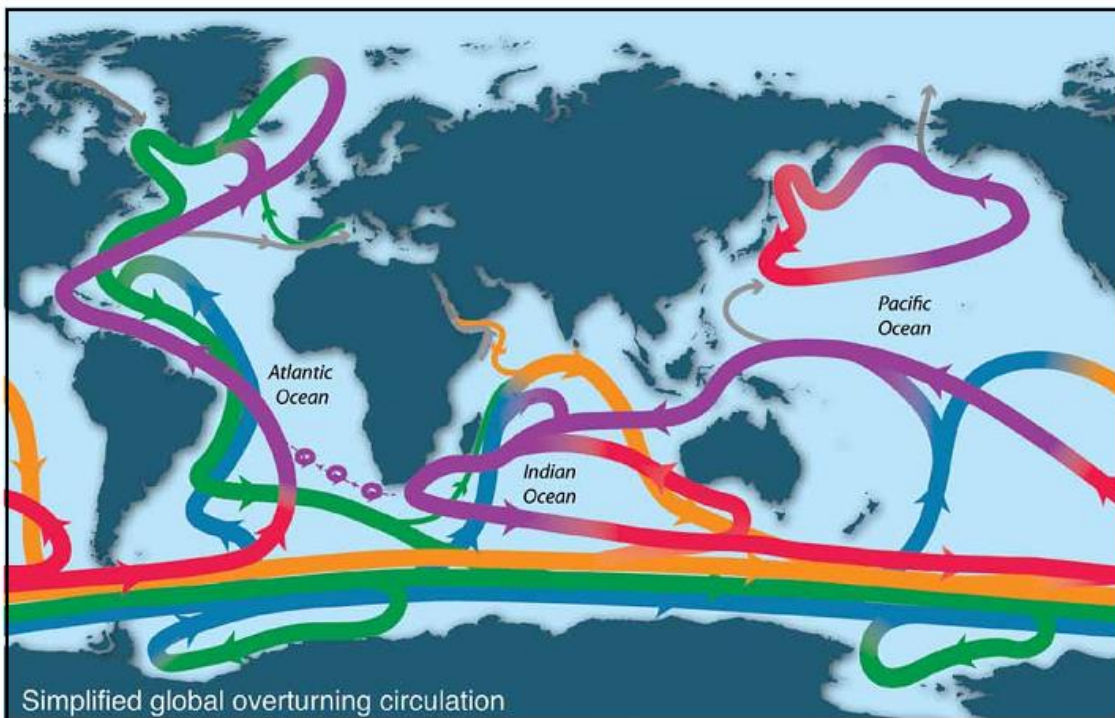


**Figura 1.** Esquema simplificado da Circulação de Revolvimento Meridional Global (MOC). As águas superficiais aquecidas são representadas pela seta roxa. As setas vermelhas representam as águas intermediárias. As águas profundas do Atlântico Norte são representadas pela seta verde que se espalham para sul no Atlântico e são transportadas pela Corrente Circumpolar Antártica (ACC) para outras bacias oceânicas. A seta azul representa as águas de fundo formadas no oceano Austral, que fluem para norte e para o entorno do continente Antártico carregadas pela Corrente Circumpolar Antártica (ACC), no Atlântico Norte são absorvidas pelas águas-fonte da Água Profunda do Atlântico Norte (NADW). Fluxos do Mediterrâneo são representados pela seta cinza. Figura de [Talley \[2013\]](#).

As distintas águas-fonte (SWT, do inglês *Source Water Type*) que formam a Água Profunda do Atlântico Norte (NADW) e a Água de Fundo da Antártica (AABW) possuem características que variam com as regiões de formação e profundidades encontradas [Orsi *et al.* 1999, Ferreira & Kerr 2017]. Essas águas ocupam exclusivamente uma determinada parte do oceano, enquanto em outras regiões compartilham o oceano com outras massas de água com as quais se misturam [Tomczack 1999]. Nos mares de Labrador, da Groenlândia, da Islândia e da Noruega, a intensa perda de calor no inverno leva à convecção profunda e à formação de águas profundas [Yashayaev *et al.* 2007,

Talley *et al.* 2011]. No Mar de Labrador é formada a Água do Mar de Labrador (LSW, do inglês *Labrador Sea Water*) e nos Mares Nórdicos são formadas a Água da Islândia-Escócia (ISOW, do inglês *Iceland-Scotland Overflow Water*) e a Água do Estreito da Dinamarca (DSOW, do inglês *Denmark Strait Overflow Water*), enquanto no Mar Mediterrâneo (Fig. 2a) forma-se uma quarta massa de água chamada Água do Mediterrâneo (MW, do inglês *Mediterranean Water*) e juntas constituem a Água Profunda do Atlântico Norte (NADW) [Reid & Lynn 1971, Dickson & Brown 1994, Talley 2013, García-Ibáñez *et al.* 2015].

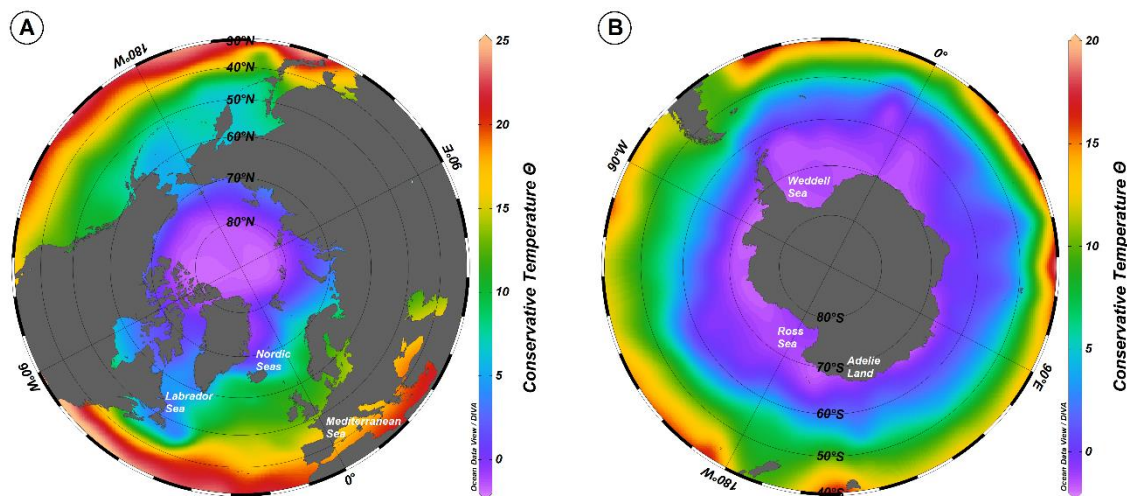


**Figura 2.** Distribuição superficial da temperatura conservativa obtida do banco de dados Global Ocean Data Analysis Project (GLODAP) e World Ocean Database 2018 (WOD18). **(a)** Localização das três áreas de formação das águas-fonte da Água Profunda do Atlântico Norte (NADW) (Mar do Labrador, Mares Nórdicos e Mar Mediterrâneo) no oceano Atlântico Norte. **(b)** Localização das três áreas de formação das águas-fonte da Água de Fundo Antártica (AABW) (Mar de Weddell, Mar de Ross e Terra de Adelie) no oceano Austral.

A Água Profunda do Atlântico Norte (NADW) afunda e ocupa o fundo do mar próximo aos seus locais de formação e se espalha para o sul (Fig. 3) [Johnson 2008]. Esta massa de água comprehende as águas mais densas de algumas regiões do Atlântico Norte, sendo relativamente mais quente, mais salgada e mais leve que a Água de Fundo Antártica (AABW) [Johnson 2008, Reid *et al.* 1977]. No Atlântico Sul, a Água Profunda do Atlântico Norte (NADW) relativamente quente e salgada flui acima da Água de Fundo Antártica (AABW)

até atingir a Corrente Circumpolar Antártica (ACC, do inglês *Antarctic Circumpolar Current*), onde é advectada para leste e propagada para norte nas bacias do Índico e Pacífico (Fig. 3) [Reid *et al.* 1977, Johnson 2008, Talley 2013].

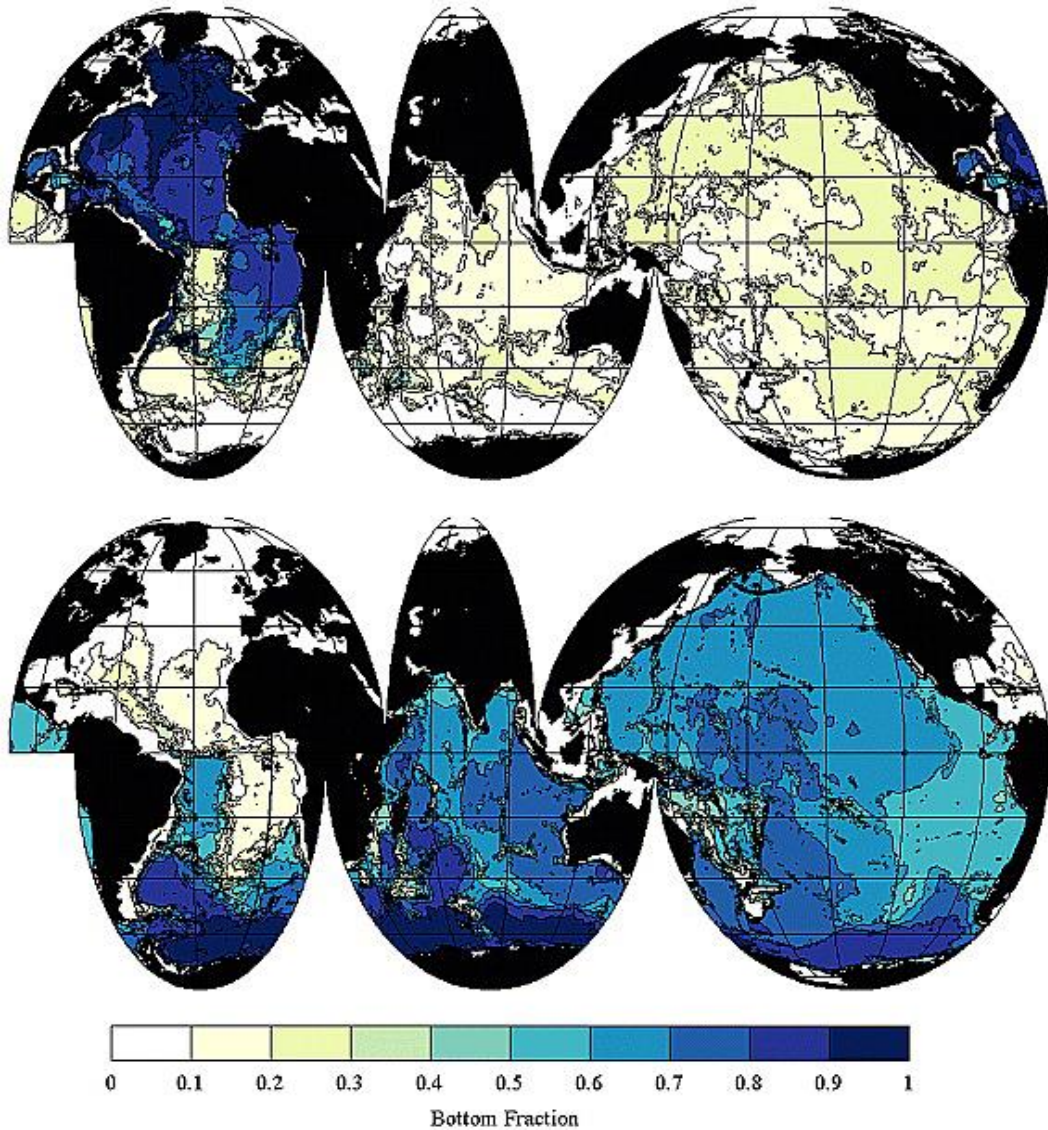


**Figura 3.** Distribuição da Água Profunda do Atlântico Norte (NADW) e da Água de Fundo Antártica (AABW) nas camadas profundas do oceano global, com a barra em cores representando as frações dessas massas de água em um intervalo de 0 a 1. As maiores frações de Água Profunda do Atlântico Norte (NADW) são encontradas na bacia do Atlântico Norte e as maiores frações da Água de Fundo Antártica (AABW) são encontradas no sul das bacias do Atlântico, Índico e Pacífico. Figura de Johnson [2008].

O processo de formação da Água de Fundo Antártica (AABW) é complexo [Gill 1973, Foster & Carmack 1976] e ocorre na margem antártica [Orsi *et al.* 1999, Talley, 2013], mais especificamente no Mar de Weddell [Gill 1973], Mar de Ross [Jacobs *et al.* 1970] e ao largo da Terra de Adélie (Fig. 2b) [Rintoul

1998]. Sua formação envolve resfriamento da superfície devido à perda de calor e aumento da salinidade devido à formação de gelo marinho e rejeição de salmoura, além de mistura com as águas circundantes durante o fluxo descendente [Foster e Carmack 1976].

A Água Profunda do Mar de Weddell (WSDW, do inglês *Weddell Sea Deep Water*), a Água de Fundo do Mar de Weddell (WSBW, do inglês *Weddell Sea Bottom Water*), a Água de Fundo do Mar de Ross (RSBW, do inglês *Ross Sea Bottom Water*) e a Água de Fundo da Terra de Adelie (ADLBW, do inglês *Adélie Land Bottom Water*) formam a Água de Fundo Antártica (AABW) [Warren 1981, Orsi *et al.* 1999], que é uma massa de água mais fria e densa do que a Água Profunda do Atlântico Norte (NADW). A Água de Fundo Antártica (AABW) se espalha para o norte em bacias profundas do oceano global (Fig. 3) e se mistura com águas mais leves sobrejacentes [Johnson 2008, Talley 2013], com exceção do Ártico e parte do Atlântico Norte, onde a Água Profunda do Atlântico Norte (NADW) cobre o fundo do oceano [Mantyla & Reid 1983, Orsi *et al.* 2001].

A distribuição das águas profundas mostra os principais fluxos dentro dos oceanos e destaca as suas rotas de exportação [Ferreira & Kerr 2017, Solodoch *et al.* 2022], que são importantes para a compreensão da circulação na camada inferior do oceano [e.g. Johnson 2008, Pardo *et al.* 2012, Tomczak 1999a], apoiando estudos biogeoquímicos [Skinner *et al.* 2010, Azar *et al.* 2021, Piñango *et al.* 2022] e projeções climáticas [Böning *et al.* 2016, O'Neill *et al.* 2016, Moorman *et al.* 2020, Nissen *et al.* 2022, Li *et al.* 2023]. Estudos anteriores e recentes sobre a distribuição de águas profundas concentram esforços principalmente nas regiões polares [Reid & Lynn 1971, Pardo *et al.* 2012, García-Ibáñez *et al.* 2015, Solodoch *et al.*, 2022]. No entanto, poucos estudos

apresentaram uma abordagem em escala global [e.g. Nakano & Sugino 2002, Johnson 2008]. Aqui a distribuição espacial e a quantificação de cada água-fonte da Água Profunda do Atlântico Norte (NADW) e da Água de Fundo Antártica (AABW) são apresentadas com base em suas porcentagens de mistura ao longo de 46 anos (1973 - 2019) através da análise Otimizada com Parâmetros Múltiplos (OMP, do inglês *Optimum Multiparameter*) [Tomczak 1981, Thompson & Edwards 1981, Mackas *et al.* 1987, Tomczak & Large 1989] no oceano global.

### **1.1. Formação e distribuição das águas-fonte da NADW e AABW**

Regiões polares são os principais locais de formação de massas de água profundas e de fundo [Mantyla & Reid 1983, Orsi *et al.* 1999]. Nessas regiões, as águas superficiais tornam-se densas o suficiente para perder flutuabilidade e afundar em direção as camadas profundas do oceano [Orsi *et al.* 1999]. No Mar de Labrador e nos Mares Nôrdicos, as águas-fonte da Água Profunda do Atlântico Norte (NADW) superior e inferior originam-se a partir de processos associados à interação entre o oceano e a atmosfera, principalmente no inverno, o que leva à convecção profunda e à formação de águas profundas (Fig. 4) [Talley & Mccartney 1982, Johnson 2008]. Por outro lado, mecanismos que envolvem processos de plataforma e a interação entre o oceano e a atmosfera na margem Antártica originam as variedades da Água de Fundo Antártica (AABW) [Orsi *et al.* 1999, Talley 2013], as quais são mais frias e relativamente doces em comparação com as águas que compõem a Água Profunda do Atlântico Norte (NADW) [Johnson 2008].

No mar de Labrador, o resfriamento durante o inverno e a convecção profunda levam à formação da Água do Mar de Labrador (LSW), a qual é a componente mais leve da Água Profunda do Atlântico Norte (NADW) e compõem

o seu ramo superior, predominante em profundidades entre 1500 e 2500 m [Clarke & Gascard 1983, García-Ibáñez *et al.* 2015], com espalhamento para sul via Corrente Profunda de Contorno Oeste (DWBC, do inglês *Deep Western Boundary Current*) e através de caminhos interiores dentro das bacias oceânicas [Stramma *et al.* 2004, Bower *et al.* 2019].

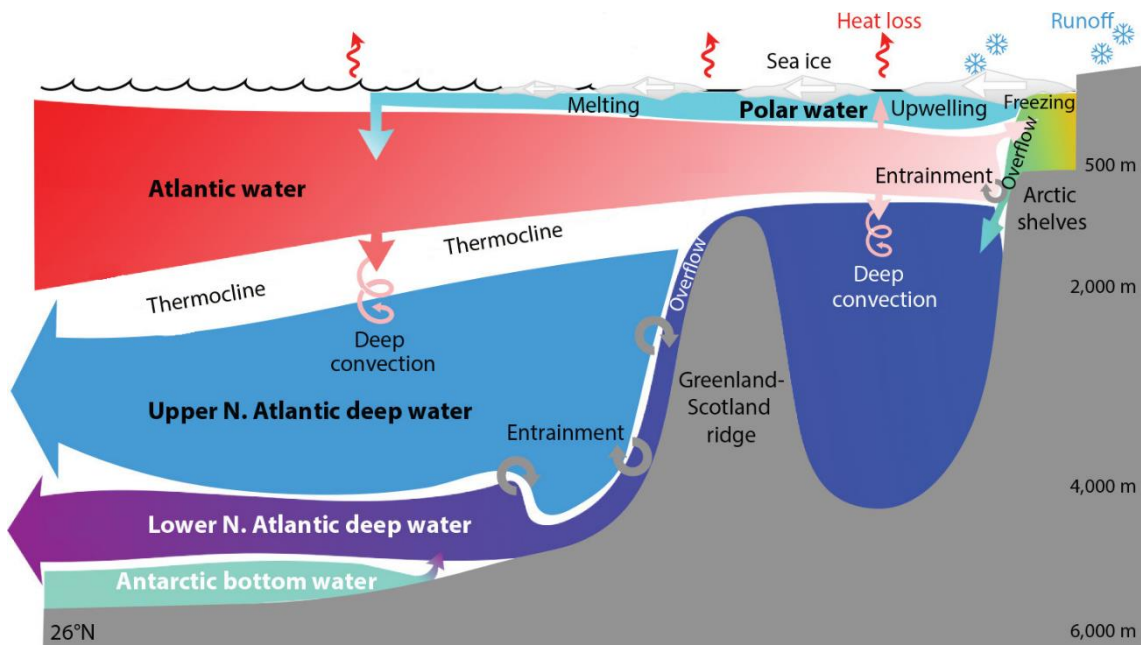


**Figura 4.** Esquema de formação da Água Profunda do Atlântico Norte (NADW). As setas em vermelho escuro indicam a perda de calor da superfície do oceano para a atmosfera; setas em vermelho claro indicam a convecção profunda das águas superficiais após perder flutuabilidade e aumentar suas densidades. As águas mais densas fluem por camadas mais profundas, compondo a Água Profunda do Atlântico Norte (NADW) inferior, enquanto as águas ventiladas para profundidades menos profundas compõem a Água Profunda do Atlântico Norte (NADW) superior. Figura modificada de Weijer *et al.* [2022].

As águas fonte que compõem a Água Profunda do Atlântico Norte (NADW) inferior são formadas quando as águas quentes do Atlântico Norte encontram as densas águas do Ártico [Read 2000, Dickson *et al.* 2002]. Estas águas do Ártico entram no oceano Atlântico através de passagens localizadas no leste da Islândia e através do Estreito da Dinamarca [Fogelqvist *et al.* 2003, Dickson *et al.* 2002], onde se misturam com águas adjacentes e originam a Água da Islândia-Escócia (ISOW) e a Água do Estreito da Dinamarca (DSOW), respectivamente [Yashayaev & Dickson 2008, Fogelqvist *et al.* 2003]. A Água da

Islândia-Escócia (ISOW) espalha-se nas camadas profundas da bacia da Islândia e flui para a Bacia de Irminger através da Zona de Fratura Charlie-Gibbs (CGFZ, do inglês *Charlie-Gibbs Fracture Zone*), onde encontra a Água do Estreito da Dinamarca (DSOW) [Bower & Furey 2017, Lozier *et al.* 2022]. Parte da Água da Islândia-Escócia (ISOW) flui em direção a sul dentro da porção leste da bacia do Atlântico Norte [Garcia-Ibanez *et al.* 2015], sendo reconhecida pela alta salinidade e baixas temperaturas em comparação com outras águas fontes da Água Profunda do Atlântico Norte (NADW) nos mares nórdicos. Dentre as várias componentes da Água Profunda do Atlântico Norte (NADW), a Água do Estreito da Dinamarca (DSOW) é considerada a variedade mais fria e densa, sendo encontrada nas camadas mais profundas das bacias de Irminger e Labrador [LeBel *et al.* 2008, Lozier *et al.* 2022], fluindo em direção a sul dentro da Deep Western Boundary Current (DWBC) com outras componentes da Água Profunda do Atlântico Norte (NADW) [Garcia-Ibanez *et al.* 2015, Lozier *et al.* 2022]. Outros caminhos de exportação no interior das bacias têm sido relatados para a Água do Estreito da Dinamarca (DSOW) [LeBel *et al.* 2008, Lozier *et al.* 2022]. A Água Profunda do Atlântico Norte (NADW) superior também é composta pela Água do Mediterrâneo (MW), a qual é formada no Mar Mediterrâneo e caracterizada pela sua máxima salinidade, o que favorece a sua elevada densidade [Garcia-Ibanez *et al.* 2015, Ferreira & Kerr 2017]. Ao sair do Mar Mediterrâneo através do Estreito de Gibraltar, esta massa de água afunda e ocupa profundidades intermediárias entre 600 e 2000 m no leste do Atlântico Norte [Tsuchiya *et al.* 1992, Álvarez *et al.* 2004, Bozec *et al.* 2011, Ferreira & Kerr 2017] e espalha-se para oeste e norte desta bacia, misturando-se com massas de água circundantes [Lozier *et al.* 1995, Bozec *et al.* 2011]. Estudos

anteriores mostram a distribuição de Água Profunda do Atlântico Norte (NADW) nas bacias do Atlântico, Índico, Pacífico e Oceano Antártico [Johnson 2008, Pardo *et al.* 2012, Talley 2013]. Ferreira e Kerr [2017] observaram contribuições da Água do Mar de Labrador (LSW) dentro da Corrente Circumpolar Antártica (ACC), com Água da Islândia-Escócia (ISOW) e Água do Estreito da Dinamarca (DSOW) estendendo-se até aproximadamente 40°S na bacia do Atlântico em profundidades entre 2000 m e 5000 m. Contribuições da Água Profunda do Atlântico Norte (NADW) foram observadas desde ~45°S até a margem Antártica nas bacias do oceano global [Pardo *et al.* 2012]. Contudo, destaca-se que os estudos sobre a distribuição das variedades da Água Profunda do Atlântico Norte (NADW) no oceano global têm recebido menos atenção devido à dificuldade de rastrear o trajeto de uma única massa de água fonte, uma vez que essas águas estão bem misturadas longe de sua área de formação. Assim, vários trabalhos têm considerado a Água Profunda do Atlântico Norte (NADW) coletivamente [Johnson 2008, Nakano & Sugino 2002], principalmente fora do oceano Atlântico, não sendo possível identificar os níveis de profundidade correspondentes a cada massa de água que a compõe.

A Água Profunda do Mar de Weddell (WSDW), Água de Fundo do Mar de Weddell (WSBW), Água de Fundo do Mar de Ross (RSBW) e a Água de Fundo da Terra de Adelie (ADLBW) resultam da mistura das águas relativamente quentes e salgadas da Corrente Circumpolar Antártica (ACC) (e.g. CDW, do inglês *Circumpolar Deep Water*), Águas de Plataforma (SW, do inglês *Shelf Water*) frias e salgadas e/ou Águas de Plataforma de Gelo (ISW, do inglês *Ice Shelf Water*) no Mar de Weddell, Mar de Ross e Terra de Adelie, respectivamente [Jacobs *et al.* 1970, Foster & Carmack 1976, Foldvik *et al.* 1985, Rintoul 1998,

Purkey *et al.* 2018]. As polínias costeiras antárticas formadas pela ação de ventos catabáticos do continente, resultam na rejeição do sal e no aumento da salinidade superficial, contribuindo para a produção de AABW (Fig. 5) [Fahrbach *et al.* 1994, Arrigo & Van Dijken 2003].

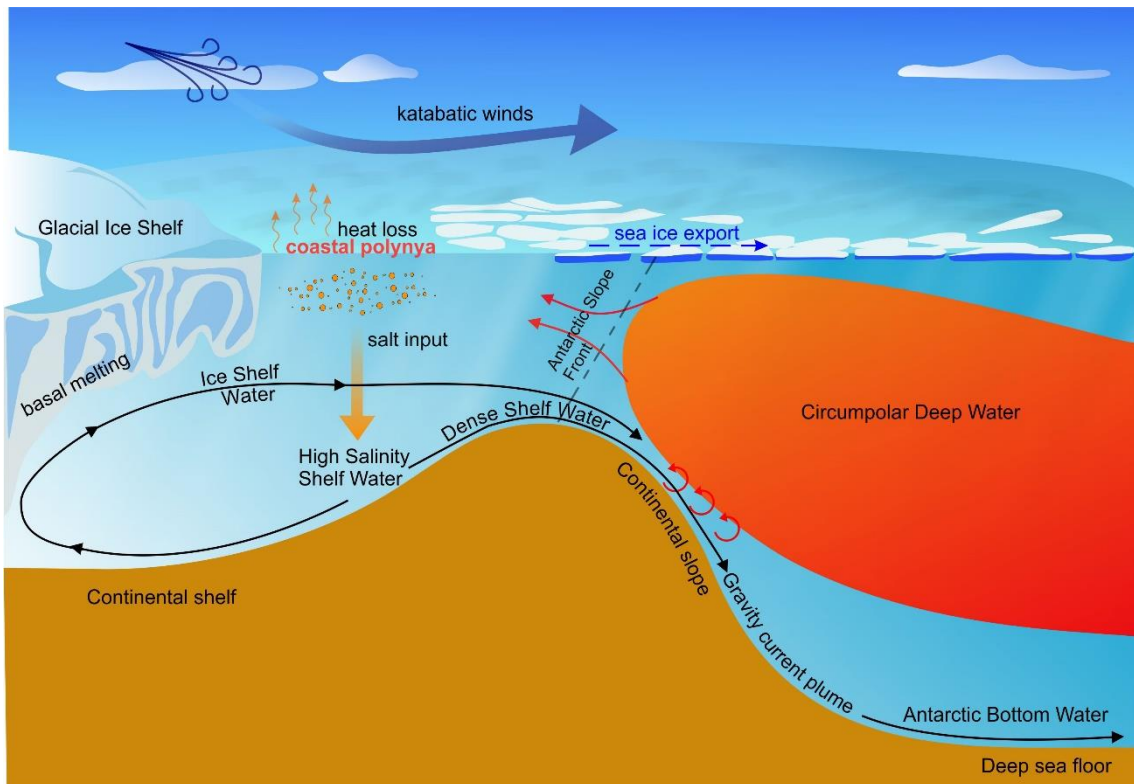


**Figura 5.** Esquema de formação da Água de Fundo Antártica (AABW) por meio do processo de convecção profunda na plataforma. As setas laranjas indicam a perda de calor da superfície do oceano para a atmosfera na polínia costeira; a seta laranja para baixo indica a rejeição de sal e a convecção profunda das águas superficiais após perder flutuabilidade e aumentar suas densidades. A SW e a ISW misturam-se com a Circumpolar Deep Water (CDW) e formam a Água de Fundo Antártica (AABW). Figura de [Silvano et al. \[2023\]](#).

A Água Profunda do Mar de Weddell (WSDW) é a componente menos densa e mais quente da Água de Fundo Antártica (AABW) e é exportada para o norte, no oceano Atlântico, através de canais profundos na Cordilheira da Escócia do Sul (SSR, do inglês *South Scotia Ridge*) e na Fossa Sandwich do Sul (SSTr, do inglês *South Sandwich Trench*) [Meredith *et al.* 2013]. Parte da Água Profunda do Mar de Weddell (WSDW) também é exportada para leste através da Corrente Circumpolar Antártica (ACC) [Orsi *et al.* 1999], espalhando-se pelas bacias do Atlântico, Índico, Pacífico e oceano Antártico, enquanto a densa Água

de Fundo do Mar de Weddell (WSBW), a componente mais fria e doce da Água de Fundo Antártica (AABW), é exportada através de caminhos similares ao da Água Profunda do Mar de Weddell (WSDW) (*e.g. South Sandwich Trench*), mas está restrito a profundidades abissais em latitudes superiores a 50°S devido à sua alta densidade [Pardo *et al.* 2012, Ferreira & Kerr 2017]. A Água de Fundo do Mar de Weddell (WSBW) estende-se aproximadamente até a Terra de Adelie, enquanto a Água de Fundo da Terra de Adelie (ADLBW) e a Água de Fundo do Mar de Ross (RSBW) são encontradas acima de 60°S na Terra de Adelie e áreas adjacentes ao Mar de Ross, com a Água de Fundo do Mar de Ross (RSBW) estendendo-se até perto da Passagem de Drake [Pardo *et al.* 2012]. Aqui, a Água de Fundo do Mar de Ross (RSBW) e a Água de Fundo da Terra de Adelie (ADLBW) estão restritas à bacia Antártica e são mais quentes e salgadas que a Água de Fundo do Mar de Weddell (WSBW). A Água de Fundo do Mar de Ross (RSBW) é a variedade mais quente e salgada da Água de Fundo Antártica (AABW), enquanto a Água de Fundo da Terra de Adelie (ADLBW) está entre a Água de Fundo do Mar de Weddell (WSBW) e a Água de Fundo do Mar de Ross (RSBW).

# **Capítulo II: Objetivos**

## **2.1. Objetivo geral**

- O objetivo geral deste estudo é determinar a distribuição espacial das massas de águas-fonte da NADW e da AABW no oceano global.

## **2.2. Objetivos específicos**

- Quantificar a contribuição das massas de águas-fonte da NADW e da AABW no oceano global a partir do percentual de mistura;
- Apontar as possíveis causas que influenciam a distribuição das massas de águas-fonte da NADW e da AABW no oceano global.

# Capítulo III: Dados e Métodos

## 3.1. Dados oceanográficos

Neste estudo, foi utilizado um conjunto de dados históricos disponível no *World Ocean Database* (WOD) 2018, [www.ncei.noaa.gov/products/world-ocean-database](http://www.ncei.noaa.gov/products/world-ocean-database)) e no *Global Ocean Data Analysis Project 2020* (GLODAP, [www.glodap.info/](http://www.glodap.info/)), que abrange 46 anos (1973 - 2019). Este conjunto de dados inclui os seguintes parâmetros: temperatura conservativa ( $\Theta$ ), salinidade absoluta ( $S_A$ ), oxigênio dissolvido ( $O_2$ ), fosfato ( $PO_4^{3-}$ ), nitrato ( $NO_3^-$ ), silicato ( $SiOH_4^{4-}$ ) e vorticidade potencial (PV). Para restringir a análise às massas de água profundas no oceano global, foram selecionados apenas dados encontrados em profundidades superiores a 1500 m. O conjunto de dados foi separado por bacias oceânicas e a análise da distribuição das águas profundas foi realizada separadamente para cada bacia (bacias do Atlântico, Índico e Pacífico). O conjunto de dados utilizado neste trabalho passou por um processo de controle de qualidade antes de ser disponibilizado, no qual foram

aplicados ajustes para remover vieses significativos, respeitando a ocorrência de quaisquer tendências ou variações temporais conhecidas ou prováveis [Boyer *et al.* 2018; Olsen *et al.* 2016]. Os dados identificados como espúrios foram removidos.

### **3.2. Análise Otimizada com Parâmetros Múltiplos (OMP)**

Para obter a distribuição e a quantificação das massas de água foi utilizada a análise Otimizada com Parâmetros Múltiplos (OMP), inicialmente proposta por Tomczak [1981] e implementada por Tomczak e Large [1989] como uma extensão da análise clássica de mistura entre massas de água, anteriormente realizada através do diagrama TS [Mamayev 1975]. Neste método, parâmetros conservativos e não conservativos são utilizados para traçar as massas de água, calculando as contribuições de cada uma delas através de equações de mistura linear [Tomczak & Large 1989]. Neste contexto, o método Otimizado com Parâmetros Múltiplos (OMP) determina a contribuição percentual de cada água-fonte previamente definida [Tomczak & Large 1989]. A água-fonte representa os valores dos parâmetros de uma massa de água original não misturada, ou seja, corresponde a água com características típicas das propriedades da região onde se originou [Poole & Tomczak 1999]. Desta forma, além de determinar a contribuição entre todas as águas-fonte selecionadas, o método Otimizado com Parâmetros Múltiplos (OMP) permite analisar a distribuição espacial das massas de água [Tomczak & Large 1989]. Posteriormente, a circulação oceânica pode ser deduzida através da distribuição das massas de água [e.g. Johnson 2008]. Porém, o método apresenta duas restrições: (i) a contribuição de todas as águas-fonte deve ser igual a 100% para garantir a conservação da massa; e (ii) esta contribuição não deve ser negativa [Tomczak *et al.* 1989]. Neste estudo, sete

parâmetros foram utilizados na análise Otimizada com Parâmetros Múltiplos (OMP) (Tab. 1).

Este método pode ser utilizado na sua forma básica ou estendida dependendo, principalmente, da escala espacial da análise e da disponibilidade de traçadores de massas de água [Karstensen & Tomczak 1999]. Neste estudo foi aplicado o método Otimizado com Parâmetros Múltiplos (OMP) estendido, pois o objetivo é analisar a distribuição de águas profundas em larga escala. A forma estendida considera que parâmetros não conservativos apresentam alterações em suas concentrações devido a processos biogeoquímicos, como remineralização e respiração à medida que as massas de água evoluem [Karstensen & Tomczak 1999]. Por esse motivo, a Razão de Redfield é incorporada às equações como fator de correção dessas modificações [Anderson & Sarmiento 1994, Karstensen & Tomczak 1999]. O sistema linear de equações de mistura da análise Otimizada com Parâmetros Múltiplos (OMP) é então mostrado na equação 1 abaixo:

$$\begin{aligned}
 x_1T_1 + x_2T_2 + x_3T_3 + x_4T_4 + x_5T_5 + x_6T_6 + x_7T_7 &+ 0 = T_{\text{obs}} + R_T \\
 x_1S_1 + x_2S_2 + x_3S_3 + x_4S_4 + x_5S_5 + x_6S_6 + x_7S_7 &+ 0 = S_{\text{obs}} + R_S \\
 x_1O_{2,1} + x_2O_{2,2} + x_3O_{2,3} + x_4O_{2,4} + x_5O_{2,5} + x_6O_{2,6} + x_7O_{2,7} &- r_{O/P}\Delta P = O_{2,\text{obs}} + R_{O2} \\
 x_1PO_{4,1} + x_2PO_{4,2} + x_3PO_{4,3} + x_4PO_{4,4} + x_5PO_{4,5} + x_6PO_{4,6} + x_7PO_{4,7} &+ \Delta P = PO_{4,\text{obs}} + R_{PO4} \\
 x_1NO_{3,1} + x_2NO_{3,2} + x_3NO_{3,3} + x_4NO_{3,4} + x_5NO_{3,5} + x_6NO_{3,6} + x_7NO_{3,7} &+ r_{N/P}\Delta P = NO_{3,\text{obs}} + R_{NO3} \\
 x_1SiO_{3,1} + x_2SiO_{3,2} + x_3SiO_{3,3} + x_4SiO_{3,4} + x_5SiO_{3,5} + x_6SiO_{3,6} + x_7SiO_{3,7} &+ r_{N/P}\Delta P = SiO_{3,\text{obs}} + R_{SiO3} \\
 x_1PV_1 + x_2PV_2 + x_3PV_3 + x_4PV_4 + x_5PV_5 + x_6PV_6 + x_7PV_7 &+ 0 = PV_{\text{obs}} + R_{PV} \\
 x_1 + x_2 + x_3 + x_4 + x_5 + x_6 + x_7 &+ 0 = 1 + R_{\Sigma}
 \end{aligned} \tag{1}$$

Os valores observados de  $T_{\text{obs}}$ ,  $S_{\text{obs}}$ ,  $O_{\text{obs}}$ ,  $P_{\text{obs}}$ ,  $N_{\text{obs}}$ ,  $Si_{\text{obs}}$ ,  $PV_{\text{obs}}$ , and  $R$  representam os valores dos parâmetros temperatura, salinidade, oxigênio, fosfato, nitrato, silicato, vorticidade potencial e o resíduo de cada parâmetro,

respectivamente;  $r\Delta P$  representa a razão de Redfield;  $T_j$ ,  $S_j$ ,  $O_j$ ,  $P_j$ ,  $N_j$ ,  $S_{ij}$  e  $PV_j$  com  $j$  variando de 1 a 7, representam os valores dos parâmetros de cada água-fonte;  $x_j$  representa as contribuições de cada água-fonte (incógnitas) e a última equação representa a condição de conservação da massa [Anderson & Sarmiento 1994, Karstensen & Tomczak 1999]. O sistema de equações acima pode ser escrito em notação matricial conforme mostrado abaixo na equação 2:

$$G x - d = R \quad (2)$$

onde  $G$  representa a matriz com os valores das propriedades de cada água-fonte,  $x$  é um vetor das contribuições calculadas para cada água-fonte,  $d$  é um vetor dos dados observados e  $R$  é o valor residual [Tomczak & Large 1989].

Na análise Otimizada com Parâmetros Múltiplos (OMP), os parâmetros muitas vezes não apresentam a mesma representação, devido à influência da variabilidade ambiental e da precisão analítica e instrumental das medições [Ferreira & Kerr 2017]. Portanto, foi aplicada uma versão ponderada da matriz  $G$ , incluindo uma matriz  $W$ , que possui respectivos pesos para cada parâmetro (Eq. 3), conforme método descrito por Tomczak e Large [1989].

$$W_j = \sigma_j^2 / \delta_{j \max} \quad (3)$$

onde  $W$  representa os pesos,  $\sigma_j^2$  é a variância para cada parâmetro das águas-fonte e  $\delta_{j \max}$  é a variância máxima do parâmetro entre todas as fontes de água [Tomczak & Large 1989]. Cada parâmetro recebe seu próprio peso, indicando que cada propriedade pode influenciar de forma diferente no cálculo da mistura. Os índices das águas-fonte estão resumidos na tabela 1.

**Tabela 1.** Índices das águas-fonte (SWT) com os respectivos desvios padrão considerados no estudo. Os pesos e a Razão de Redfield para cada parâmetro utilizado na análise Otimizada com Parâmetros Múltiplos (OMP) também são fornecidos. As siglas das massas de água correspondem à a Água do Mar de Labrador (LSW), Água do Estreito da Dinamarca (DSOW), Água da Islândia-Escócia (ISOW), Água do Mediterrâneo (MW), Água Profunda do Mar de Weddell (WSDW), Água de Fundo do Mar de Weddell (WSBW), Água de Fundo da Terra de Adelie (ADLBW), Água de Fundo do Mar de Ross (RSBW), Água Intermediária da Antártica (AAIW), Água do Mar Vermelho (RSOW) e Água Intermediária do Pacífico Norte (NPIW).

SWT	$\Theta$ (°C)	$S_A$ (g kg <sup>-1</sup> )	DO μmol/kg	PO <sub>4</sub> μmol/kg	NO <sub>3</sub> μmol/kg	SiOH <sub>4</sub> μmol/kg	PV 10 <sup>8</sup> ms <sup>-1</sup>
LSW	3.072 ± 0.182	35.055 ± 0.015	284 ± 9.0	1.08 ± 0.003	16.2 ± 0.05	10 ± 0.05	0.0116 ± 0.002
DSOW	1.494 ± 0.200	35.054 ± 0.002	299 ± 2.0	0.94 ± 0.010	14.0 ± 0.25	8 ± 0.23	0.0675 ± 0.006
ISOW	2.822 ± 0.112	35.136 ± 0.006	274 ± 0.4	1.08 ± 0.001	16.2 ± 0.08	13 ± 0.56	0.0329 ± 0.002
MW	9.936 ± 0.119	36.125 ± 0.033	186 ± 0.4	1.00 ± 0.009	16.6 ± 0.06	9 ± 0.12	0.0664 ± 0.002
WSDW	0.000 ± 0.050	34.823 ± 0.018	223 ± 5.0	2.25 ± 0.050	32.8 ± 0.40	114 ± 8.0	-0.0095 ± 0.005
WSBW	-1.000 ± 0.119	34.810 ± 0.013	257 ± 8.0	2.22 ± 0.040	32.2 ± 0.40	112 ± 4.0	-0.0078 ± 0.006
ADLBW	-0.470 ± 0.055	34.835 ± 0.008	239 ± 3.0	2.22 ± 0.005	31.9 ± 0.01	109 ± 0.04	-0.0076 ± 0.001
RSBW	-0.250 ± 0.006	34.863 ± 0.003	229 ± 2.0	2.24 ± 0.007	31.5 ± 0.18	99 ± 0.54	-0.0109 ± 0.0002
AAIW	3.403 ± 0.214	34.429 ± 0.013	222 ± 4.0	2.15 ± 0.007	30.81 ± 0.02	34 ± 0.83	-0.0797 ± 0.003
RSOW	11.168 ± 0.862	35.754 ± 0.169	15 ± 8.0	2.59 ± 0.006	31.59 ± 1.99	49 ± 2.61	0.0376 ± 0.010
NPIW	3.803 ± 0.198	34.344 ± 0.090	54 ± 12	2.89 ± 0.070	40.47 ± 1.13	108 ± 9.0	0.0909 ± 0.013
Weights	7.9395	7.9395	6.0938	1.3421	5.7383	1.1201	0.0574
Redfield Ratio	n/a	n/a	-170	1	16	40	n/a

### 3.3. Definição das águas-fonte

O número de massas de água utilizadas na análise Otimizada com Parâmetros Múltiplos (OMP) depende do número de parâmetros disponíveis [Tomzack & Large 1989]. Aqui, foram utilizadas as seguintes massas de água para a análise: Água do Mar de Labrador (LSW), Água do Estreito da Dinamarca (DSOW), Água da Islândia-Escócia (ISOW) e Água do Mediterrâneo (MW), definidas como águas-fonte da Água Profunda do Atlântico Norte (NADW) [Dickson & Brown 1994, Johnson 2008, Garcia-Ibanez *et al.* 2015, Ferreira & Kerr 2017]; Água Profunda do Mar de Weddell (WSDW), Água de Fundo do Mar de Weddell (WSBW), Água de Fundo da Terra de Adelie (ADLBW) e Água de Fundo do Mar de Ross (RSBW), definidas como águas-fonte da Água de Fundo Antártica (AABW) [Orsi *et al.* 1999, Johnson 2008, Pardo *et al.* 2012, Ferreira & Kerr 2017]; e a água intermediária da Antártica (AAIW, do inglês *Antarctic Intermediate Water*), a água intermediária do Mar Vermelho (RSOW, do inglês

*Red Sea Overflow Water)* e a água intermediária do Pacífico Norte (NPIW, do inglês *North Pacific Intermediate Water*), adicionadas à análise para reduzir possíveis erros de mistura com a Água do Mar de Labrador (LSW) [Johnson 2008], totalizando onze massas de água. Além disso, foram utilizados sete parâmetros, a temperatura conservativa ( $\Theta$ ), salinidade absoluta ( $S_A$ ), oxigênio dissolvido (DO), fosfato ( $PO_4^{3-}$ ), nitrato ( $NO_3^-$ ), silicato ( $SiOH_4^{4-}$ ) e vorticidade potencial (PV), o que limita a análise em até sete massas de água. Para resolver o problema entre a limitação das massas de água pelo número de parâmetros, as rodadas da análise Otimizada com Parâmetros Múltiplos (OMP) foram realizadas separadamente por bacias oceânicas e foi considerada a melhor combinação linear de mistura entre as massas de água, com cada bacia oceânica envolvendo a mistura de sete massas de água, o que resulta em sete parâmetros para as bacias do Atlântico, do Índico e do Pacífico, conforme mostra a tabela 2.

**Tabela 2.** Bacias oceânicas com as respectivas massas de água e parâmetros utilizados em cada uma das aplicações da análise Otimizada com Parâmetro Múltiplos (OMP). As siglas das massas de água correspondem à a Água do Mar de Labrador (LSW), Água do Estreito da Dinamarca (DSOW), Água da Islândia-Escócia (ISOW), Água do Mediterrâneo (MW), Água Profunda do Mar de Weddell (WSDW), Água de Fundo do Mar de Weddell (WSBW), Água de Fundo da Terra de Adelie (ADLBW), Água de Fundo do Mar de Ross (RSBW), Água Intermediária da Antártica (AAIW), Água do Mar Vermelho (RSOW) e Água Intermediária do Pacífico Norte (NPIW).

Bacias oceânicas	Massas de água	Parâmetros
Atlantic basin	LSW, DSOW, ISOW, MW, WSDW, WSBW, AAIW	$\Theta$ , $S_A$ , DO, $PO_4$ , $NO_3$ , $SiO_2$ , PV
Indian basin	LSW, ISOW, WSDW, WSBW, ADLBW, AAIW, RSOW	$\Theta$ , $S_A$ , DO, $PO_4$ , $NO_3$ , $SiO_2$ , PV
Pacific basin	LSW, ISOW, WSDW, ADLBW, RSBW, AAIW, NPIW	$\Theta$ , $S_A$ , DO, $PO_4$ , $NO_3$ , $SiO_2$ , PV

### *3.3.1. Cálculo dos índices das águas-fonte*

Os índices das massas de água (Tab. 1) que compõem a matriz G foram definidos a partir de regressão linear utilizando dados oceânicos da região onde cada massa de água foi formada. Inicialmente, foi definida uma variável independente de  $\Theta$  para cada água-fonte com base na literatura [Johnson 2008, Pardo *et al.* 2012, Garcia-Ibanez *et al.* 2015, Ferreira & Kerr 2017, Fuhr *et al.* 2021]. Vale ressaltar que alguns destes valores de temperatura que definem as águas-fonte foram transformados com as novas equações de estado da água do mar - TEOS-10. O limite mínimo e máximo de  $\Theta$  de cada água-fonte foi calculado a partir do desvio padrão dos dados da área de formação de cada água-fonte. Posteriormente, foram plotados os parâmetros dependentes (salinidade absoluta -  $S_A$ , oxigênio dissolvido -  $O_2$ , fosfato -  $PO_4$ , nitrato -  $NO_3$ , silicato -  $SiOH_4^{4-}$  e vorticidade potencial -  $PV$ ) de cada massa de água em função do parâmetro independente previamente definido. A partir da regressão linear, os valores mínimo e máximo do parâmetro independente definem os limites mínimo e máximo dos parâmetros dependentes. Os valores de  $\Theta$  e  $S_A$  das águas-fonte podem ser observados no diagrama TS (Fig. 6).

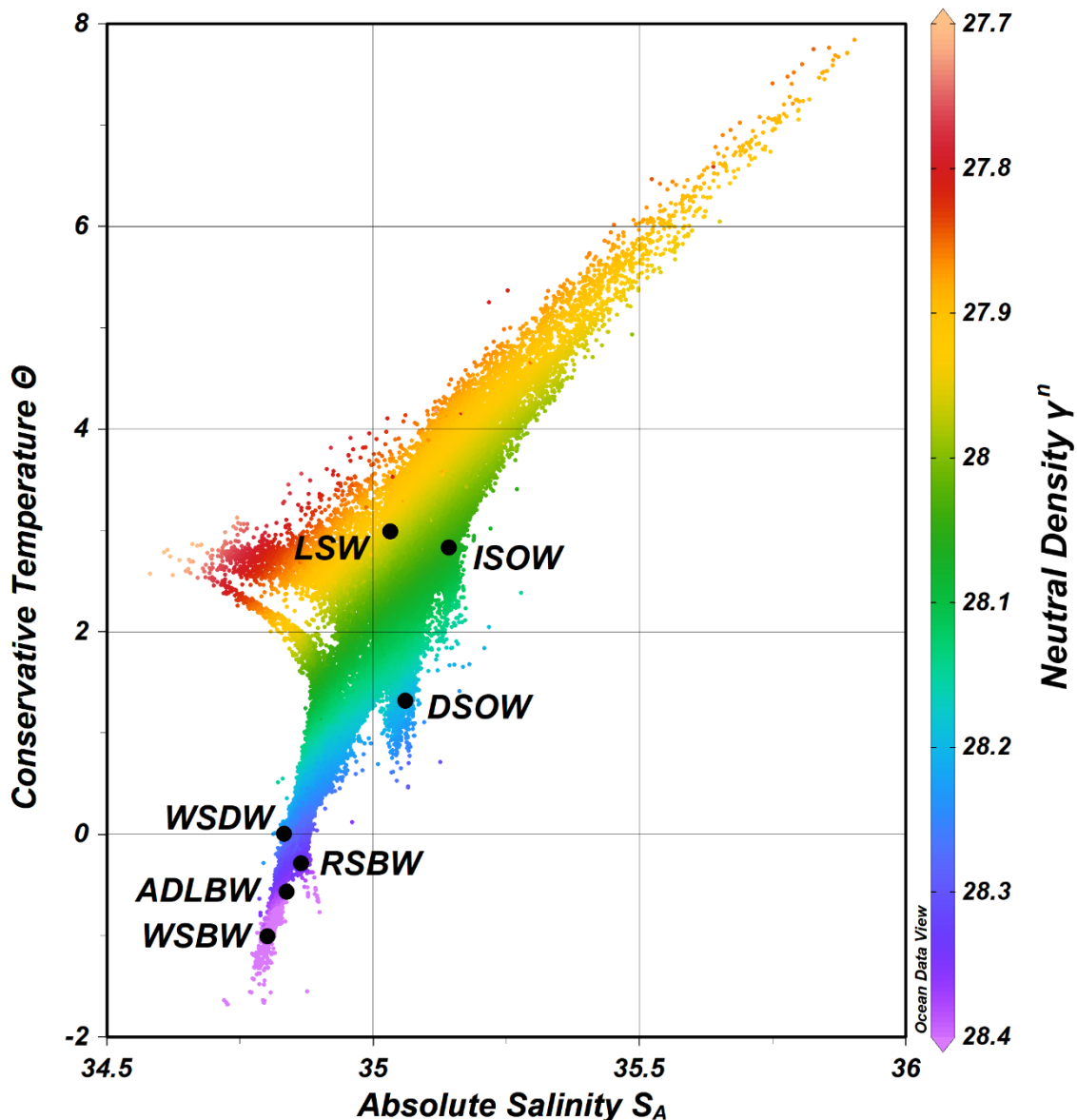


**Figura 6.** Diagrama TS de dados dos oceanos Atlântico e Antártico obtidos do banco de dados WOD18 e GLODAP, com os pontos pretos definindo as massas de água profundas usadas na análise: Água do Mar de Labrador (LSW), Água da Islândia-Escócia (ISOW), Água do Estreito da Dinamarca (DSOW), Água Profunda do Mar de Weddell (WSDW), Água de Fundo do Mar de Weddell (WSBW), Água de Fundo da Terra de Adelie (ADLBW) e Água de Fundo do Mar de Ross (RSBW). As cores representam a densidade neutra ( $Y^n$ ;  $\text{kg m}^{-3}$ ).

### 3.3.2. Teste de sensibilidade

Um teste de sensibilidade foi aplicado para garantir a robustez dos resultados. Portanto, optou-se por aplicar uma abordagem de Monte Carlo para variar aleatoriamente os índices das águas-fonte dentro da faixa de propriedades de cada massa de água, uma vez que a análise Otimizada com Parâmetros Múltiplos (OMP) não considera mudanças temporais na definição dessas águas-

fonte. Um total de 50 execuções da análise Otimizada com Parâmetros Múltiplos (OMP) foram realizadas com os parâmetros das águas-fonte ligeiramente modificados considerando a faixa de propriedades representadas na tabela 1. Somente resultados que obtiveram um resíduo de conservação de massa até 10% foram considerados. Os resultados apresentados são a média de todas as execuções da análise Otimizada com Parâmetros Múltiplos (OMP) realizadas [Almeida *et al.* 2018, Kerr *et al.* 2018].

## Capítulo IV: Artigo Científico

Para a obtenção do título de Mestre pelo Programa de Pós-Graduação em Oceanologia, é requerido que o discente realize a submissão de pelo menos um artigo científico como primeiro autor em periódico com corpo indexado. Desse modo, os resultados da pesquisa desenvolvida durante o período de mestrado e a discussão dos resultados serão apresentados em forma de artigo neste Capítulo. O manuscrito de autoria de David Antonio de Lima Silva e Rodrigo Kerr, é intitulado “***Revisiting the distribution and sources contribution of Deep Water Masses in the global ocean basins***” e foi submetido para publicação no periódico “***Deep Sea Research Part I***”.

# Revisiting the distribution and sources contribution of Deep Water Masses in the global ocean basins

David de Lima and Rodrigo Kerr

## 4.1. Introduction

The global ocean plays a fundamental role modulating the global climate balance due to the heat transport from low latitudes to polar regions through the Meridional Overturning Circulation (MOC) ([Gordon, 1986](#), [Orsi et al., 1999](#); [Wunsch, 2005](#); [Stocker, 2013](#); [Bryden et al., 2020](#)). The lower branch of the MOC is driven by deep and bottom waters that move through the deep basins of the global ocean, transporting CO<sub>2</sub> ([Yu et al., 2014](#); [Rae et al., 2018](#)), nutrients, salt, and minerals which are tracers of oceanographic changes over different time scales ([Goodman, 1988](#); [Williams et al., 2019](#); [Mokedemm and McManus, 2017](#); [Martínez-Fontaine et al., 2019](#)). This branch is widely represented by the North Atlantic Deep Water (NADW) and the Antarctic Bottom Water (AABW, [Gordon, 1986](#); [Broecker and Denton, 1989](#); [Elliot et al., 2002](#); [Lynch-Stieglitz et al., 2007](#)), which are formed in high latitudes of the northern and southern hemisphere, respectively ([Foster and Carmack, 1976](#); [Mantyla and Reid, 1983](#); [Orsi et al., 1999](#); [Ferreira and Kerr, 2017](#)). The different varieties of the NADW and AABW have characteristics that vary with regions and depths ([Orsi et al., 1999](#); [Ferreira and Kerr, 2017](#)). These waters occupy exclusively a certain part of the ocean, whereas in other regions, they share the ocean with other masses of water with which they mix ([Tomczack, 1999](#)).

In Greenland, Iceland and Norwegian Seas, intense winter heat loss leads to deep convection and formation of deep water ([Yashayaev et al., 2007](#); [Talley et al., 2011](#)). In the Labrador Sea ([Fig. 1a](#)), the Labrador Sea Water (LSW) is

formed, and in the Nordic Seas (Fig. 1a) the Iceland-Scotland Overflow Water (ISOW) and the Denmark Strait Overflow Water (DSOW) are formed, whereas in the Mediterranean Sea (Fig. 1a) a fourth water mass called Mediterranean Water (MW) is formed and together they constitute the NADW (Reid and Lynn, 1971; Dickson and Brown, 1994; Talley, 2013; García-Ibáñez et al., 2015). The NADW sinks and occupies the seafloor close to its formation sites and spreads southwards (Johnson, 2008). This water mass comprises the densest waters in some regions of the North Atlantic Ocean, being relatively warmer, saltier and lighter than the AABW (Johnson, 2008; Reid et al., 1977). In the South Atlantic Ocean, the relatively warm and salty NADW flows above the AABW until it reaches the Antarctic Circumpolar Current (ACC), where it is advected eastward and propagated northward into the Indian and Pacific Oceans (Reid et al., 1977; Johnson, 2008; Talley, 2013).

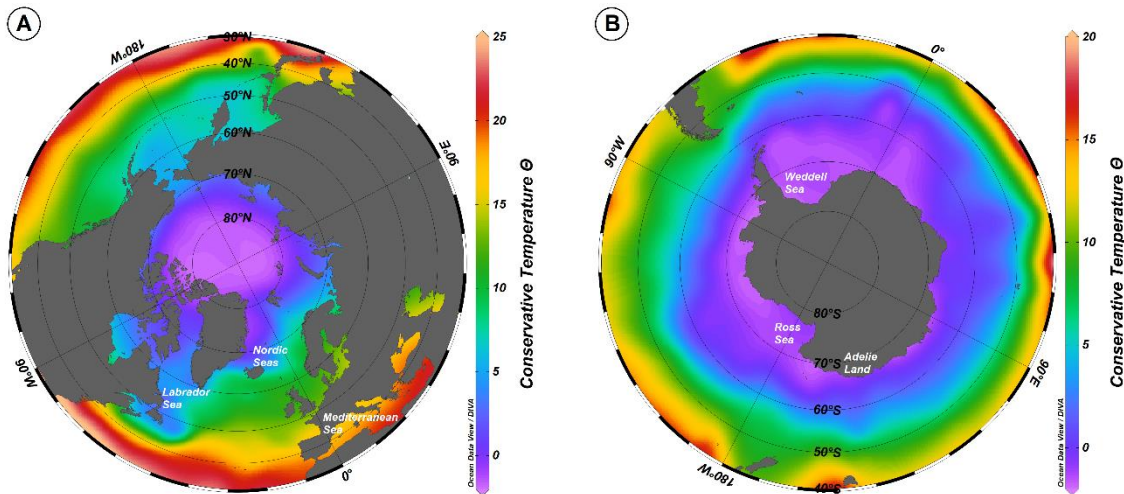


**Figure 1.** Surface distribution of conservative temperature ( $^{\circ}\text{C}$ ) from the compiled data of GLODAP and WOD18 databases. (a) Location of the three formation areas of the North Atlantic Deep Water (NADW) source waters (i.e. Labrador Sea, Nordic Seas, and Mediterranean Sea) in the North Atlantic Ocean. (b) Location of the three formation areas of the Antarctic Bottom Water (AABW) source waters (i.e. Weddell Sea, Ross Sea, and Adelie Land) in the Southern Ocean.

The formation process for AABW is complex (Gill, 1973; Foster and Carmack, 1976) and takes place on the Antarctic margin (Orsi et al., 1999; Talley,

2013), more specifically in the Weddell Sea (Gill, 1973), Ross Sea (Jacobs et al., 1970) and off Adélie Land (Rintoul, 1998) (Fig. 1b). Its formation involves surface cooling due to heat loss, and salinity increase due to sea ice formation and brine rejection, in addition to mixing with surrounding waters during downslope flow (Foster and Carmack, 1976). The Weddell Sea Deep Water (WSDW), Weddell Sea Bottom Water (WSBW), Ross Sea Bottom Water (RSBW) and Adélie Land Bottom Water (ADLBW) forms the AABW (Warren, 1981; Orsi et al., 1999), which is a colder and denser water mass than NADW. It spreads northward into deep basins of the global ocean and mixes with overlying lighter waters (Johnson, 2008; Talley, 2013), except for the Arctic and some of the North Atlantic Ocean, where NADW overlies the ocean bottom (Mantyla and Reid, 1983; Orsi et al., 2001).

The distribution of deep waters show the main flows within the oceans and highlight their export pathways (Ferreira and Kerr 2017; Solodoch et al., 2022), which are important for understanding circulation in the lower ocean layer (e.g., Johnson, 2008; Pardo et al., 2012; Tomczak, 1999a), and supports biogeochemical (Skinner et al., 2010; Azar et al., 2021; Piñango et al., 2022) and climate projections studies (Böning et al., 2016; O'Neill et al., 2016; Moorman et al., 2020; Nissen et al., 2022; Li et al., 2023). Past and recent studies on the distribution of deep waters concentrate efforts mainly in polar regions (Reid and Lynn, 1971; Pardo et al., 2012; García-Ibáñez et al., 2015; Solodoch et al., 2022). Nevertheless, few studies have presented a global-scale approach (e.g., Nakano and Sugihara, 2002; Johnson, 2008).

Here, the spatial distribution and quantification of the source water masses of NADW and AABW are presented based on the percentage of mixing over 46

years (1973–2019) through the use of the inverse method Optimum Multiparameter (OMP) analysis (Tomczak, 1981; Thompson and Edwards, 1981; Mackas et al., 1987; Tomczak and Large, 1989) in the global ocean. The manuscript is organized as follows: section 4.2 describes the formation and distribution of the main source water masses of the NADW and AABW; section 4.3 describes the methodology and data set; in section 4.4 the results of the analysis for the Atlantic, Indian and Pacific basins are presented using vertical sections and horizontal maps of distribution and contribution of water masses; the distribution and contribution of water masses are discussed in section 4.5; and finally, the main findings are summarized in section 4.6.

#### **4.2. Formation and distribution context: source water masses of NADW and AABW**

Polar regions are the main sites of formation of deep and bottom water masses (Mantyla & Reid, 1983; Orsi et al., 1999). In these regions, surface waters become dense enough to lose buoyancy and sink into the interior layers of the ocean (Orsi, et al., 1999). In the Labrador Sea and Nordic Seas, the varieties of upper and lower NADW originate from processes involving the interaction between the atmosphere and the ocean, mainly during winter (Talley and Mccartney, 1982; Johnson, 2008). On the other hand, mechanisms involving shelf processes and the interaction between atmosphere and the ocean in the Antarctic margin originate the AABW varieties (Orsi et al., 1999, Talley 2013), which are colder and relatively fresh compared to the waters that make up the NADW (Johnson, 2008).

In the Labrador Sea, winter cooling and deep ocean convection lead to the formation of LSW, which is the lightest component of NADW, predominant at

depths between 1500 m and 2500 m (Clarke and Gascard, 1983; García-Ibáñez et al., 2015), with spreading southward via the Deep Western Boundary Current (DWBC) and through interior pathways within the basins (Stramma et al., 2004; Bower et al., 2019). The lower components of the NADW are formed when the warm waters of the North Atlantic meet the overflow waters of the Arctic (Read, 2000; Dickson et al., 2002). These deep overflow waters enter the Atlantic Ocean through passages located east of Iceland and through the Denmark Strait (Fogelqvist et al., 2003; Dickson et al., 2002), mixing with adjacent waters and originating ISOW and DSOW, respectively (Yashayaev and Dickson, 2008; Fogelqvist et al., 2003). The ISOW spreads in the deep layers of the Iceland Basin and flows into the Irminger Basin through the Charlie-Gibbs Fracture Zone, where it meets the DSOW (Bower and Furey, 2017; Lozier et al., 2022). Part of the ISOW flows southward within the eastern North Atlantic basin (Garcia-Ibanez et al., 2015) and is recognized for its high salinity and low temperatures compared to the other NADW source waters in the Nordic Seas. Among the components of NADW, the DSOW is considered the coldest and densest variety and is found in the deeper layers of the Irminger and Labrador Basin (LeBel et al., 2008; Lozier et al., 2022) flowing southward within the DWBC along with the other components of NADW (Garcia-Ibanez et al., 2015; Lozier et al., 2022), other export pathways within the basins have also been reported for it (LeBel et al., 2008; Lozier et al., 2022). The upper NADW is also composed of the MW, which is formed in the Mediterranean Sea and characterized by its maximum salinity, which favors its high density (Garcia-Ibanez et al., 2015; Ferreira and Kerr, 2017). Upon leaving the Mediterranean Sea through the Strait of Gibraltar, this mass of water sinks and occupies intermediate depths between 600 m and 2000 m in the eastern

North Atlantic (Tsuchiya et al., 1992; Álvarez et al., 2004; Bozec et al., 2011; Ferreira and Kerr, 2017) and spreads to the west and north of this basin, mixing with surrounding water masses (Lozier et al., 1995; Bozec et al., 2011). Previous studies show the distribution of NADW in the Atlantic, Indian, Pacific and Southern Ocean basins (Johnson, 2008; Pardo et al., 2012; Talley, 2013). Ferreira and Kerr (2017) observed LSW contributions within the ACC, with ISOW and DSOW extending to approximately 40°S in the Atlantic basin at depths between 2000 m and 5000 m. NADW contributions have been observed from ~45°S to the Antarctic margin in global ocean basins (Pardo et al., 2012). It is noteworthy that studies on the distribution of NADW varieties in the global ocean have received less attention due to the difficulty of tracking the path of a single NADW water mass, since these waters are well mixed far from their area of formation. Thus, several works have considered NADW collectively (Johnson, 2008; Nakano and Sugino, 2002), particularly outside the Atlantic Ocean, and it is not possible to identify the depth levels corresponding to each water mass that composes it.

The WSDW, WSBW, RSBW and ADLBW result from the mixing of the relatively warm and salty waters of the ACC with cold and salty Shelf Waters (SW) and/or Ice Shelf Water (ISW) in the continental slope of Weddell Sea, Ross Sea, and Adelie Land, respectively (Jacobs et al., 1970; Foster and Carmack, 1976; Foldvik et al., 1985; Rintoul, 1998; Purkey et al., 2018). Antarctic coastal polynyas resulting from katabatic winds from the continent result in the rejection of salt and an increase in surface salinity, contributing to the production of AABW (Fahrbach et al., 1994; Arrigo and Van Dijken, 2003). The WSDW is the less dense and warmest component of AABW and is exported northward into the

Atlantic Ocean through deep channels in the South Scotia Ridge and South Sandwich Trench ([Meredith et al., 2013](#)). Part of the WSDW is also exported eastward through the ACC ([Orsi et al., 1999](#)) spreading to the Atlantic, Indian, Pacific basins and Southern Ocean, whereas the dense WSBW, the coldest and freshest component of the AABW, is exported through similar pathways to the WSDW (e.g., South Sandwich Trench), but it is restricted to abyssal depths at latitudes greater than 50°S due to its high density ([Pardo et al., 2012; Ferreira and Kerr, 2017](#)). The WSBW extends to approximately Adelie Land, whereas ADLBW and RSBW are found above 60°S in Adelie Land and areas adjacent to the Ross Sea, with RSBW extending to near Drake Passage ([Pardo et al., 2012](#)). The RSBW is the warmer and saltier variety of AABW, whereas the ADLBW have properties in between the WSBW and RSBW.

### 4.3. Data and methods

#### 4.3.1. Databases compiled and used in this study

Here, we compiled and used a historical dataset available at the World Ocean Database (WOD 2018, [www.ncei.noaa.gov/products/world-ocean-database](http://www.ncei.noaa.gov/products/world-ocean-database)) and Global Ocean Data Analysis Project 2020 (GLODAP, [www.glodap.info/](http://www.glodap.info/)), which spans 46 years (1973 - 2019). This dataset includes the following parameters: conservative temperature ( $\Theta$ ), absolute salinity ( $S_A$ ), dissolved oxygen ( $O_2$ ), phosphate ( $PO_4$ ), nitrate ( $NO_3$ ), silicate ( $SiOH_4^{4-}$ ) and potential vorticity (PV). To restrict the analysis to deep water masses in the global ocean, only data found at depths greater than 1500 m were selected. The dataset was separated by ocean basins ([Fig. 2a](#)) and the analysis of the distribution of deep waters was carried out separately for each ocean basin (i.e. Atlantic, Indian, and Pacific basins).

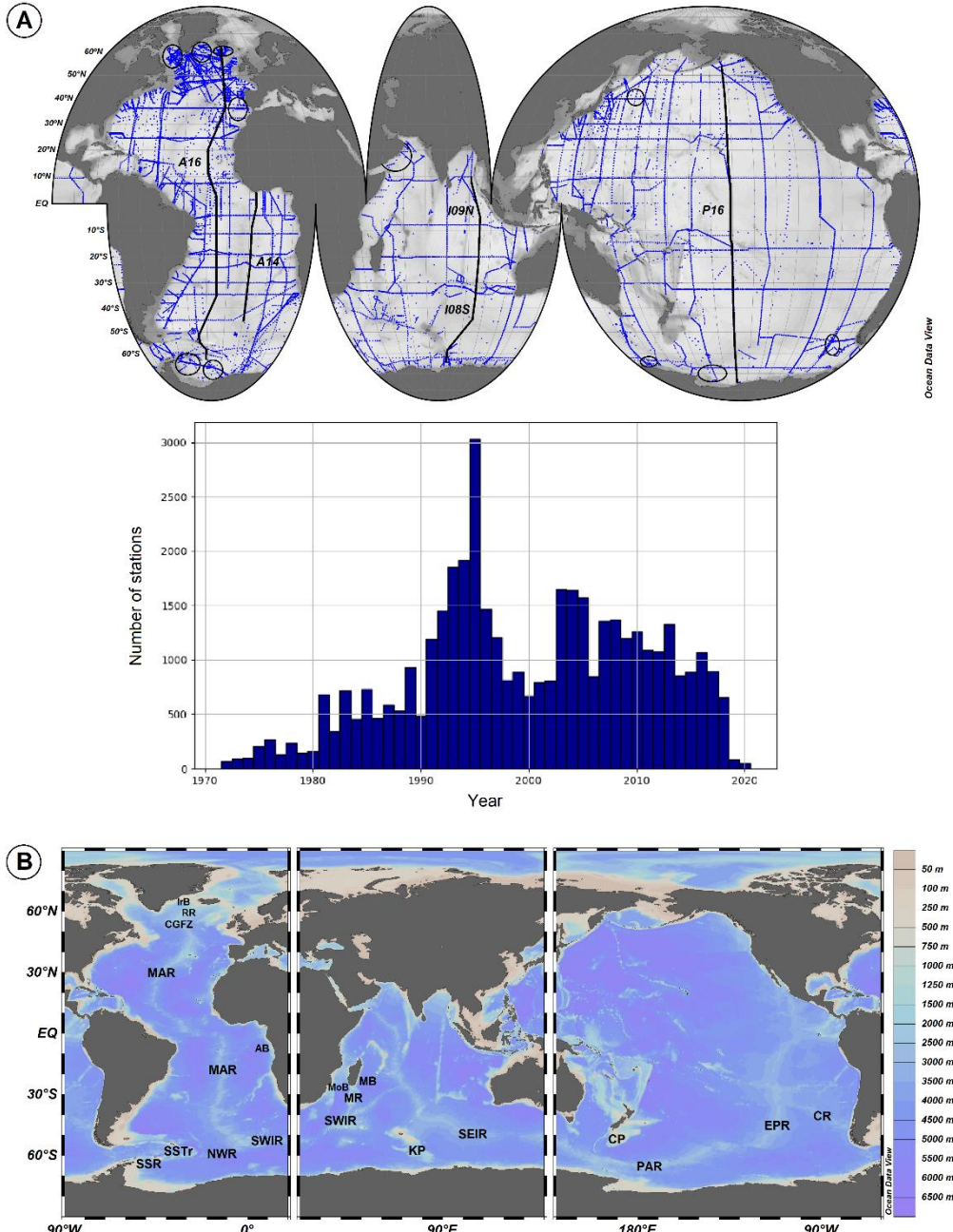


**Figure 2.** (a) Distribution of the hydrographic stations and locations of the three WOCE hydrographic sections (black lines) running through the Atlantic (A16 and A14), the Indian (I09N and I08S) and the Pacific (P16) basins. The black outlined ellipses represent the source areas where parameters were obtained to determine the source waters of North Atlantic Deep Water in the North Atlantic Ocean and Antarctic Bottom Water in the Southern Ocean, in addition to three more intermediate waters (Antarctic Intermediate Water - AAIW, Red Sea Overflow Water - RSOW, and North Pacific Intermediate Water - NPIW) in the Indian and Pacific basins. The histogram shows the number of stations per year for the global ocean basin. (b) Ocean Basins bathymetric features. The acronyms for bathymetric features in the Atlantic Ocean basin are Irminger Basin (IrB), Reykjanes Ridge (RR), Charlie-Gibbs Fracture Zone (CGFZ), Mid-Atlantic Ridge (MAR), Angola Basin (AB), South Scotia Ridge (SSR), South Sandwich Trench (SSTr), North Weddell Ridge (NWR), and Southwest Indian Ridge (SWIR). The acronyms for bathymetric features in the Indian Ocean basin are Southwest Indian Ridge (SWIR), Mozambique Basin (MoB), Madagascar Ridge (MR), Madagascar Basin (MB), Kerguelen Plateau (KP), and Southeast Indian Ridge (SEIR). The acronyms for bathymetric features in the Pacific Ocean basin are Campbell Plateau (CP), Pacific Antarctic Ridge (PAR), East Pacific Rise (EPR), and Chile Ridge (CR).

The dataset used in this work underwent a quality control process before being made available, in which adjustments were applied to remove significant biases (if any), while respecting the occurrence of any known or likely trends or time variations (Boyer et al., 2018; Olsen et al., 2016). A check to avoid repeated oceanographic stations in the two databases was applied.

#### 4.3.2. Optimum Multiparameter (OMP) analysis

The Optimum Multiparameter Analysis (OMP) was initially proposed by Tomczak (1981) and implemented by Tomczak and Large (1989) as an extension of classical mass mixing analysis of water, previously carried out using the TS diagram (Mamayev, 1975). In this method, conservative and non-conservative parameters are used to trace the water masses by calculating the contributions of each of them through linear mixing equations (Tomczak and Large, 1989). In this context, the OMP method determines the percentage contribution of each source water type (SWT) previously defined (Tomczak and Large, 1989). The SWT represents the values of the parameters of an original unmixed water mass, that is, it corresponds to water with characteristics typical of the properties of the region where it originated (Poole and Tomczak, 1999). In this way, in addition to determining the contribution between all selected SWT, the OMP method allows the spatial distribution of water masses to be analyzed (Tomczak and Large, 1989). Subsequently, ocean circulation can be deduced through the distribution of water masses (e.g., Johnson, 2008). However, the method presents two restrictions: (i) the contribution of all SWT must be equal to 100% to ensure mass conservation; and (ii) this contribution should not be negative (Tomczak et al., 1989). In this study, seven ocean parameters were used in the OMP analysis (see Table 1).

This method can also be used in its basic or extended form depending, mainly, on the spatial scale of the analysis and the availability of water mass tracers (Karstensen and Tomczak, 1999). In this study, the extended OMP method was applied, since the objective is to analyze the distribution of deep waters on a large scale. The extended form considers that non-conservative parameters present changes in their concentrations due to biogeochemical processes, such as remineralization and respiration as water masses evolve (Karstensen and Tomczak, 1999). For this reason, the Redfield Ratio is incorporated into the equations as a correction factor for these modifications (Anderson and Sarmiento, 1994; Karstensen and Tomczak, 1999). The linear system of mixing equations from OMP analysis is then shown in equation 1 below:

$$\begin{aligned}
 x_1T_1 + x_2T_2 + x_3T_3 + x_4T_4 + x_5T_5 + x_6T_6 + x_7T_7 &+ 0 = T_{\text{obs}} + R_T \\
 x_1S_1 + x_2S_2 + x_3S_3 + x_4S_4 + x_5S_5 + x_6S_6 + x_7S_7 &+ 0 = S_{\text{obs}} + R_S \\
 x_1O_{2,1} + x_2O_{2,2} + x_3O_{2,3} + x_4O_{2,4} + x_5O_{2,5} + x_6O_{2,6} + x_7O_{2,7} &- r_{O/P}\Delta P = O_{2,\text{obs}} + R_{O2} \\
 x_1PO_{4,1} + x_2PO_{4,2} + x_3PO_{4,3} + x_4PO_{4,4} + x_5PO_{4,5} + x_6PO_{4,6} + x_7PO_{4,7} &+ \Delta P = PO_{4,\text{obs}} + R_{PO4} \\
 x_1NO_{3,1} + x_2NO_{3,2} + x_3NO_{3,3} + x_4NO_{3,4} + x_5NO_{3,5} + x_6NO_{3,6} + x_7NO_{3,7} &+ r_{N/P}\Delta P = NO_{3,\text{obs}} + R_{NO3} \\
 x_1SiO_{3,1} + x_2SiO_{3,2} + x_3SiO_{3,3} + x_4SiO_{3,4} + x_5SiO_{3,5} + x_6SiO_{3,6} + x_7SiO_{3,7} + r_{N/P}\Delta P &= SiO_{3,\text{obs}} + R_{SiO3} \\
 x_1PV_1 + x_2PV_2 + x_3PV_3 + x_4PV_4 + x_5PV_5 + x_6PV_6 + x_7PV_7 &+ 0 = PV_{\text{obs}} + R_{PV} \\
 x_1 + x_2 + x_3 + x_4 + x_5 + x_6 + x_7 &+ 0 = 1 + R_{\Sigma}
 \end{aligned} \tag{1}$$

The observed values of  $T_{\text{obs}}$ ,  $S_{\text{obs}}$ ,  $O_{\text{obs}}$ ,  $P_{\text{obs}}$ ,  $N_{\text{obs}}$ ,  $Si_{\text{obs}}$ , and  $PV_{\text{obs}}$ , represent the values of the conservative temperature, absolute salinity, dissolved oxygen, phosphate, nitrate, silicate and potential vorticity, respectively, while  $R$  represent the residue of each parameter;  $r \Delta P$  represents the Redfield ratio;  $T_j$ ,  $S_j$ ,  $O_j$ ,  $P_j$ ,  $N_j$ ,  $Si_j$  and  $PV_j$  with  $j$  varying from 1 to 7, represent the parameter values of each SWT;  $x_j$  the contributions of each SWT (unknowns) and the last equation

represents the mass conservation condition (Anderson and Sarmiento, 1994; Karstensen and Tomczak, 1999). The above system of equations can be written in matrix notation as shown below in equation 2:

$$G x - d = R \quad (2)$$

where G represents the matrix with the values of the properties of each SWT, x is a vector of the contributions calculated for each SWT, d is a vector of the observed data and R is the residual value (Tomczak and Large, 1989).

In the OMP analysis, the parameters often do not present the same representation, due to the influence of environmental variability and the analytical and instrumental precision of the measurements (Ferreira and Kerr, 2017). Therefore, a weighted version of the G matrix was applied, including a W matrix, which has respective weights for each parameter (equation 3), according to the method described by Tomczak and Large (1989).

$$W_j = \sigma_j^2 / \delta_{j \max} \quad (3)$$

The W represents the weight,  $\sigma_j^2$  is the variance for each SWT parameter and  $\delta_{j \max}$  is the maximum variance of the parameter among all source waters (Tomczak and Large, 1989). Each parameter receives its own weight, indicating that each thermohaline property can influence the mixing calculation differently.

The SWT indices are summarized in [Table 1](#).

**Table 1.** Source waters type (SWT) indices with the respective standard deviations considered in the study. The weights and Redfield ratio for each parameter used in the Optimum Multiparameter analysis (OMP) are also given. The acronyms for the source water masses correspond to Labrador Sea Water (LSW), Denmark Strait Overflow Water (DSOW), Iceland-Scotland Overflow Water (ISOW), Mediterranean Water (MW), Weddell Sea Deep Water (WSDW), Weddell Sea Bottom Water (WSBW), Adelie Land Bottom Water (ADLBW), Ross Sea Bottom Water (RSBW), Antarctic Intermediate Water (AAIW), Red Sea Overflow Water (RSOW), and North Pacific Intermediate Water (NPIW).

SWT	$\Theta$ (°C)	$S_A$ (g kg <sup>-1</sup> )	DO μmol/kg	PO <sub>4</sub> μmol/kg	NO <sub>3</sub> μmol/kg	SiOH <sub>4</sub> μmol/kg	PV 10 <sup>8</sup> ms <sup>-1</sup>
LSW	3.072 ± 0.182	35.055 ± 0.015	284 ± 9.0	1.08 ± 0.003	16.2 ± 0.05	10 ± 0.05	0.0116 ± 0.002
DSOW	1.494 ± 0.200	35.054 ± 0.002	299 ± 2.0	0.94 ± 0.010	14.0 ± 0.25	8 ± 0.23	0.0675 ± 0.006
ISOW	2.822 ± 0.112	35.136 ± 0.006	274 ± 0.4	1.08 ± 0.001	16.2 ± 0.08	13 ± 0.56	0.0329 ± 0.002
MW	9.936 ± 0.119	36.125 ± 0.033	186 ± 0.4	1.00 ± 0.009	16.6 ± 0.06	9 ± 0.12	0.0664 ± 0.002
WSDW	0.000 ± 0.050	34.823 ± 0.018	223 ± 5.0	2.25 ± 0.050	32.8 ± 0.40	114 ± 8.0	-0.0095 ± 0.005
WSBW	-1.000 ± 0.119	34.810 ± 0.013	257 ± 8.0	2.22 ± 0.040	32.2 ± 0.40	112 ± 4.0	-0.0078 ± 0.006
ADLBW	-0.470 ± 0.055	34.835 ± 0.008	239 ± 3.0	2.22 ± 0.005	31.9 ± 0.01	109 ± 0.04	-0.0076 ± 0.001
RSBW	-0.250 ± 0.006	34.863 ± 0.003	229 ± 2.0	2.24 ± 0.007	31.5 ± 0.18	99 ± 0.54	-0.0109 ± 0.0002
AAIW	3.403 ± 0.214	34.429 ± 0.013	222 ± 4.0	2.15 ± 0.007	30.81 ± 0.02	34 ± 0.83	-0.0797 ± 0.003
RSOW	11.168 ± 0.862	35.754 ± 0.169	15 ± 8.0	2.59 ± 0.006	31.59 ± 1.99	49 ± 2.61	0.0376 ± 0.010
NPIW	3.803 ± 0.198	34.344 ± 0.090	54 ± 12	2.89 ± 0.070	40.47 ± 1.13	108 ± 9.0	0.0909 ± 0.013
Weights	7.9395	7.9395	6.0938	1.3421	5.7383	1.1201	0.0574
Redfield Ratio	n/a	n/a	-170	1	16	40	n/a

#### 4.3.3. Source waters type definition

The number of water masses used in the OMP analysis depends on the number of parameters available (Tomzack and Large, 1989). Here, the following water masses were used for the OMP analysis: LSW, DSOW, ISOW and MW, defined as source waters of NADW (Dickson and Brown, 1994; Johnson, 2008; Garcia-Ibanez et al., 2015; Ferreira and Kerr, 2017); WSDW, WSBW, ADLBW and RSBW, defined as source waters of AABW (Orsi et al., 1999; Johnson, 2008; Pardo et al., 2012; Ferreira and Kerr, 2017); and the intermediate waters AAIW, RSOW and NPIW, added to the analysis to reduce possible errors regarding mixing with the upper layer of NADW (Johnson, 2008), totaling eleven water masses. Furthermore, seven parameters were used, the conservative temperature –  $\Theta$ , absolute salinity –  $S_A$ , dissolved oxygen – O<sub>2</sub>, phosphate – PO<sub>4</sub><sup>3-</sup>, nitrate – NO<sub>3</sub><sup>-</sup>, silicate – SiOH<sub>4</sub><sup>4-</sup> and potential vorticity - PV, which limits

the analysis to up to seven source water masses. In order to solve the problem between the limitation of water masses by the number of parameters, the OMP rounds were carried out separately by basins and the best linear combination of mixing between water masses was considered to obtain the following arrangement (i): the Atlantic basin involving the mixing of LSW, DSOW, ISOW, MW, WSDW, WSBW and AAIW; (ii) the Indian basin involving the mixing of LSW, ISOW, WSDW, WSBW, ADLBW, AAIW and RSOW; and (iii) the Pacific basin involving the mixing of LSW, ISOW, WSDW, ADLBW, RSBW, AAIW and NPIW.

#### 4.3.4. Calculation of source water type indices

The indices of the SWT ([Table 1](#)) that make up the G matrix were defined from linear regression using oceanic data from the region where each water mass was formed ([Fig. 2a](#)). Initially,  $\Theta$  was defined as the independent variable for each SWT based on the literature ([Johnson, 2008](#); [Pardo et al., 2012](#); [Garcia-Ibanez et al., 2015](#); [Ferreira and Kerr, 2017](#); [Fuhr et al., 2021](#)). It is noteworthy that some of these studies report potential temperature values, thus those values were transformed to  $\Theta$  using the TEOS-10 equations. The minimum and maximum  $\Theta$  limit of each SWT was calculated from the standard deviation of the formation area data of each SWT ([Fig. 2a](#)). Subsequently, the dependent parameters ( $S_A$ ,  $O_2$ ,  $PO_4$ ,  $NO_3$ ,  $SiOH_4^{4-}$  and  $PV$ ) of each water mass were plotted as a function of the previously defined independent parameter. From linear regression, the minimum and maximum values of the independent parameter define the minimum and maximum limits of the dependent parameters. The  $\Theta$  and  $S_A$  values of the SWT can be observed in the  $\Theta-S_A$  diagram ([Fig. 3](#)).

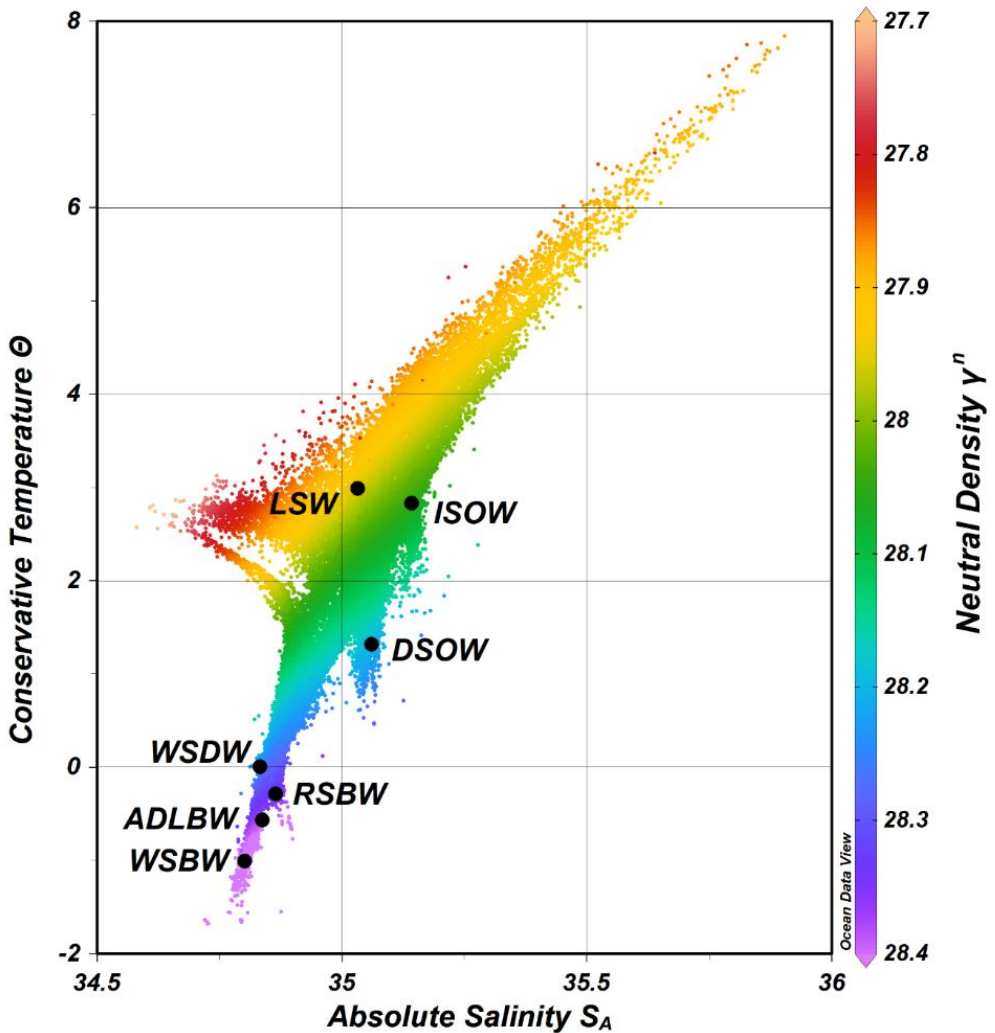


**Figure 3.**  $\Theta$ - $S_A$  diagram ( $^{\circ}\text{C}$ - $\text{g kg}^{-1}$ ) of Atlantic and Southern Oceans data obtained from the GLODAP and WOD18 database, with the black dots defining each source waters type used in the analysis: Labrador Sea Water (LSW), Iceland-Scotland Overflow Water (ISOW), Denmark Strait Overflow Water (DSOW), Weddell Sea Deep Water (WSDW), Weddell Sea Bottom Water (WSBW), Adelie Land Bottom Water (ADLBW), and Ross Sea Bottom Water (RSBW). The colorbar represent the neutral density ( $\rho^n$ ;  $\text{kg m}^{-3}$ ).

#### 4.3.5. Sensitivity test

A sensitivity test was applied to ensure the robustness of the results. Therefore, it was applied a Monte Carlo approach to randomly vary the SWT indices within the range of properties of each water mass, as the OMP does not consider temporal changes in the definition of these SWT. A total of 50 OMP runs were performed with slightly modified SWT parameters considering the range of properties represented in Table 1. Only results that obtained a mass conservation

residual up to 10% were considered. The results presented are the average of all OMP runs performed (Almeida et al., 2018; Kerr et al., 2018).

## 4.4. Results

### 4.4.1. Water mass distributions in the Atlantic basin

The distribution and quantification of the contribution of NADW and AABW source water masses infers their main pathways in the Global Ocean basin. Total contributions were quantified in the western and eastern Atlantic Ocean basins. The western and eastern basins of the Atlantic Ocean show greater contributions to LSW, ISOW and WSDW ([Table 2](#)), highlighting the strong influence of these source waters in these basins. DSOW presented a greater contribution in the western basin of the Atlantic Ocean, whereas the largest MW contribution was in the eastern basin, close to its formation area ([Table 2](#)). WSBW showed greater contribution in the western basin and slightly less contribution in the eastern basin ([Table 2](#)). As expected, LSW is predominant in the Labrador Basin with significant contributions in the Iceland Basin and the Irminger Basin ([Fig. 4a](#)). In the Labrador Basin, the LSW is found from 1500 m to greater depths and has a higher concentration between 1800 m and 2500 m. From about 55°N to equatorial latitudes, LSW is found between 1500 m and ~3000 m, with highest concentrations between 1800 m and 2400 m, reaching a contribution of approximately 70% ([Fig. 5a](#)). From the equatorial to subtropical regions of the South Atlantic, the LSW is enriched from ~70% to 80% coevally with its deepening between 30°S and 50°S ([Figs. 4a, b, c and 5a](#)).

**Table 2.** Total contribution (%; first line) and averaged contributions with the respective standard deviations (%; second line) of source waters in each ocean basin. The acronyms represent the source waters: Labrador Sea Water (LSW), Denmark Strait Overflow Water (DSOW), Iceland-Scotland Overflow Water (ISOW), Mediterranean Water (MW), Weddell Sea Deep Water (WSDW), Weddell Sea Bottom Water (WSBW), Adelie Land Bottom Water (ADLBW) and, Ross Sea Bottom Water (RSBW).

Source Waters	Atlantic Ocean Basin	West Atlantic Ocean Basin	East Atlantic Ocean Basin	Indian Ocean Basin	West Indian Ocean Basin	East Indian Ocean Basin	Pacific Ocean Basin	West Pacific Ocean Basin	East Pacific Ocean Basin
LSW	36.6%	36.8%	36.9%	30.4%	29.3%	29.2%	42%	42.1%	41.7%
	$32.3 \pm 14\%$	$32.8 \pm 14\%$	$32.2 \pm 14\%$	$25 \pm 9\%$	$25.7 \pm 9\%$	$24.2 \pm 8\%$	$37 \pm 6\%$	$37 \pm 5\%$	$36.9 \pm 8\%$
ISOW	29.6%	27.7%	32.4%	1.7%	1.8%	1.8%	0.3%	0.2%	0.6%
	$26\% \pm 12\%$	$24 \pm 11\%$	$28.2 \pm 13\%$	$1.4 \pm 0.5\%$	$1.4 \pm 0.5\%$	$1.4 \pm 0.5\%$	$0.2 \pm 0.04\%$	$0.1 \pm 0.02\%$	$0.5 \pm 0.1\%$
DSOW	6.1%	8.6%	2.5%	-	-	-	-	-	-
	$4 \pm 1\%$	$6 \pm 2\%$	$1 \pm 0.6\%$						
MW	4.7%	3.7%	6%	-	-	-	-	-	-
	$3.6 \pm 1\%$	$3 \pm 1.3\%$	$4 \pm 1\%$						
WSDW	19%	19.1%	18.4%	57%	58.4%	58.3%	55.3%	56%	53.7%
	$12 \pm 5\%$	$12 \pm 5\%$	$12 \pm 4\%$	$46.6 \pm 16\%$	$45.3 \pm 15\%$	$48 \pm 16\%$	$48.7 \pm 10\%$	$49.2 \pm 11\%$	$47.4 \pm 10\%$
WSBW	4%	4%	3.8%	8.1%	8%	7.8%	-	-	-
	$2.7 \pm 0.7\%$	$2.7 \pm 0.7\%$	$2.6 \pm 0.6\%$	$6.6 \pm 2\%$	$6.6 \pm 2\%$	$6.6 \pm 2\%$			
ADLBW	-	-	-	2.7%	2.5%	2.5%	0.7%	0.6%	1%
				$2.1 \pm 0.6\%$	$2.2 \pm 0.6\%$	$2.1 \pm 0.5\%$	$0.6 \pm 0.1\%$	$0.5 \pm 0.1\%$	$0.8 \pm 0.1\%$
RSBW	-	-	-	-	-	-	1.6%	1%	2.9%
							$1.3 \pm 0.2\%$	$0.9 \pm 0.1\%$	$2.5 \pm 0.5\%$

At these latitudes, this water mass core is found between 2000 m and 2500 m (Figs. 4a, b and 5a) and below 2500 m it gradually decreases its contribution until a depth of 4000 m with values reaching ~10% west of Mid-Atlantic Ridge (Fig. 5a). Between 40°S and 50°S the LSW has a high contribution above 2000 m, which suggests the upwelling of LSW to shallower layers (Fig. 5a). From 50°S the LSW decreases its contribution from 50% to 10% at approximately 60°S (Fig. 5a).

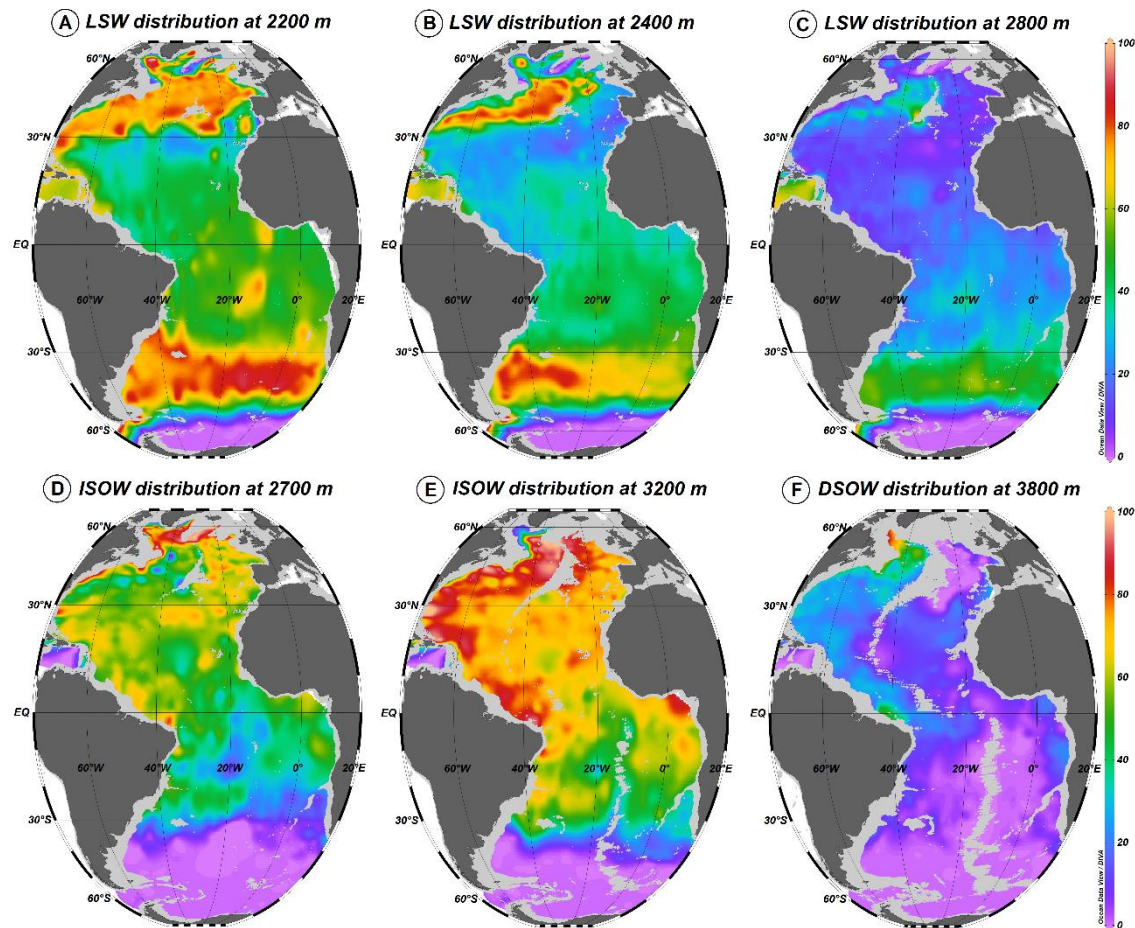


**Figure 4.** Distribution and contribution (%) of North Atlantic Deep Water (NADW) source waters in the Atlantic basin. Labrador Sea Water (LSW) at (a) 2200 m, (b) 2400 m and (c) 2800 m. Iceland-Scotland Overflow Water (ISOW) at (d) 2700 m and © 3200 m. Denmark Strait Overflow Water (DSOW) at (f) 3800 m.

The ISOW showed higher concentration to the south of Iceland between 2100 m and 2800 m with values above 90% (Figs. 4d and 5b). The ISOW is also found in the western Reykjanes Ridge, in the Irminger and Labrador basins, with

contributions above 75% (Fig. 4d). As well LSW, the ISOW occupies the entire North Atlantic basin, but it is found at greater depths (Fig. 4e). From ~55°N to 40°N, the ISOW presents a core between 2800 m and 3500 m, contributing with values above 80% (Figs. 4e and 5b).

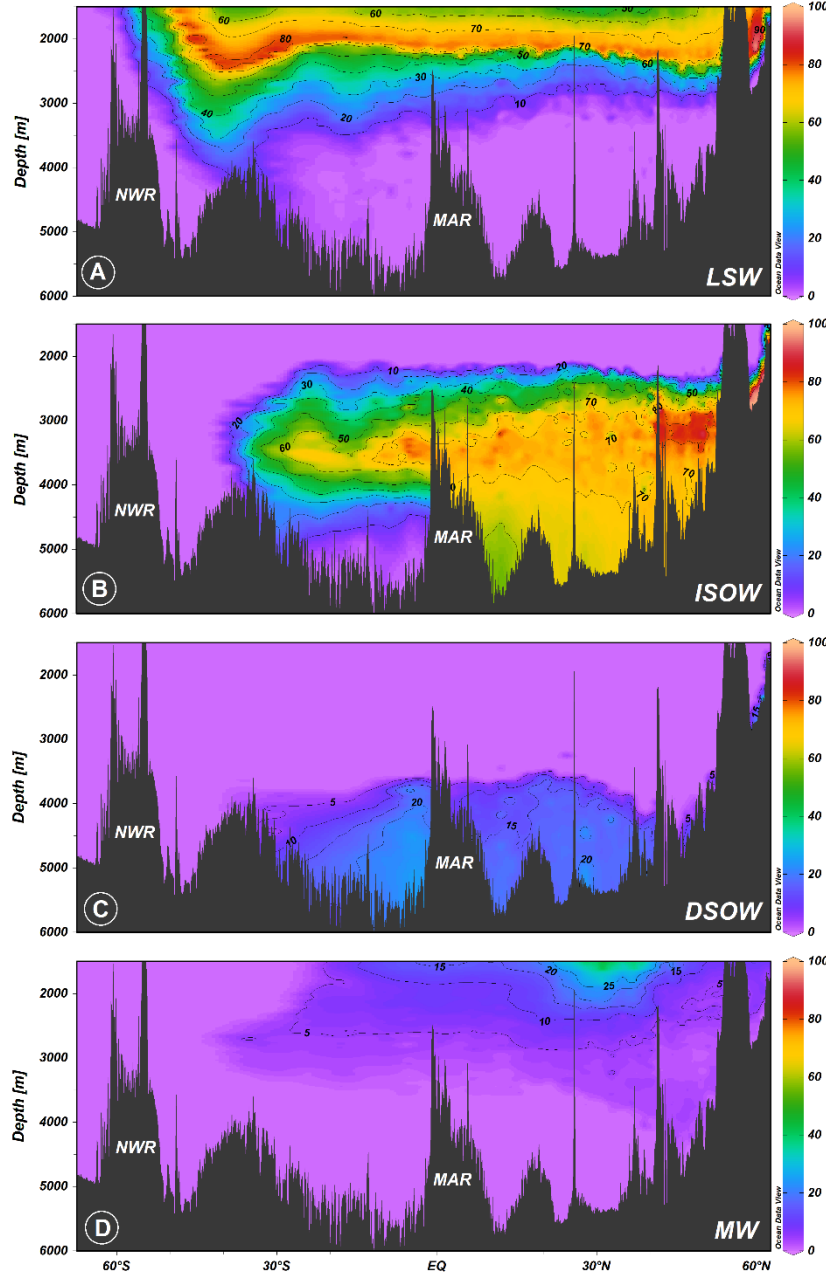


**Figure 5.** Distribution and contribution (%) of North Atlantic Deep Water (NADW) source waters in the Atlantic basin along the WOCE A16 section (Fig. 2a). The names of the source waters type (SWT) are on the bathymetry: (a) Labrador Sea Water (LSW), (b) Iceland-Scotland Overflow Water (ISOW), (c) Denmark Strait Overflow Water (DSOW), and (d) Mediterranean Water (MW). The acronyms of the bathymetric features are the North Weddell Ridge (NWR) and Mid-Atlantic Ridge (MAR).

From  $40^{\circ}\text{N}$  to the equatorial region, the ISOW distribution presents the largest contributions (above 80%) at the extreme western boundary (Fig. 4e). Whereas in the interior of the Atlantic basin, from  $40^{\circ}\text{N}$  to  $\sim 10^{\circ}\text{S}$ , the ISOW shows relatively lower contributions, with values of up to 70% (Figs. 4e and 5b). From  $10^{\circ}\text{S}$  the ISOW decreases its contribution from 70% to less than 10% at  $40^{\circ}\text{S}$  between 3000 m and 4000 m (Figs. 4e and 5b). The ISOW occupies the entire North Atlantic basin, from 2100 m to the bottom (Fig. 5b). However, from the equator it reaches depths of approximately 4700 m at the western boundary of the South Atlantic basin (Fig. 5b), below this are WSDW and DSOW, while at the eastern boundary ISOW is found throughout the water column from 2100 m to the lower layers (Fig. 6). Nonetheless, south of the Walvis Ridge the ISOW shows a significant decrease in its contribution (Figs. 4d, e and 6). From  $\sim 35^{\circ}\text{S}$  the ISOW is found in the southern basin of South Africa with contributions between 40% and 10% (Fig. 4e).

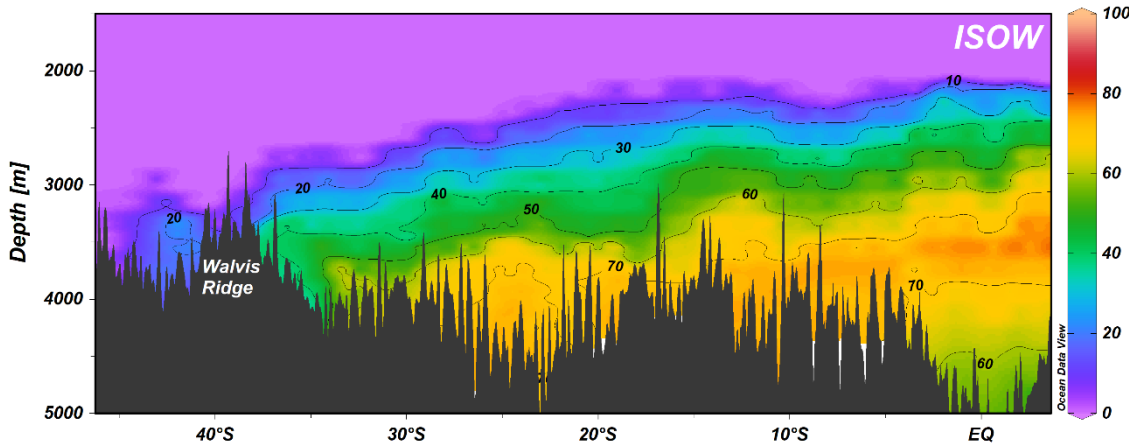


**Figure 6.** Distribution and contribution (%) of Iceland-Scotland Overflow Water (ISOW) in the Atlantic basin along the WOCE A14 section (Fig. 2a).

The distribution of DSOW shows that it is the coldest and densest of the NADW source waters, occupying the bottom layer. DSOW has a core in the bottom layers of the Greenland, Labrador and Irminger basins, with contributions between 90% and 50%. South of about 36°N the DSOW distribution shows values below 30% from 3500 m to the bottom layer ([Fig. 5c](#)). From 10°S to ~38°S, the DSOW decreases its concentration and presents values of up to 10% ([Fig. 4f](#)). The DSOW distribution shows higher contributions (30% - 20%) in the western Mid-Atlantic Ridge ([Fig. 4f](#)), whereas in the eastern Mid-Atlantic Ridge its contributions are relatively lower due to higher ISOW contributions. The DSOW in the Angola basin shows higher contributions due to the lower presence of ISOW ([Fig. 4f](#)).

The MW is mainly found in the intermediate layers of the Iberian basin, with the highest concentrations of this water mass found near 36°N in the Iberian basin at 1500 m with contributions reaching 85% ([Fig. 7a](#)). From 1800 m to 2000 m, MW presents a contribution of around ~45% ([Fig. 7b](#)) and as depth increases its contribution decreases. Part of the MW spreads to the north, with contributions of 80% to the south of Portugal and 50% to the north of Spain ([Fig. 7a](#)). Another part spreads westward towards the central Atlantic with contributions from ~40% at 1500 m ([Figs. 5d and 7a](#)) to 20% at 2000 m ([Fig. 5d](#)). The MW extends to approximately 30°S with a contribution of ~5% ([Figs. 5d and 7a](#)).

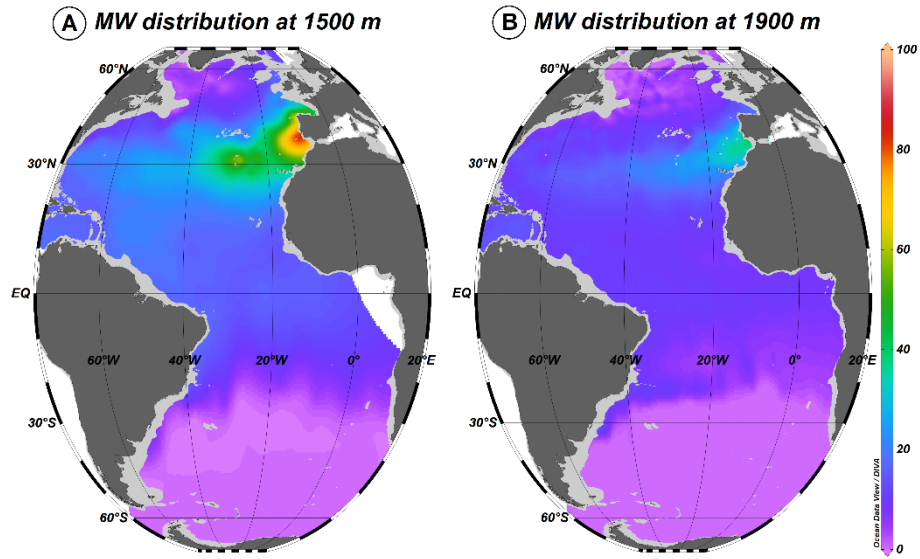


**Figure 7.** Distribution and contribution (%) of North Atlantic Deep Water (NADW) source water in the Atlantic basin. Mediterranean Water (MW) at (a) 1500 m and (b) 1900 m.

The WSDW and WSBW dominate the bottom layer of the South Atlantic and the Antarctic basins. The WSDW is the lightest variety of AABW and presents high contributions (greater than 90%) from 1500 m to the bottom layers (Figs. 8a, b and 9a). South of 60°S at depths greater than 3500 m the contribution of WSDW is lower (less than 60%) (Figs. 8a, b and 9a). The WSDW distribution on the western boundary shows high contributions up to approximately 30°S with values above 80% and from 30°S onwards the contribution of this water mass gradually decreases (Fig. 8a and b). The WSDW contribution decreases from 70% in the Cape Basin to ~25% in the Angola basin (Fig. 8b), whereas on the western boundary WSDW shows contributions above 80% at ~30°S and 70% - 60% at tropical latitudes (Fig. 8a and b). North of the equator, the WSDW extends to approximately 50°N, reaching contributions of 10% at depths greater than 3600 m (Figs. 8a, b and 9a). The WSBW core is mainly found below 4000 m depth at latitudes higher than 60°S with values above 60% (Figs. 8c, d and 9b). This water mass is the densest variety of the AABW in the Atlantic basin (Johnson, 2008) and extends to near 50°S with a contribution of ~6% (Figs. 8c, d and 9b).

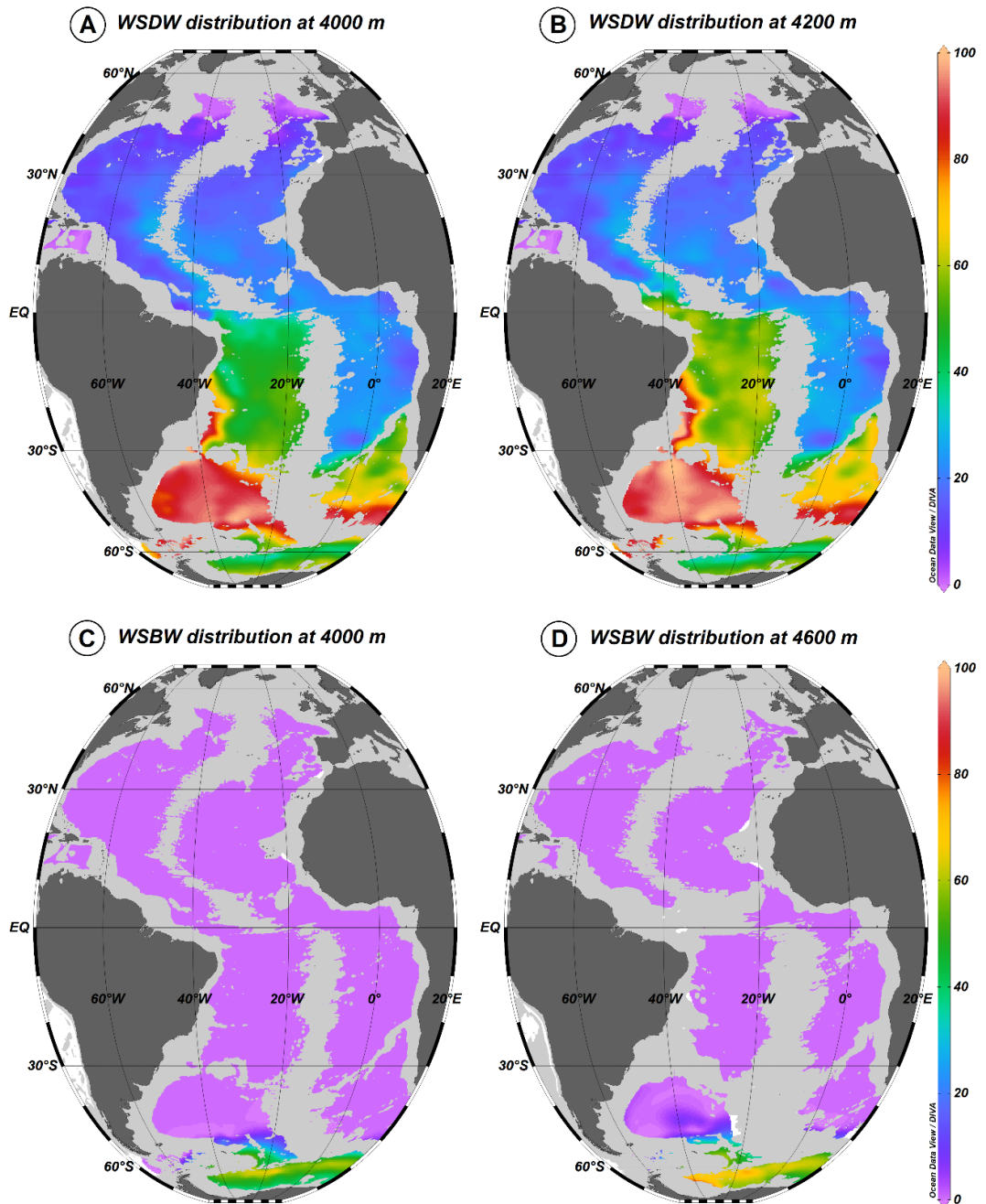


**Figure 8.** Distribution and contribution (%) of Antarctic Bottom Water (AABW) source waters in the Atlantic basin. Weddell Sea Deep Water (WSDW) at (a) 4000 m and (b) 4200 m. Weddell Sea Bottom Water (WSBW) at (c) 4000 m and (d) 4600 m.

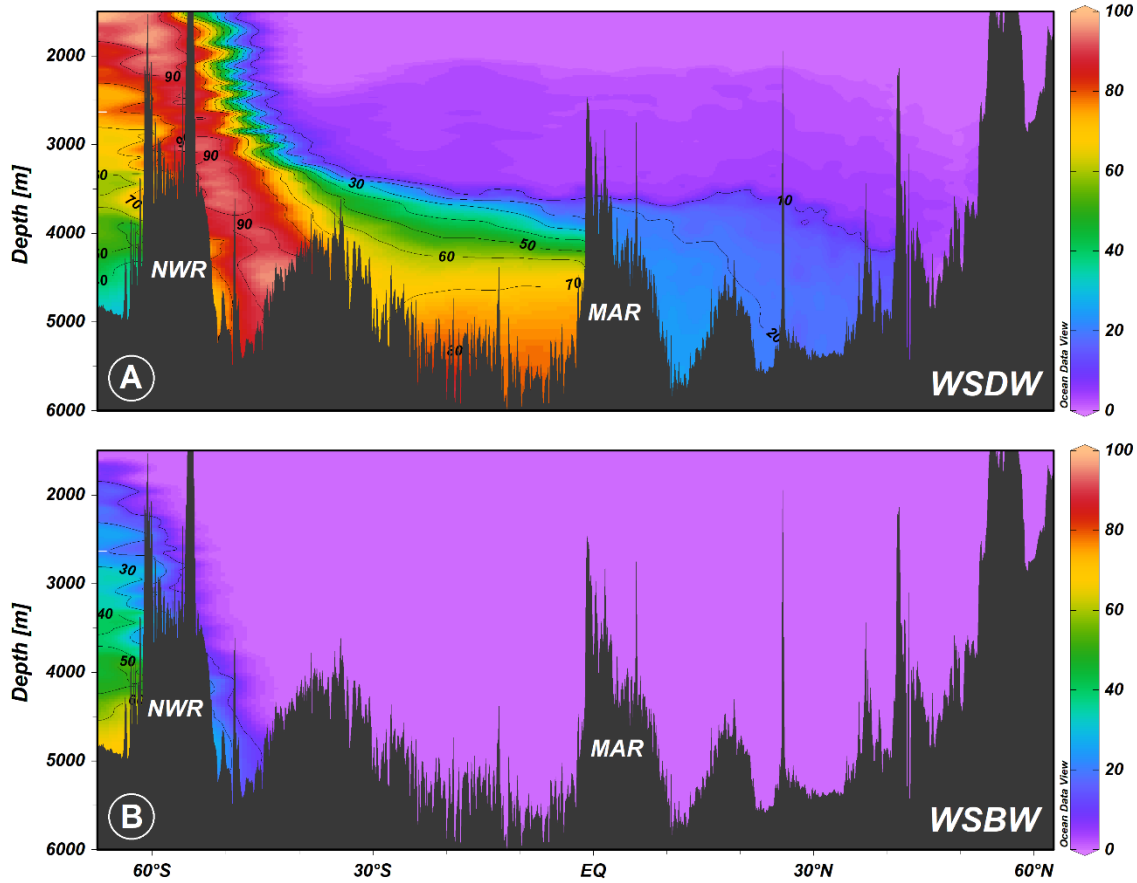


**Figure 9.** Distribution and contribution (%) of Antarctic Bottom Water (AABW) source waters in the Atlantic basin along the WOCE A16 section (Fig. 2a). The names of the source waters type (SWT) are on the bathymetry: (a) Weddell Sea Deep Water (WSDW), and (b) Weddell Sea Bottom Water (WSBW). The acronyms of the bathymetric features are the North Weddell Ridge (NWR) and Mid-Atlantic Ridge (MAR).

#### 4.4.2. Water mass distributions in the Indian basin

Total contributions were quantified in the western and eastern Indian Ocean basins. The WSDW and LSW showed the largest contributions in the western and eastern basins of the Indian Ocean (Table 2), highlighting the dominance of these waters in relation to the other source waters analyzed in these basins (ISOW, WSBW and ADLBW).

The LSW fraction is mainly found between 1800 m and 3000 m with contributions between 65% and 30% (Figs. 10a and 12a). This water mass extends from ~60°S to the north of the Indian basin with maximum contribution (65%) found between 40°S and 10°S between 2000 m and 2500 m (Figs. 10a

and Fig. 12a). The distribution of the LSW shows relatively high contributions in the Mozambique, Madagascar and Australian basins, suggesting a main northward path of the LSW across the western and eastern Indian basin (Fig. 10a). In the north of the equator, the LSW values vary around 55% between 1800 m and 2400 m, whereas below 2400 m to 4000 m the values found are between ~50% and ~15% (Fig. 12a). Throughout the Indian basin, the LSW reduces its contribution (up to ~30%) at depths greater than 4000 m (Fig. 12a). The ISOW fraction in the Indian basin reaches values of up to 11% and is restricted to depths greater than 2500 m with greater distribution at depths around 4000 m (Figs. 10c and 12b). This water mass is found in the Mozambique basin, where it reaches its maximum extent near 25°S with contributions of around ~10% (Fig. 10b and c). However, part of the ISOW is found south of 50°S in the western and eastern Indian and Antarctic basins (Fig. 10b and c).

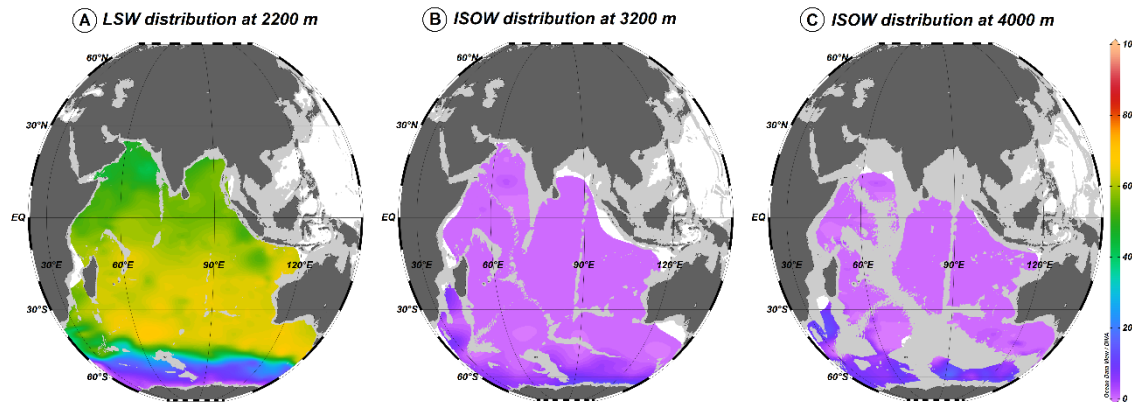


**Figure 10.** Distribution and contribution (%) of North Atlantic Deep Water (NADW) source waters in the Indian basin. Labrador Sea Water (LSW) at (a) 2200 m. Iceland-Scotland Overflow Water (ISOW) at (b) 3200 m and (c) 4000 m.

The WSDW fills much of the bottom of the Indian basin, with a total contribution of  $57 \pm 12\%$ , with maximum values around 80% and 85% between 3000 m and 3500 m in the eastern and central Indian basin (Fig. 11a), and below 3500 m WSDW shows a contribution of approximately 70%, dominating the bottom layer of the Indian basin (Figs. 11b and 12c). The WSDW shows

contributions around 70% at 2000 m in the Antarctic basin, however from  $\sim 50^{\circ}$ S its contribution decreases above this depth and the highest WSDW values are found in the bottom layers (Fig. 12c).

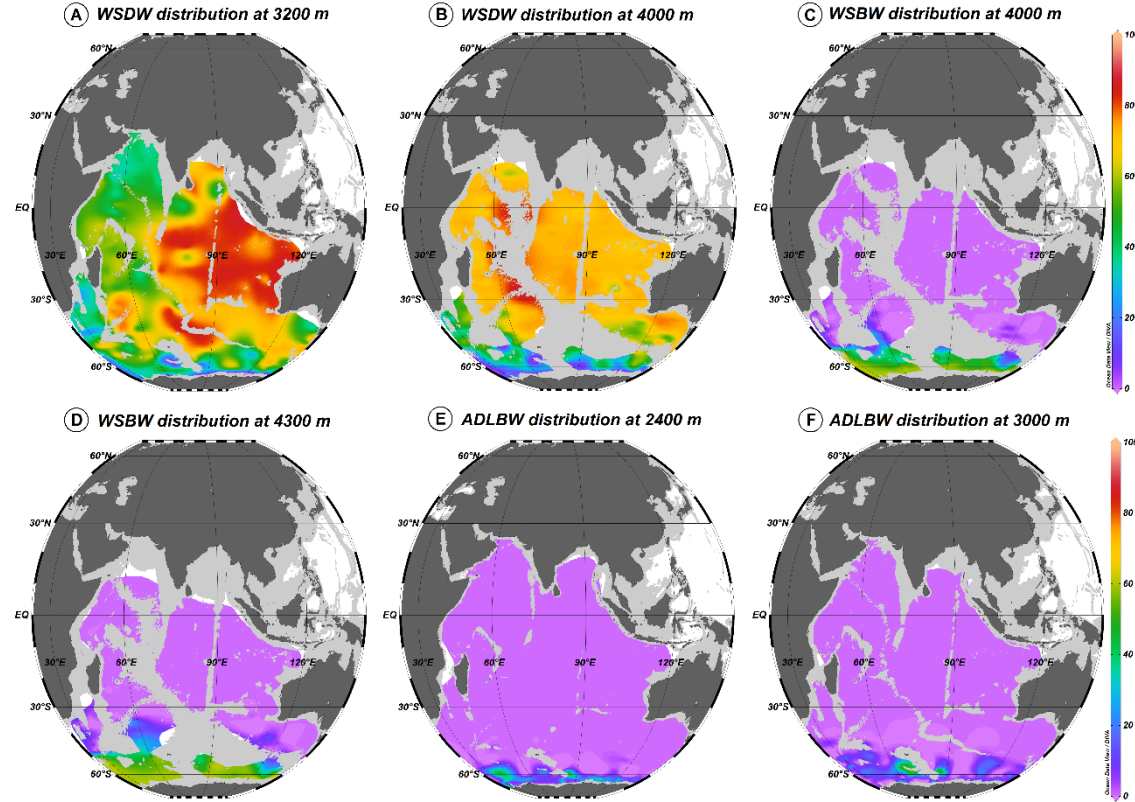


**Figure 11.** Distribution and contribution (%) of Antarctic Bottom Water (AABW) source waters in the Indian basin. Weddell Sea Deep Water (WSDW) (a) at 3200 m and (b) 4000 m. Weddell Sea Bottom Water (WSBW) (c) at 4000 m and (d) 4300 m. Adelie Land Bottom Water (ADLBW) (e) at 2400 and (f) 3000 m.

Fractions of the WSBW and ADLBW contribute a total of  $8.1 \pm 0.3\%$  and  $2.6 \pm 0.06\%$ , respectively. The distribution of these water masses shows the dominant role of the AABW source waters in the bottom layers of the South Indian and Antarctic basins (Figs. 11c, e and 12d and e), with WSBW achieving contributions of up to 60% at 4000 m (Fig. 11c), whereas the ADLBW fraction only exceeds 30% from  $\sim 2400$  m to 3000 m (Fig. 11e and f).

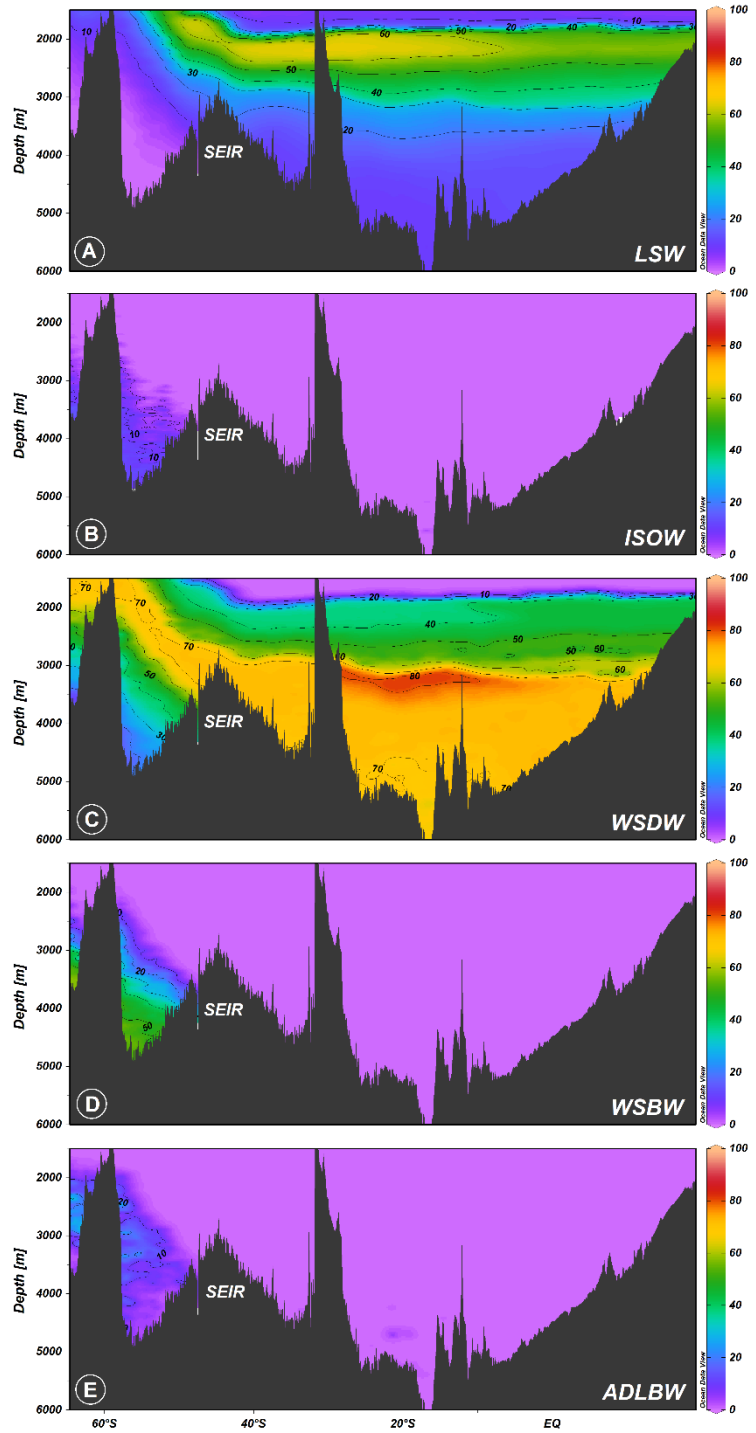


**Figure 12.** Distribution and contribution (%) of North Atlantic Deep Water (NADW) and Antarctic Bottom Water (AABW) source waters in the Indian basin along the WOCE I09N and I08S sections (Fig. 2a). The names of the source waters type (SWT) are on the bathymetry: (a) Labrador Sea Water (LSW), (b) Iceland-Scotland Overflow Water (ISOW), (c) Weddell Sea Deep Water (WSDW), (d) Weddell Sea Bottom Water (WSBW), and (e) Adelie Land Bottom Water (ADLBW). The acronym of the bathymetric feature is the Southeast Indian Ridge (SEIR).

The WSBW fraction extends up to  $\sim 35^{\circ}\text{S}$  at 4300 m in the southwest Indian basin, reaching values of up to 10% contribution, while much of its contribution is

restricted to south of 50°S ([Fig. 11c, d and 12d](#)). The distribution of ADLBW also shows a limit of ~50°S in its extension to the north ([Fig. 11e, f and 12e](#)).

#### *4.4.3. Water mass distributions in the Pacific basin*

Total contributions were quantified in the western and eastern Atlantic Ocean basins. The WSDW and LSW showed the largest contributions in the western and eastern basins of the Pacific Ocean ([Table 2](#)), highlighting the dominance of these waters in relation to the other source waters analyzed in these basins (ISOW, RSBW and ADLBW).

Relatively high LSW contributions are found in the western South Pacific basin and as it spreads eastward its contribution shows a short decrease ([Fig. 13a](#)). At depths around 2200 m the LSW shows a decrease in its contribution as it spreads towards the North Pacific basin ([Figs. 13a and 14a](#)). Between approximately 58°S and 48°S, between 1500 m and 3400 m, the LSW fraction shows higher contributions (50%) and below 3400 m the contributions vary around 41% and 25% ([Fig. 14a](#)). Below 3400 m from 30°S to the North Pacific basin the contribution of the LSW vary around 41% and 38% ([Fig. 14a](#)). From the Southern Pacific basin to ~35°N the LSW above 2200 m shows contributions of ~40% and north of 35°N the LSW above 2200 m has values up to 30% ([Fig. 14a](#)). Above ~1700 m the LSW is enriched in the equatorial region, reaching values of up to 50% ([Fig. 14a](#)). The ISOW is restricted to approximately 60°S south of the Pacific Antarctic Ridge ([Fig. 13b](#)) and shows contributions ranging from 2% to ~10% from 2000 m to the bottom layers, with a core between 2800 m and 3200 m ([Fig. 14b](#)).

The WSDW fraction fills much of the bottom of the Pacific basin, with a total contribution of  $55.3 \pm 11\%$ , with maximum values above 70% below 3000 m ([Fig.](#)

13c). In the western Pacific basin, the maximum WSDW contribution (~70%) extends near to the equator, while in the eastern basin the maximum contribution extends to near 35°S (Fig. 13c). In the northern, western, and eastern Pacific basins, at depths below 3200 m the WSDW contributions reach values of 60% and above this depth the WSDW contribution decreases, reaching values of 50% at 3000 m to below 15% at 1600 m (Fig. 14c).

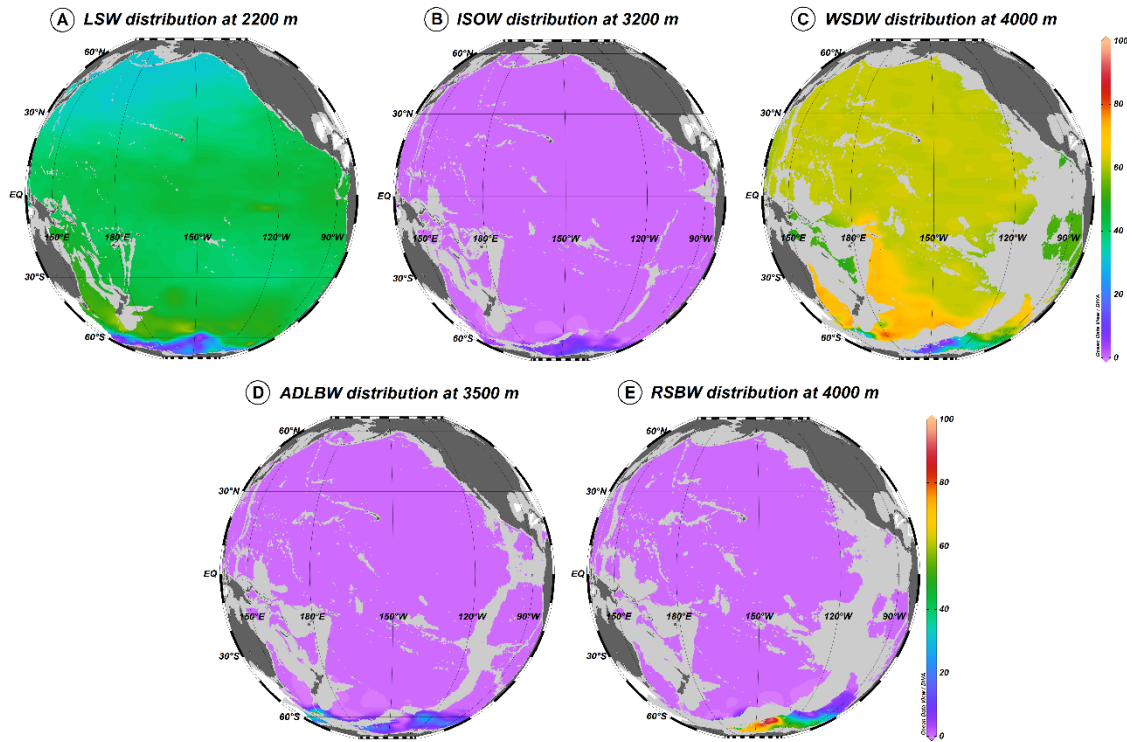


**Figure 13.** Distribution and contribution (%) of North Atlantic Deep Water (NADW) and Antarctic Bottom Water (AABW) source waters in the Indian basin. Labrador Sea Water (LSW) (a) at 2200 m and, Iceland-Scotland Overflow Water (ISOw) (b) at 3200 m. Weddell Sea Deep Water (WSDW) at (c) 4000 m, Adelie Land Bottom Water (ADLBW) (d) at 3500 m and, Ross Sea Bottom Water (RSBW) (e) at 4000.

Fractions of the ADLBW and the RSBW contribute a total of  $1.6 \pm 0.1\%$  and  $0.8 \pm 0.2\%$ , respectively. As in the Indian basin, these waters are distributed mainly south of 60°S of the Pacific Ocean basin, with ADLBW contributing 40% at ~3500 m near Adelie Land (Fig. 13d), whereas RSBW shows maximum contribution from 60% to 90% below 3500 m (Fig. 13e) and contributions of 30% at depths above 2600 m (Fig. 14 e).

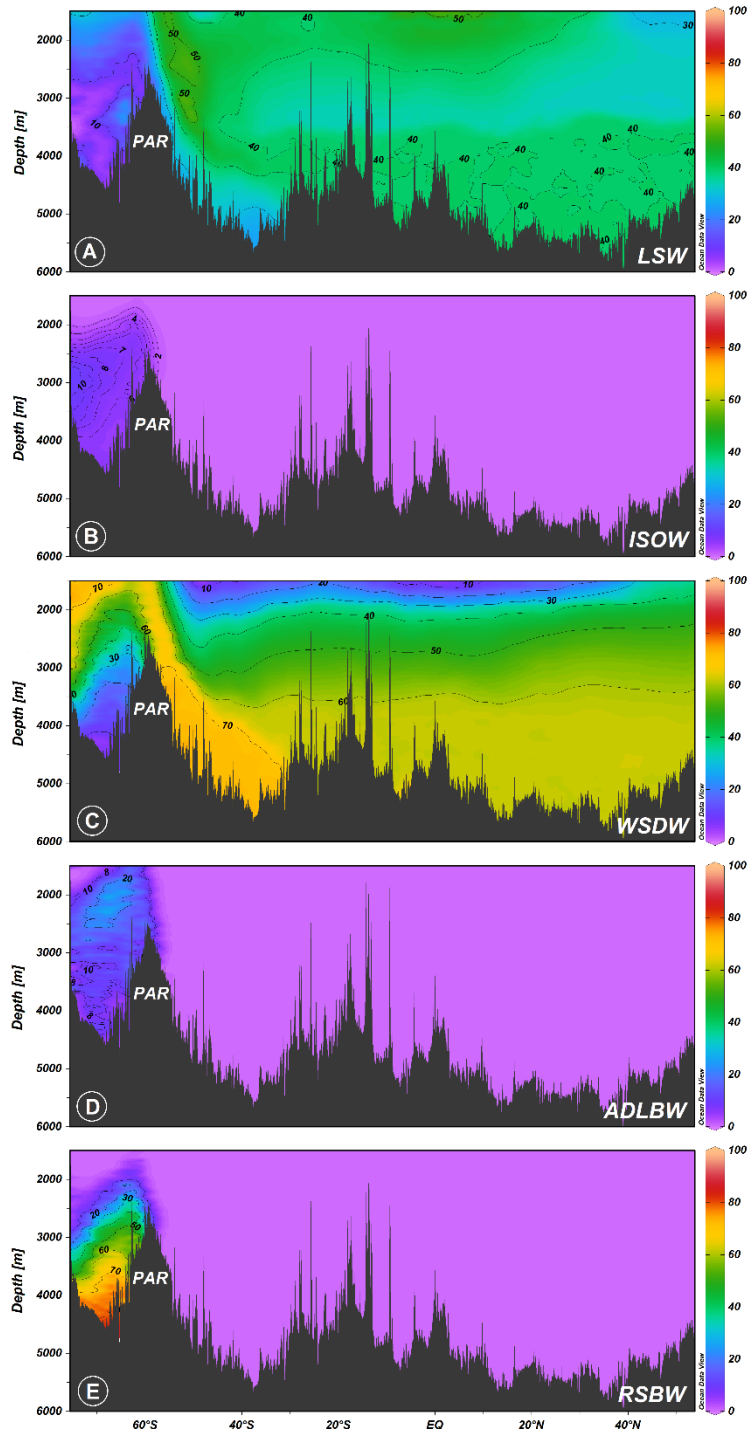


**Figure 14.** Distribution and contribution (%) of North Atlantic Deep Water (NADW) and Antarctic Bottom Water (AABW) source waters in the Pacific basin along the WOCE P16 section (Fig. 2a). The names of the source waters type (SWT) are on the bathymetry: (a) Labrador Sea Water (LSW), (b) Iceland-Scotland Overflow Water (ISOW), (c) Weddell Sea Deep Water (WSDW), (d) Adelie Land Bottom Water (ADLBW), and (e) Ross Sea Bottom Water (RSBW). The acronym of the bathymetric feature is the Pacific Antarctic Ridge (PAR).

Most of the ADLBW and RSBW are restricted south of the Pacific Antarctic Ridge at approximately 60°S (Figs. 13d, e and 14d and e). North of the Pacific

Antarctic Ridge the ADLBW extends to ~55°S with values up to 40% in the southwest Pacific basin near Adelie Land ([Fig. 13e](#)).

## 4.5. Discussion

### 4.5.1. Water mass distributions in the Atlantic basin

The distribution of the LSW, ISOW and DSOW in the Nordic and Labrador Seas ([Fig. 4a, b, c, d, e and f](#)) agree with studies on their paths (e.g., [García-Ibáñez et al., 2015](#); [Biló and Johns, 2019](#); [Bower et al., 2019](#)) indicating the recirculation of these water masses to the north through the North Atlantic Current ([Zou et al., 2020](#); [Bower et al., 2019](#)). The LSW fraction reaches greater depths at the western boundary of the North Atlantic basin up to ~30°N ([Fig. 4b](#)), which is a region where the Deep Western Boundary Current (DWBC) carries LSW from its site of formation to the south along the western boundary ([Stramma et al., 2004](#); [Yashayaev, 2007](#)). From ~30°N the LSW contributions are at similar depth levels at the western and eastern boundary of the Atlantic basin ([Fig. 4b](#)), which apparently agrees with the northward recirculation of DWBC, decreasing the transport within the DWBC ([Lozier 1997](#); [Schott et al., 2006](#)). The LSW also shows high contributions (~70%) at the eastern boundary of the North Atlantic ([Figs. 4a and 5a](#)), indicating eastward flow over the Mid-Atlantic Ridge by North Atlantic Current ([Lozier, 1997](#); [Bower et al., 2009](#); [Biló and Johns, 2019](#)), consistent with studies on interior recirculation pathways in LSW export to the subtropical gyre ([Zou and Lozier, 2016](#); [Bower et al., 2019](#)). The LSW is found between 1500 m and ~4000 m with largest contributions at ~2200 m ([Fig. 5a](#)), agreeing with studies on its distribution in the Atlantic Ocean (e.g., [Johnson, 2008](#); [Ferreira and Kerr, 2017](#); [Romera-Castillo et al., 2022](#)), this water mass is one of the source waters of NADW and is considered as the main origin of the

upper NADW (Talley et al., 2011). The upward flow of LSW near the ACC to shallower depths (Fig. 5a), likely causes an increase in its contribution in the South Atlantic between 40°S and 50°S (Ferreira and Kerr, 2017). The Ekman transport generated by wind stress in the surface layers is responsible for causing the upwelling of deeper waters (Rintoul et al., 2001). Furthermore, the deepening of isopycnals observed at ~40°S (Figs. 4a, b, c and 5a) is due to the subtropical gyre (Talley et al., 2011) and the presence of AAIW in this area, which also suggests an increase in contribution from LSW (Ferreira and Kerr, 2017). This LSW deepening behavior is also evident in other studies (e.g., Ferreira and Kerr, 2017; Romera-Castillo et al., 2022). Once outcropped into the upper ocean in the Antarctic basin, the LSW becomes a source of AABW (Talley, 2013). The presence of LSW in the Cape Basin (Fig. 4a, b and c), suggests that fractions of this water mass exit the South Atlantic basin via southern South Africa (Arhan et al., 2003; van Sebille et al., 2012; Garzoli et al., 2015).

The distribution of ISOW and DSOW across Iceland, Irminger and Labrador basins (Fig. 4d, e and f) agrees with studies on their transport by the DWBC before continuing towards the equator (Bower et al., 2019; Zou et al., 2020). Interior ISOW pathways in the North Atlantic show westward flow through the Charlie-Gibbs Fracture Zone, spreading toward the Irminger and Labrador Basins (Fig. 4d) via cyclonic flow west of the Reykjanes Ridge (Stramma et al., 2004; Lozier et al., 2022) explaining the presence of ISOW in the Irminger and Labrador Basins (Fig. 5c). The southward transport of the ISOW by the DWBC likely contributes to the largest contributions of this water mass at the western boundary of the North Atlantic basin, whereas at the eastern boundary it flows equatorward following a dominant flow (Fleischmann et al., 2001; Zou et al., 2017, 2020) with

minor contributions ([Fig. 4e](#)). In the eastern South Atlantic basin, the ISOW is blocked by the Walvis Ridge ([Fig. 6](#)), which explains the lower contributions in the Cape basin. ISOW make up the lower NADW and is present in the bottom layer of the North Atlantic basin, which does not happen in most of the South Atlantic basin, where denser water masses (DSOW and WSDW) are present in these depths ([Figs. 5c and 9a](#)). The DSOW was found in the Labrador Sea at 3800 m ([Fig. 4f](#)) is possibly advected along the deep boundary currents of the Irminger Sea to Labrador Sea ([Lozier et al., 2022](#)). Model results showed the DSOW spread into the interior of the Labrador Sea from the Greenland side, likely due to topographic interactions ([Xu et al., 2015; Lozier et al., 2022](#)). The distribution of DSOW in the North Atlantic basin ([Fig. 4f](#)) with a predominant presence in the western basin suggests a dominant transport to the south by the deep boundary current according to studies on its paths (e.g., [Lozier et al., 2022](#)). Southward transport of DSOW along the DWBC and interior pathways are likely impacted by eddy-driven recirculations within the North Atlantic basin ([Lozier, 1997; Gary et al., 2012](#)) and its highest density among the NADW source waters makes it spread through layers of bottom close to the ground ([Fig. 5c](#)). The LSW, ISOW and DSOW spread south in the zonal direction transported mainly by the DWBC ([Bower et al., 2019](#)), covering the deep and overflow layers as distributions shown in the Atlantic Ocean basin ([Fig. 4a, b, c, d, e and f](#)). However, it is likely that only LSW and part of ISOW are exported and mixed within other ocean basins from ACC, while DSOW is restricted to the Atlantic basin due to its greater depth (density) and interactions with the bottom ([Fig. 5c](#)). The MW enters the North Atlantic through the Strait of Gibraltar from the Mediterranean Sea ([Bozec et al., 2011](#)) with a core on the Iberian basin shelf ([Fig. 7a](#)). Its distribution

is associated with a northward advective flow (Reid, 1979) and westward transport by meddies (Mazé et al., 1997), consistent with the distribution presented here (Fig. 7a and b). In regions far from the MW core (zonal direction and deeper regions) the presence of LSW fractions induces a decrease in MW, suggesting a mixing between these water masses (Figs. 5d and 7a and b).

The distribution pattern of the WSBW and WSDW along their paths suggests their interaction with sills and narrow passages of the ocean floor in addition to mixing processes (Bryden and Nurser, 2003; Solodoch et al., 2022). The WSBW is blocked by the North Weddell Ridge and the Southwest Indian Ridge and is restricted to ~50°S (Figs. 8c, d and 9b), whereas the more buoyant and warmer WSDW has a greater range spreading northward (Figs. 8a, b and 9a), consistent with the study by Ferreira and Kerr (2017). In the bottom layer south of North Weddell Ridge and Southwest Indian Ridge, the presence of dense WSBW induces a decrease in WSDW (Figs. 8a, b, c, d and 9b), respecting mass conservation. The distribution of WSDW and WSBW shows the main route of AABW into the South Atlantic basin through passages in the Scotia Sea and the South Sandwich Trench (Figs. 8a, b, c and d), whereas on the eastern boundary part of the WSDW is bounded by the Walvis Ridge in the Angola Basin (Fig. 8a and b), these pathways are consistent with the available observations about AABW (Johnson, 2008; Meredith et al., 2013; Ferreira and Kerr, 2017). The lower WSDW contributions from ~30°S on the western boundary suggest its blocking by the bottom topography (Fig. 8a and b). The WSDW found in the Argentina basin spreads into the Brazil basin through the Vema Channel (Fig. 8b), the main pathway for the northward flow of AABW (Talley et al., 2011; Morozov et al., 2018; Campos et al., 2021), where it is exported via the deep

western boundary current and through recirculation pathways within the basins (Reid, 1994; 1997; Talley et al., 2011; Purkey et al., 2018). The contribution of WSDW decreases as it spreads northward, suggesting its absorption by NADW, highlighting the influence of WSDW on deep water mixing at high latitudes (Figs. 8a, b and 9a). Here, WSDW mixes most strongly with DSOW and ISOW in the North Atlantic basin at higher depths (greater than 4000 m), whereas mixing with LSW occurs at 60°S between 1500 m and 4000 m (Figs. 5a, b, c and 9a), supporting that AABW mixes with lighter overlying waters (Johnson, 2008). The presence of WSDW and WSBW at the extremities of the eastern South Atlantic basin (Fig. 8a, b, c and d), supports eastward transport of AABW through the ACC, spreading into the Indian and Pacific basins (Reid and Lynn, 1971; Johnson, 2008).

#### 4.5.2. Water mass distributions in the Indian basin

The distribution of LSW shows it spreading from South Africa (Yuzhu, 2000) to join the eastward flow in the South Indian basin and a portion spreading northward into the southwest Indian basin, mainly through the Mozambique and Madagascar basins (Fig. 10a), consistent with NADW studies (e.g., Johnson, 2008; Talley et al., 2013). Part of the LSW that enters the ACC emerges at the sea surface (Fig. 12a) in regions south of the ACC, contributing to mixing with AABW water masses (Talley et al., 2013). In the eastern Indian basin, the LSW carried by the ACC appears to spread northward above the Southeast Indian Ridge and across the Australian basin to afterwards fill the eastern and central Indian basins up to the Bengal basin (Fig. 10a), consistent with available studies on NADW (e.g., Johnson, 2008; Talley et al., 2013). The reduction in LSW contribution as depth and northward latitude increase indicates the presence of

WSDW that dominates the bottom layer in the Indian basin (Fig. 12a), which is corroborated by other studies (Aoki et al., 2020; Strass et al., 2020). The ISOW shows low signal in the Mozambique basin and south of 50° (Fig. 10b and c), suggesting strong mixing with other water masses in these areas. South of 50°S in the southwestern Indian basin, ISOW appears to spread southward through Southwest Indian Ridge gaps and is restricted to the east, southern of the Southeast Indian Ridge, suggesting its blockage by Southeast Indian Ridge (Fig. 10b, c and 12b). Considered a denser mass of water than LSW, the ISOW showed a shorter range into the Indian basin from its formation area (Fig. 10b and c).

The distribution of WSDW in the Indian basin shows a cascade deepening in the Antarctic basin from 1500 m to the bottom layer, showing a northward spreading from the shallower layers to the bottom layers (Fig. 12c), as evidenced by Johnson (2008) for the AABW. The AABW carried by the ACC distributes northward into the western and eastern Indian basins (Talley et al., 2013). The northward flow of AABW from the ACC is strongly influenced by the bathymetry of the Southwest Indian Ridge (Boswell and Smythe-Wright, 2002), suggesting that high WSDW contributions east of Madagascar (Fig. 11b) indicates a northward flow exiting the southern flank through gaps in the Southwest Indian Ridge (Kolla et al., 1976). Therefore, this may be a main pathway of the WSDW northward along the western Indian basin to reach the Somali and Arabian bays (e.g., Johnson, 2008). On the other hand, some fraction of the WSDW coming from the South African basin spreads to the Agulhas and Mozambique basins where it is recirculated and restricted by the Madagascar Ridge (Fig. 11a and b; Barker and Heezen, 1973; Kolla et al., 1976), consistent with studies on the

distribution of Southern Ocean bottom waters (e.g., [Johnson, 2008](#); [Solodoch et al., 2022](#)). In the eastern portion of the South Indian basin, part of the WSDW probably transported by the ACC ([Solodoch et al., 2022](#)), spreads northward across the Southeast Indian Ridge and enters the southern Australian basin, spreading northward into the eastern and central Indian basins, whereas another part spreads to the Pacific basin, according to studies on the distribution of AABW (e.g., [Kennett and Watkins, 1975](#); [Kolla et al., 1976](#); [Johnson, 2008](#)). Although the distribution of WSDW in the central and eastern Indian Ocean basins is close to the distributions of AABW found by Johnson (2008), the high contribution from WSDW at 3000 m ([Figs. 11a and 12c](#)) may indicate a patchiness in the water mass concentration estimates, as contributions from CDW (water mass not analyzed here) can influence the mixing of water masses at this depth (e.g., [Yuzhu, 2000](#)). The WSBW and ADLBW are restricted to the South Indian basin, suggesting the blockage of these water masses by the Southwest Indian Ridge and the Southeast Indian Ridge ([Figs. 11d, e, f and 12d and e](#)). Adelie-sourced AABW is recirculated on the Kerguelen Plateau to the east ([Solodoch et al., 2022](#)), whereas some part of it extends westward along latitude ~60°S ([Fig. 11e and f](#)). The presence of WSBW in the eastern portion of the South Indian basin ([Fig. 11c and d](#)) may indicate its eastward transport by the ACC along with other AABW source waters, consistent with the available observations ([Johnson, 2008](#); [Pardo et al., 2012](#)).

#### *4.5.3. Water mass distributions in the Pacific basin*

The distribution of the LSW shows it spreading from southern Australia to eastward in the South Pacific basin and northward mainly east of Australia ([Figs. 13a](#)). As it spreads eastward into the South Pacific basin the LSW mixes

with the surrounding waters in the circumpolar region (Broecker et al., 1998). Part of the LSW that enters the ACC emerges at the sea surface in regions south of the ACC (Fig. 14a), contributing to the production of AABW (Talley et al., 2013). In the eastern Pacific basin, LSW carried by the ACC appears to spread far east above the East Pacific Rise, to afterwards fill this area (Fig. 13a), consistent with studies about the NADW (e.g., Nakano and Sugino, 2002; Johnson, 2008). In the interior layers throughout almost the entire extent of the Pacific basin, it is suggested that the LSW presents strong mixing with the WSDW, as they are the two main water masses found in this region (Fig. 14a and c) and the decrease in the contribution of the LSW in the upper layers from ~35°N indicates the presence of WSDW and NPIW in this region (Fig. 14a and c). The high contribution from the LSW above 1800 m in the equatorial region (Fig. 14a) may indicate a patchiness in the water mass concentration estimates, as contribution of UCDW (not considered in the analysis) can influence the mixing of water masses at this depth (e.g., Fuhr et al., 2021). It is suggested that the ISOW, the densest branch of NADW carried by the ACC, is constrained south of 60°S by the Pacific Antarctic Ridge and as it spreads eastwards its contribution decreases (Fig. 13b), which can be explained by the presence of other masses of water in this region, suggesting its mixture with the AABW varieties, as available studies on NADW have shown (Broecker et al., 1998, Talley et al., 2013).

The distribution of WSDW in the Pacific basin shows a cascade deepening in the Antarctic basin from 1500 m to the bottom layer, showing a northward spreading from the shallower layers to the bottom layers (Fig. 14c), as evidenced by Johnson (2008) for the AABW. The WSDW is carried by the ACC in an eastward flow and spreads from southeastern Australia in deep layers (Solodoch

et al., 2022) to fill the floor of the Pacific basin (Fig. 13c), consistent with studies on AABW (e.g., Johnson, 2008; Rintoul, 2012; Talley et al., 2013). The high contributions in the western South Pacific basin indicate a main northward path of AABW (Fig. 13c; e.g., Johnson, 2008; Solodoch et al., 2022). The presence of WSDW in the eastern portion of the South Pacific, may indicate its eastward flow through the Drake Passage (Fig. 13c). However, its low contributions in the Chile and Peru basins indicate its blockage by the East Pacific Rise and the Chile Ridge (Fig. 13c), consistent with the results of available studies (Nakano and Sugino, 2002; Johnson, 2008). In the North Pacific basin, WSDW shows a decrease in its contribution (Fig. 13c), suggesting its mixing with the LSW.

The ADLBW and RSBW are restricted south of 60°S, suggesting their blockages by the Pacific Antarctic Ridge and the East Pacific Rise (Figs. 13d, e and 14d and e), consistent with the study by Pardo et al. (2012). However, some eastward advected ADLBW crosses the Pacific Antarctic Ridge and spreads toward the Campbell Plateau (Solodoch et al., 2022), whereas south of the East Pacific Rise its signal is almost lost (Fig. 13d). The RSBW shows an eastward spread south of ~60°, with contributions close to the Drake Passage (Fig. 13e; Pardo et al., 2012). However, the RSBW advection moves part of it westward near the coast (Orsi et al., 1999), pushing the ADLBW from its formation region in the bottom layers (Pardo et al., 2012).

#### 4.6. Conclusions

In this study we show the use of OMP mixing analysis to determine the distribution and quantify the contribution of NADW and AABW source waters in the Atlantic, Indian, and Pacific basins. The choice of source water masses and their indices is appropriate, considering residuals up to 10% for OMP

applications. The results evidence that LSW and ISOW presented greater total contributions than DSOW and MW in the Atlantic basins. Furthermore, LSW and ISOW are the major source water masses of NADW that spread to the Indian and Pacific basins. Which confirms the mixing and export of these waters within the ACC in the South Atlantic basin, with LSW being the dominant water mass of NADW. On the other hand, the dominant source water of AABW is the WSDW, found throughout the global ocean. It extends to approximately 50°N in the Atlantic basin, where it is absorbed by NADW source waters in the bottom layers. The LSW and WSDW are the dominant waters in the global ocean contributing to the deep layers in the oceanic basins, and they show similar export paths from the South Atlantic basin, spreading to the Indian Ocean basin and subsequently to the Pacific Ocean basin through the east to west current system. In these basins, they also spread northward, with WSDW spreading mainly along the western basins in the lower layers. The ISOW showed a pathway through the Mozambique basin, extending to ~38°S in the southwestern Indian basin. ISOW contributions were also observed south of 50°S in the Indian and Pacific basins, always with low signals, indicating its mixing with other water masses. The WSBW extends up to ~50°S in the western South Atlantic basin and up to ~35°S in the western Indian basin. South of 50°S in the southeastern Indian basin the WSBW is blocked by the Southeast Indian Ridge. The ADLBW showed low contributions in the Indian and Pacific Ocean basins in relation to the Weddell Sea source waters, in agreement with the study by [Solodoch et al. \(2022\)](#), which showed lower concentrations for ADLBW in the Indian basin. This water mass was restricted to the south of the Indian and Pacific basins by the ridges present

in these areas. The same happens with RSBW, which is found in the Pacific basin and is limited to 60°S by Pacific Antarctic Ridge.

Additionally, the results of this work provide useful information to support future climate studies involving modeling and biogeochemistry. New insights into the distribution and major contribution of source waters in the global deep ocean have been gained, mainly in context of upwelling diapycnal mixing. The largest contributions and wider ranges in distributions show that LSW and WSDW are the main source water masses contributing to NADW and AABW layers, respectively. These findings contribute to the understanding of the main source waters in the Global Ocean and how they evolve during their transport (e.g., mixing and pathways). Finally, the distribution and quantification of NADW and AABW source waters provide new information about deep circulation and upwelling diapycnal mixing in ocean basins.

### **Declaration of competing interest**

The authors declare that they have no known competing financial interests or personal relationships that could have appeared to influence the work reported in this paper.

### **Acknowledgements**

This study provides a contribution to the activities of the Brazilian High Latitudes Oceanography Group (GOAL; [www.goal.furg.br](http://www.goal.furg.br)), which is part of the Brazilian Antarctic Program (PROANTAR). GOAL has been funded by and/or has received logistical support from the Brazilian Ministry of the Environment (MMA), the Brazilian Ministry of Science, Technology, and Innovation (MCTI), the Brazilian Navy, the Secretariat of the Interministerial Commission for the

Resources of the Sea (SECIRM), and the Council for Research and Scientific Development of Brazil (CNPq) through grants from the Brazilian National Institute of Science and Technology of Cryosphere (INCT-CRIOSFERA; CNPq Grants nos. 573720/2008-8 and 465680/2014-3; FAPERGS Grant no. 17/2551-0000518-0), NAUTILUS, INTERBIOTA, PROVOCCAR, ECOPELAGOS, PRO-SAMBA and IMPACTANT projects (CNPq Grants nos. 405869/2013-4, 407889/2013-2, 442628/2018-8, 442637/2018-7, 440859/2023-9 and 440865/2023-9, respectively), and Higher Education Personnel Improvement Coordination/CMAR2 (CAPES Grant no. 23038.001421/2014-30). D.L.S acknowledges financial support from CAPES scholarship Grant no. 88887.595779/2020-00 and was supervised by R.K., who received a CNPq research Grant no. 309978/2021-1. We appreciate the availability of data from WOD and GLODAP projects.

# **Capítulo V: Síntese da Discussão e Conclusões**

Neste estudo mostramos o uso da análise OMP para determinar a distribuição e quantificar a contribuição das águas-fonte da Água Profunda do Atlântico Norte e da Água de Fundo Antártica nas bacias oceânicas do Atlântico, Índico e Pacífico. A escolha das águas-fonte e de seus índices é adequada, considerando os resíduos de até 10% para as aplicações OMP. Os resultados evidenciam que a Água do Mar de Labrador e a Água da Escócia-Islândia apresentaram maiores contribuições totais que a Água do Estreito da Dinamarca e a Água do Mediterrâneo nas bacias do Atlântico. Além disso, a Água do Mar de Labrador e a Água da Escócia-Islândia são as principais águas-fonte da Água Profunda do Atlântico Norte que se espalham pelas bacias do Índico e do Pacífico. O que confirma a mistura e exportação destas águas dentro da Corrente Circumpolar Antártica na bacia do Atlântico Sul, sendo a Água do Mar de Labrador a massa de água dominante da Água Profunda do Atlântico Norte. Por outro lado, a água-fonte dominante da Água de Fundo Antártica é a Água Profunda do Mar de Weddell, encontrada em todo o oceano global. Estende-se

até aproximadamente 50°N na bacia do Atlântico, onde é absorvida pelas águas-fonte da Água Profunda do Atlântico Norte nas camadas inferiores, principalmente pela Água da Escócia-Islândia e Água do Estreito da Dinamarca. A Água do Mar de Labrador e a Água de Fundo do Mar de Weddell são as águas dominantes no oceano global, contribuindo para as camadas profundas das bacias oceânicas, e mostram caminhos de exportação semelhantes a partir da bacia do Atlântico Sul, espalhando-se para a bacia do Oceano Índico e subsequentemente para a bacia do Oceano Pacífico através da Corrente Circumpolar Antártica. Nestas bacias, também se espalham para norte, com a Água de Fundo do Mar de Weddell a espalhar-se principalmente ao longo das bacias ocidentais nas camadas inferiores. A Água da Escócia-Islândia mostrou um caminho através da bacia de Moçambique, estendendo-se até ~38°S na bacia do sudoeste da Índia. Contribuições da Água da Escócia-Islândia também foram observadas ao sul de 50°S nas bacias do Índico e do Pacífico, sempre com sinais baixos, indicando sua mistura com outras massas de água. A Água de Fundo do Mar de Weddell estende-se até ~50°S na bacia ocidental do Atlântico Sul e até ~35°S na bacia oeste da Índia. Ao sul de 50°S na bacia do sudeste da Índia, a Água de Fundo do Mar de Weddell é bloqueada pela Southeast Indian Ridge. A Água de Fundo da Terra de Adelie apresentou baixas contribuições nas bacias dos oceanos Índico e Pacífico em relação às águas-fonte do Mar de Weddell, em concordância com o estudo de Solodoch *et al.* [2022], que mostrou menores concentrações para a Água de Fundo da Terra de Adelie na bacia do oceano Índico. Esta massa de água está restrita ao sul das bacias dos oceanos Índico e Pacífico pelas cordilheiras presentes nestas áreas.

O mesmo acontece com a Água de Fundo do Mar de Ross, que se encontra na bacia do Oceano Pacífico e é limitada a 60°S pela Pacific Antarctic Ridge.

Além disso, os resultados deste trabalho fornecem informações úteis que apoiam estudos climáticos envolvendo modelagem e biogequímica de massas de água. Foram obtidos novos conhecimentos sobre a distribuição e a principal contribuição das águas-fonte no oceano profundo global. As maiores contribuições e variações mais amplas nas distribuições mostram que a Água do Mar de Labrador e a Água Profunda do Mar de Weddell são as principais massas de água fonte que contribuem para as camadas da Água Profunda do Atlântico Norte e da Água de Fundo Antártica, respectivamente. Estas descobertas contribuem para a compreensão das principais águas-fonte no Oceano Global e como elas evoluem durante o seu transporte (por exemplo, mistura e caminhos). Finalmente, a distribuição e quantificação das águas-fonte da Água Profunda do Atlântico Norte e da Água de Fundo Antártica fornecem novas informações sobre a circulação profunda e a mistura diapicnal ascendente nas bacias oceânicas.

## **Capítulo VI: Referências Bibliográficas**

Almeida L, Azevedo JLL, Kerr R, Araujo M, Mata MM (2018) Impact of the new equation of state of seawater (TEOS-10) on the estimates of water mass mixture and meridional transport in the Atlantic Ocean. *Prog Oceanogr* 162:13-24. doi.org/10.1016/j.pocean.2018.02.008

Anderson LA, Sarmiento JL (1994) Redfield ratios of remineralization determined by nutrient data analysis. *Glob Biogeochem Cycles* 8:65–80. doi.org/10.1029/93GB03318

Aoki S, Yamazaki K, Hirano D, Katsumata K, Shimada K, Kitade Y, Sasaki H, Murase H (2020) Reversal of freshening trend of Antarctic Bottom Water in the Australian-Antarctic Basin during 2010s. *Sci Rep* 10:14415. doi.org/10.1038/s41598-020-71290-6

Arrigo KR, Van Dijken GL (2003) Phytoplankton dynamics within 37 Antarctic coastal polynyas. *J Geophys Res* 108:3271. doi.org/10.1029/2002JC001739

Arhan M, Mercier H, Park Y-H (2003) On the deep water circulation of the eastern South Atlantic Ocean. *Deep Sea Res Pt I* 50:889-916. doi.org/10.1016/S0967-0637(03)00072-4

Azar E, Piñango A, Wallner-Kersanach M, Kerr R (2021) Source waters contribution to the tropical Atlantic central layer: New insights on the Indo-Atlantic exchanges. Deep Sea Res Pt I 168:103450. doi.org/10.1016/j.dsr.2020.103450

Barker P, Heezen BC (1973) Morphology of the Earth in the Antarctic and Subantarctic. Geogr J 139:572. doi.org/10.2307/1795080

Biló TC, Johns WE (2019) Interior pathways of Labrador Sea water in the North Atlantic from the Argo perspective. Geophys Res Lett 46:3340–3348. doi:10.1029/2018GL081439

Böning C, Behrens E, Biastoch A, Getzlaff K, Bamber JL (2016) Emerging impact of Greenland meltwater on deepwater formation in the North Atlantic Ocean. Nature Geosci 9:523-527. doi:10.1038/ngeo2740

Boswell SM, Smythe-Wright D (2002) The tracer signature of Antarctic Bottom Water and its spread in the Southwest Indian Ocean: Part I-CFC-derived translation rate and topographic control around the Southwest Indian Ridge and the Conrad Rise. Deep Sea Res Pt I 49:555-573. doi:10.1016/S0967-0637(01)00066-8

Boyer TP, Antonov JI, Baranova OK, Coleman C, Garcia HE, Grodsky A, Johnson DR, Locarnini RA, Mishono AV, O'Brien TD, Paver CR, Reagan JR, Seidov D, Smolyar IV, Zweng MM (2013) World Ocean Database 2013. Silver Spring, MD, National Oceanographic Data Center, 208pp. (NOAA Atlas NESDIS, 72). doi:10.25607/OPB-1454

Bower A, Lozier S, Biastoch A, Drouin K, Foukal N, Furey H, Lankhorst M, Rühs S, Zou S (2019) Lagrangian views of the pathways of the Atlantic Meridional Overturning Circulation. J Geophys Res 124:5313-5335. doi:10.1029/2019JC015014

Bower A, Lozier M, Gary S, Boning CW (2009) Interior pathways of the North Atlantic meridional overturning circulation. Nature, 459:243-247. doi.org/10.1038/nature07979

Bozec A, Lozier MS, Chassignet EP, Halliwell GR (2011) On the variability of the Mediterranean Outflow Water in the North Atlantic from 1948 to 2006. *J Geophys Res* 116:C09033. doi:10.1029/2011JC007191

Broecker WS, Peacock SL, Walker S, Weiss R, Fahrbach E, Schroeder M, Mikolajewicz U, Heinze C, Key R, Peng T-H, Rubin S (1998) How much deep water is formed in the Southern Ocean? *J Geophys Res* 103:15833-15843. doi:10.1029/98JC00248

Broecker WS, Denton GH (1989) The role of ocean-atmosphere reorganizations in glacial cycles. *Quat Sci Rev* 9:305-341. doi.org/10.1016/0277-3791(90)900267

Bryden HL, Johns WE, King BA, McCarthy G, McDonagh EL, Moat BI, Smeed DA (2020) Reduction in ocean heat transport at 26°N since 2008 cools the eastern subpolar gyre of the North Atlantic Ocean. *J Clim* 33:1677-1689. doi.org/10.1175/JCLI-D-19-0323.1

Bryden HL, Nurser AG (2003) Effects of strait mixing on ocean stratification. *J Phys Oceanogr* 33:1870-1872. doi.org/10.1175/1520-0485(2003)033<1870:EOSMOO>2.0.CO;2

Campos EJD, van Caspel MC, Zenk W, Morozov EG, Frey DI, Piola AR, Meinen CS, Sato OT, Perez RC, Dong S (2021) Warming trend in Antarctic Bottom Water in the Vema Channel in the South Atlantic. *Geophys Res Lett*, 48:e2021GL094709. doi.org/10.1029/2021GL094709

Clarke RA, Gascard JC (1983) The Formation of Labrador Sea Water. Part I: Large-Scale Processes. *J Phys Oceanogr* 13:1764-1778. doi.org/10.1175/1520-0485(1983)013<1764:TFOLSW>2.0.CO;2

Dickson R R, Brown J (1994) The production of North Atlantic Deep Water: Sources, rates, and pathways. *J Geophys Res* 99:12319-12341. doi.org/10.1029/94JC00530

Elliot M, Labeyrie L, Duplessy JC (2002) Changes in North Atlantic deep-water formation associated with the Dansgaard Oeschger temperature oscillations (60–10 ka). *Quatern Sci Rev* 21:1153–1165. doi.org/10.1016/S0277-3791(01)00137-8

Fahrbach E, Peterson RG, Rohardt G, Schlosser P, Bayer R (1994) Suppression of bottom water formation in the southeastern Weddell. *Deep Sea Res Pt I* 41:389–411. doi.org/10.1016/0967-0637(94)90010-8

Ferreira MLC, Kerr R (2017) Source water distribution and quantification of North Atlantic Deep Water and Antarctic Bottom Water in the Atlantic Ocean. *Prog Oceanogr* 153:66–83. doi.org/10.1016/j.pocean.2017.04.003

Fleischmann U, Hildebrandt H, Putzka A, Bayer R (2001) Transport of newly ventilated deep water from the Iceland Basin to the WestEuropean Basin. *Deep Sea Res Pt I* 48:1793–1819. doi.org/10.1016/S0967-0637(00)00107-2

Foldvik A, Kvinge T, Tørresen T (1985) Bottom Currents Near the Continental Shelf Break in the Weddell Sea. *Antarctic Res Ser* 43:5–20. doi.org/10.1029/AR043p0021

Foster TD, Carmack EC (1976) Frontal zone mixing and Antarctic Bottom Water formation in the southern Weddell Sea. *Deep Sea Res* 23:301–317. doi.org/10.1016/0011-7471(76)90872-X

Fuhr M, Laukert G, Yu Y, Nürnberg D, Frank M (2021) Tracing Water Mass Mixing from the Equatorial to the North Pacific Ocean With Dissolved Neodymium Isotopes and Concentrations. *Front Mar Sci* 7:61. doi.org/10.3389/fmars.2020.603761

García-Ibáñez MI, Pardo PC, Carracedo LI, Mercier H, Lherminier P, Ríos AF, Pérez FF (2015) Structure, transports and transformations of the water masses in the Atlantic Subpolar Gyre. *Prog Oceanogr* 135:18–36. doi.org/10.1016/j.pocean.2015.03.009

Gary SF, Lozier MS, Biastoch A, Bning CW (2012) Reconciling tracer and float observations of the export pathways of Labrador Sea Water. *Geophys Res Lett* 39:1–5. doi.org/10.1029/2012GL053978

Garzoli SL, Dong S, Fine R, Meinen CS, Perez RC, Schimid C, van Sebille E, Yao Q (2015) The fate of the deep western boundary current in the South Atlantic. *Deep Sea Res Pt I* 103:125-36. doi.org/10.1016/j.dsr.2015.05.008

Gill AE (1973) Circulation and bottom water production in the Weddell Sea. *Deep Sea Res* 20:I11-140. doi.org/10.1016/0011-7471(73)90048-X

Goodman PJ (1988) The Role of North Atlantic Deep Water Formation in na OGCM's Ventilation and Thermohaline Circulation. *J Phys Oceanogr* 28:1759-1785. doi.org/10.1175/1520-0485(1998)028<1759:TRONAD>2.0.CO;2

Gordon AL (1986) Intercean exchange of the thermocline waters. *J Geophys Res* 91:5037-5046. doi.org/10.1029/JC091iC04p05037

Jacobs SS, Amos AF, Bruchhausen PM (1970) Ross sea oceanography and Antarctic Bottom Water formation. *Deep Sea Res* 17:935-962. doi.org/10.1016/0011-7471(70)90046-X

Johnson GC (2008) Quantifying Antarctic Bottom Water and North Atlantic Deep Water volumes. *J Geophys Res* 113:C05027. doi.org/10.1029/2007JC004477

Karstensen J, Tomczak M (1998) Age determination of mixed water masses using CFC and oxygen data. *J Geophys Res Oceans* 103:18599-18609. doi.org/10.1029/98JC00889

Kennett JP, Watkins ND (1975) Deep-sea erosion and manganese nodule development in the southeast Indian ocean. *Science* 188:1011-1013. doi:10.1126/science.188.4192.1011

Kerr R, Dotto TS, Mata MM, Hellmer HH (2018) Three decades of deep water mass investigation in the Weddell Sea (1984-2014): Temporal variability and changes. *Deep Sea Res Pt II* 149:70-83. doi.org/10.1016/j.dsr2.2017.12.002

Kolla V, Sullivan L, Streeter S, Langseth M (1976) Spreading of Antarctic Bottom Water and its effects on the floor of the Indian Ocean inferred from bottom-water potential temperature, turbidity, and sea-floor photography. *Mar Geol* 21:171-189. doi:10.1016/0025-3227(76)90058-X

LeBel DA, Smethier WM, Rhein M, Kieke D, Fine RA, Bullister JL, Min DH, Roether W, Weiss FR, Andrié C, Wright-Smythe D, Jones EP (2008) The formation rate of North Atlantic Deep Water and Eighteen Degree Water calculated from CFC-11 inventories observed during WOCE. *Deep Sea Res Pt I* 55:891-910. doi.org/10.1016/j.dsr.2008.03.009

Li Q, England MH, Hogg AM, Rintoul SR, Morrison AK (2023) Abyssal ocean overturning slowdown and warming driven by Antarctic meltwater. *Nature* 615:841-847. doi.org/10.1038/s41586-023-05762-w

Lozier MS (1997) Evidence for large-scale eddy-driven gyres in the North Atlantic. *Sci* 277:361-364. doi:10.1126/science.277.5324.361

Lozier MS, Owens WB, Curry RG (1995) The climatology of the North Atlantic. *Progr Oceanogr* 36:1-44. doi.org/10.1016/0079-6611(95)00013-5

Lozier MS, Bower AS, Furey HH, Drouin KL, Xu X, Zou S (2022) Overflow water pathways in the North Atlantic. *Progr Oceanogr* 208:102874. doi.org/10.1016/j.pocean.2022.102874

Lynch-Stieglitz J, Adkins JF, Curry WB, Dokken T, Hall IR, Herguera JC, Hirschi JJ, Ivanova EV, Kissel C, Marchal O, Marchitto TM, McCave I., McManus JF, Mulitza S, Ninnemann U, Peeters F, Yu EF, Zahn R (2007) Atlantic meridional overturning circulation during the Last Glacial Maximum. *Sci* 316:66-69. doi:10.1126/science.1137127

Mackas DL, Denman L, Bennett AF (1987) Least squares multiple tracer analysis of water mass composition. *J Geophys Res* 92:2907-2918. doi.org/10.1029/JC092iC03p02907

Mamayev OI (1975) Temperature-Salinity Analysis of World Ocean Waters. Elsevier Oceanogr Ser 11:119-158. doi.org/10.1016/S0422-9894(08)71172-3

Mantyla AW, Reid JL (1983) Abyssal characteristics of the World Ocean Waters. Deep Sea Res Pt A 30:805-833. doi.org/10.1016/0198-0149(83)90002-X

Fontaine CM, De Pol-Holz R, Michel E, Siani G, Reyes-Macaya D, Martínez Méndez G, DeVries T, Stott L, Southon J, Mohtadi M, Hebbeln D (2019) Ventilation of the deep ocean carbon reservoir during the last deglaciation: results from the southeast pacific. Paleoceanography and Paleoclimatology, 34:2080-2097. doi:10.1029/2019PA003613

Mazé JP, Arhan M, Mercier H (1997) Volume budget of the eastern boundary layer off the Iberian Peninsula. Deep Sea Res Part I 44:1543-1574. doi.org/10.1016/S0967-0637(97)00038-1

Meredith MP, Venables HJ, Clarke A, Ducklow HW, Erickson M, Leng MJ, Lenaerts JTM, van den Broeke MR (2013) The freshwater system west of the Antarctic Peninsula: Spatial and temporal changes. J Clim 26:1669-1684. doi.org/10.1175/JCLI-D-12-00246.1

Mokeddem Z, McManus JF (2017) Insights into North Atlantic deep water formation during the peak interglacial interval of Marine Isotope Stage 9 (MIS 9). Clim Dyn 49:3193-3208. doi:10.1007/s00382-016-3505-9

Moorman R, Morrison AK, McC Hogg A (2020) Thermal Responses to Antarctic Ice Shelf Melt in an Eddy-Rich Global Ocean-Sea Ice Model. J Clim 33:6599-6620. doi.org/10.1175/JCLI-D-19-0846.1

Morozov EG, Frey DI, Zuev OA, Makarenko NI, Seliverstova AM, Mekhova OS, Krechik VA (2023) Antarctic bottom water in the Vema fracture zone. J Geophys Res 128:e2023JC019967. doi:10.1029/2023JC019967

Nakano H, Suginoara N (2002) Importance of the eastern Indian Ocean for the abyssal Pacific. J Geophys Res 107:3219. doi:10.1029/2001JC001065

Nissen C, Timmermann R, Hoppema M, Gürses O, Hauck J (2022) Abruptly attenuated carbon sequestration with Weddell Sea dense waters by 2100. *Nat Commun* 13:3402. doi.org/10.1038/s41467-022-30671-3

O'Neill BC, Tebaldi C, van Vuuren DP, Eyring V, Friedlingstein P, Hurtt G, Knutti R, Kriegler E, Lamarque J-F, Lowe J, Meehl G A, Moss R, Riahi K, Sanderson BM (2016) The scenario model intercomparison project (ScenarioMIP) for CMIP6. *Geosci Model Dev* 9:3461–3482. doi:10.5194/gmd-9-3461-2016

Olsen A, Key RM, van Heuven S, Lauvset SK, Velo A, Lin X, Schirnick C, Kozyr A, Tanhua T, Hoppema M, Jutterström S, Steinfeldt R, Jeansson E, Ishii M, Pérez FF, Suzuki T (2016) The Global Ocean Data Analysis Project version 2 (GLODAPv2) – an internally consistent data product for the world ocean. *Earth Syst Sci Data* 8:297–323. doi.org/10.5194/essd-8-297-2016

Orsi AH, Jacobs SS, Gordon AL, Visbeck M (2001) Cooling and Ventilating the Abyssal Ocean. *Geophys Res Lett* 28:2923-2926. doi.org/10.1029/2001GL012830

Orsi AH, Johnson GC, Bullister JL (1999) Circulation, mixing, and production of Antarctic Bottom Water. *Progr Oceanogr* 43:55–109. doi.org/10.1016/S0079-6611(99)00004-X

Pardo PC, Pérez FF, Velo A, Gilcoto M (2012) Water masses distribution in the Southern Ocean: improvement of an extended OMP (eOMP) analysis. *Progr Oceanogr* 103:92-105. doi.org/10.1016/j.pocean.2012.06.002

Piñango A, Kerr R, Orselli IBM, Carvalho ACO, Azar E, Karstensen J, Garcia CAE (2022) Ocean acidification and long-term changes in the carbonate system properties of the South Atlantic Ocean. *Glob Biogeochem Cycles* 36:e2021GB007196. doi:10.1029/2021GB007196

Poole P, Tomczak M (1999) Optimum Multiparameter analysis of the water mass structure in the Atlantic Ocean thermocline. *Deep Sea Res Pt I* 46:1895-1921. doi.org/10.1016/S0967-0637(99)00025-4

Purkey SG, Smethie WM, Gebbie G, Gordon AL, Sonnerup RE, Warner MJ, Bullister JL (2018) A synoptic view of the ventilation and circulation of Antarctic Bottom Water from chlorofluorocarbons and natural tracers. *Annu Rev Mar Sci* 10:503-527. doi.org/10.1146/annurev-marine-121916-063414

Era JW, Burke A, Robinson L, Adkins JF, Chen T, Cole C, et al. (2018) CO<sub>2</sub> storage and release in the deep Southern Ocean on millennial to centennial timescales. *Nature*, 562:569-573. doi:10.1038/s41586-018-0614-0

Reid JL (1994) On the total geostrophic circulation of the North Atlantic Ocean: flow patterns, tracers and transports. *Progr Oceanogr* 33:1-92. doi.org/10.1016/0079-6611(94)90014-0

Reid JL (1979) On the contribution of the Mediterranean Sea outflow to the Norwegian-Greenland Sea. *Deep Sea Res Pt A* 26:1199-1223. doi.org/10.1016/0198-0149(79)90064-5

Reid JL, Nowlin WD, Patzert WC (1977) On the Characteristics and Circulation of the Southwestern Atlantic Ocean. *J Phys Oceanogr* 7:62-91. doi.org/10.1175/1520-0485(1977)007<0062:OTCACO>2.0.CO;2

Reid JL, Lynn RJ (1971) On the influence of the Norwegian-Greenland and Weddell seas upon the bottom waters of the Indian and Pacific oceans. *Deep Sea Res* 18:1063-1088. doi.org/10.1016/0011-7471(71)90094-5

Rintoul SR, Hughes C, Olbers D (2001) The Antarctic Circumpolar Current System. *Int Geophys* 77:271-302. doi:10.1016/S0074-6142(01)80124-8

Rintoul SR (1998) On the origin and influence of Adelie Land Bottom Water. *Antarct Res Ser* 75:151-171. doi.org/10.1029/AR075p0151

Romera-Castillo C, Heras J, Álvarez M, Álvarez-Salgado XA, Mata G, Sáenz-de-Cabezón E (2022) Application of multi-regression machine learning algorithms to solve ocean water mass mixing in the Atlantic Ocean. *Front Mar Sci* 9. doi:10.3389/fmars.2022.904492

Schott FA, Fischer J, Dengler M, Zantopp R (2006) Variability of the Deep Western Boundary Current east of the Grand Banks. *Geophys Res Lett* 33:L21S07. doi:10.1029/2006GL026563

Silvano A, Purkey S, Gordon AL, et al. (2023) Observing Antarctic Bottom Water in the Southern Ocean. *Front Mar Sci* 10. doi.org/10.3389/fmars.2023.1221701

Skinner LC, Fallon S, Waelbroeck C, Michel E, Barker S (2010) Ventilation of the deep Southern Ocean and deglacial CO<sub>2</sub> rise. *Science*, 328:1147–1151. doi:10.1126/science.1183627

Solodoch A, Stewart AL, Hogg AM, Morrison AK, Kiss AE, Thompson AF, Purkey SG, Cimoli L (2022) How does Antarctic Bottom Water cross the Southern Ocean? *Geophys Res Lett* 49:e2021GL097211. doi.org/10.1029/2021GL097211

Stocker TF (2013) Chapter 1 - The ocean as a component of the climate system. *Int Geophys* 103:3-30. doi.org/10.1016/B978-0-12-391851-2.00001-5

Stramma L, Kieke D, Rhein M, Schott F, Yashayaev I, Koltermann KP (2004) Deep Water changes at the western boundary of the subpolar North Atlantic during 1996 to 2001. *Deep Sea Res Pt I* 51:1033-1056. doi.org/10.1016/j.dsr.2004.04.001

Strass VH, Rohardt G, Kanzow T, Hoppema M, Boebel O (2020) Multidecadal warming and density loss in the deep Weddell Sea Antarctica. *J Clim* 33:9863-9881. doi.org/10.1175/JCLI-D-20-0271.1

Talley LD (2013) Closure of the global overturning circulation through the Indian, Pacific, and Southern Oceans: Schematics and transports. *Oceanography* 26:80-97. doi:10.5670/oceanog.2013.07

Talley LD, Pickard G, Emery W, Swift J (2011) Descriptive physical oceanography: An Introduction (6th edn.). Elsevier, Boston.

Thompson RORY, Edwards RJ (1981) Mixing and water-mass formation in the Australian Subantarctic. *J Phys Oceanogr* 11:1399–1406. doi.org/10.1175/1520-0485(1981)011<1399:MAWMFI>2.0.CO;2

Tomczak M (1999) Some historical, theoretical and applied aspects of quantitative water mass analysis. *J Mar Res* 57:275-303. doi.10.1357/002224099321618227

Tomczak M (1981) A multi-parameter extension of temperature/salinity diagram techniques for the analysis of non-isopycnal mixing. *Progr Oceanogr* 10:147-171. doi.org/10.1016/0079-6611(81)90010-0

Tomczak M, Large DGB (1989) Optimum multiparameter analysis of mixing in the thermocline of the eastern Indian Ocean. *J Geophys Res* 94:16141-16149. doi.org/10.1029/JC094iC11p16141

Tsuchiya M, Talley DL, McCartney MS (1992) An eastern Atlantic section from Iceland southward across the equator. *Deep Sea Res Pt A* 39:1885-1917. doi.org/10.1016/0198-0149(92)90004-D

Van Sebille E, England MH, Froyland G (2012) Origin, dynamics and evolution of ocean garbage patches from observed surface drifters. *Environ Res Lett* 7:044040. doi: 10.1088/1748-9326/7/4/044040

Warren BA (1981) Deep circulation of the World Ocean. In: Evolution of Physical Oceanography. Cambridge, USA, pp 6-41.

Weijer W, Haine TWN, Siddiqui AH, Cheng W, Veneziani M, Kurtakoti P (2022) Interactions between the Arctic Mediterranean and the Atlantic Meridional Overturning Circulation: A Review. *Oceanography*. 35:118-127. doi.org/10.5670/oceanog.2022.130

Williams TJ, Hillenbrand C-D, Piotrowski AM, Allen CS, Frederichs T, Smith JA, Ehrmann W, Hodell DA (2019) Paleocirculation and ventilation history of Southern Ocean sourced deep water masses during the last 800,000 years. *Paleoceanogr. Paleoclimatology* 34:833–852. doi:10.1029/2018PA003472

Wunsch C (2005) The total meridional heat flux and its oceanic and atmospheric partition. *J Clim* 18:4374 - 4380. doi.org/10.1175/JCLI3539.1

Xu Z, Schrama E, van der Wal W (2015) Optimization of regional constraints for estimating the Greenland mass balance with GRACE level-2 data. *Geophys J Int* 202:381-393. doi.org/10.1093/gji/ggv146

Yashayaev I, van Aken HM, Holliday NP, Bersch M (2007) Transformation of the Labrador Sea Water in the subpolar North Atlantic. *Geophys Res Lett* 34:L22605. doi:10.1029/2007GL031812

Yu J, Anderson RF, Rohling E (2014) Deep Ocean Carbonate Chemistry and Glacial-Interglacial Atmospheric CO<sub>2</sub> Changes. *Oceanography* 27:16-25. doi.org/10.5670/oceanog.2014.04

Yuzhu Y (2000) Implications of the deep circulation and ventilation of the Indian Ocean on the renewal mechanism of North Atlantic Deep Water. *J Geophys Res* 105:23895-23926. doi:10.1029/2000JC900105

Zou S, Bower A, Furey H, Susan Lozier M, Xu X (2020) Redrawing the IcelandScotland Overflow Water pathways in the North Atlantic. *Nat Commun* 11:1-8. doi:10.1038/s41467-020-15513-4

Zou S, Lozier S, Zenk W, Bower A, Johns W (2017) Observed and modeled pathways of the Iceland Scotland Overflow Water in the eastern North Atlantic. *Prog Oceanogr* 159:211–222. doi.org/10.1016/j.pocean.2017.10.003

Zou S, Lozier MS (2016) Breaking the Linkage Between Labrador Sea Water Production and Its Advection Export to the Subtropical Gyre. *J Phys Oceanogr* 46:2169-2182. doi:10.1175/JPO-D-15-0210.1